CHARACTERIZATION OF MASS TRANSFER IN ADSORBENTS FOR USE IN

OXYGEN SEPARATION FROM AIR

by

Timothy J. Giesy

Dissertation

Submitted to the Faculty of the

Graduate School of Vanderbilt University

in partial fulfillment of the requirements

for the degree of

DOCTOR OF PHILOSOPHY

in

Chemical Engineering

May, 2014

Nashville, Tennessee

Approved:

M. Douglas LeVan

Kenneth A. Debelak

Peter N. Pintauro

Eugene J. LeBoeuf

ACKNOWLEDGMENTS

TABLE OF CONTENTS

LIST OF TABLES

LIST OF FIGURES

CHAPTER I

INTRODUCTION

Gas adsorption is an established technology for separating gas mixtures. Materials used as adsorbents in adsorptive separation are typically porous materials with large internal surface area. Examples of such materials are zeolites, porous alumina, porous carbons, and silica gel. During adsorption, adsorbate molecules diffuse through the porous structure of the adsorbent until equilibrium has been reached throughout the adsorbent. For a particular adsorbent, gases will differ both in their equilibrium adsorption capacity and in the rate at which they diffuse through the adsorbent. It is these differences that are utilized to effect the separation.

Pressure swing adsorption (PSA) is a technique in which an adsorbent is used repeatedly, with adsorption occurring at high pressure, and regeneration of the adsorbent occurring at low pressure. The less adsorbable components are the product of the adsorption step, while the more adsorbable components are recovered during regeneration.[1] Since PSA is a non-equilibrium process, the rigorous design of a PSA system relies heavily on being able to characterize the diffusion of each gas in the mixture to be separated. Though PSA technologies for many gas separations exist already, it is nevertheless advantageous to improve upon existing technologies by characterizing the diffusion of gases in new adsorbents.

One potential application for PSA is in the development of a medical oxygen concentrator for use in manned space missions. A recognized risk associated with the NASA human space flight program is the inability to adequately treat an ill or injured astronaut in space. A crucial aspect of addressing this risk is the development of a suitable medical oxygen source. The compressed oxygen tanks currently used aboard the International Space Station have some critical disadvantages. Notably,

these tanks are hazardous, heavy, and offer a limited supply of oxygen. Furthermore, the continual discharge of pure oxygen during medical treatment causes the spacecraft oxygen limit to be rapidly exceeded. Medical oxygen concentrators based on pressure swing adsorption have neither the hazards nor constraints of compressed oxygen cylinders, and do not increase the oxygen concentration in their surrounding environment. However, current PSA oxygen concentrators are too heavy and use too much power to be used in space. The development a lighter, more efficient medical oxygen concentrator is a comprehensive effort, but of fundamental importance are the identification and characterization of new, more effective adsorbents.

Multiple experimental methods exist for measuring diffusion rates in adsorbents. These include chromatography, NMR, differential adsorption bed, zero-length column, frequency response (FR), and constant-volume techniques.[2] Frequency response consists of perturbing one system variable periodically around an equilibrium state and monitoring the response of one or more other system variables in order to characterize the system. By measuring the response of an adsorption system over a wide range of frequencies, these techniques can distinguish between mass transfer mechanisms.

In this work, frequency response methods are used to characterize the transport behavior of atmospheric gases in adsorbents that are relevant to the development of a new, PSA-based medical oxygen concentrator. In Chapter 2, a new combined-technique frequency response apparatus is presented, and this apparatus is used to study transport of pure CO_2 in 13X zeolite. Then, in Chapter 3, the apparatus is used to study transport of pure N_2, O_2, and Ar in two varieties of carbon molecular sieve. Chapter 4 presents a study of transport of binary mixtures of O_2 and Ar in one of the carbon molecular sieve varieties from the pure gas study. In Chapter 5, analytical frequency response models are presented to aid in the interpretation and characterization of transport in different adsorbents. Finally, Chapter 6 summa-

rizes the major conclusions and contributions of this work. Preliminary results from frequency response studies of N_2 and O_2 on LiLSX zeolite are given in Appendix B.

References

[1] Suzuki, M. Adsorption Engineering. Tokyo: Kodansha LTD, 1990.

[2] Wang, Y.; LeVan, M. D. Investigation of mixture diffusion in nanoporous adsorbents via the pressure-swing frequency response method. 1. Theoretical treatment. *Ind. Eng. Chem. Res.* **2005**, *44*, 3692.

CHAPTER II

MEASUREMENT OF MASS TRANSFER RATES IN ADSORBENTS: NEW
COMBINED-TECHNIQUE FREQUENCY RESPONSE APPARATUS AND
APPLICATION TO CO_2 IN 13X ZEOLITE

2.1 Introduction

The effective design of adsorption-based gas separation processes depends upon accurate knowledge of the dynamic behavior of adsorbent/gas systems. It is usually assumed that uptake in porous adsorbents is limited by mass transfer, so studies of adsorption dynamics are often mass transfer studies in practice. Mass transfer of gases in porous adsorbents can be complex due to the existence of one or more mechanisms. Possible mechanisms include micropore diffusion (surface diffusion), Knudsen diffusion, macropore diffusion, Poiseuille flow, transport across a surface barrier, and external mass transfer. Also, changes in the adsorbent temperature caused by heats of adsorption can further complicate dynamic behavior.

Frequency response (FR) methods have proven useful for studies of adsorption dynamics due to their ability to discriminate among limiting mass transfer mechanisms. Commonly in studies of adsorption dynamics, a system is perturbed using a step change in the concentration of gas in contact with the adsorbent. By contrast, FR experiments employ a periodic (typically sinusoidal) perturbation of a system variable around an equilibrium point. The frequency of perturbation is thus introduced as an additional degree of freedom by which similar mass transfer mechanisms might be distinguished from one another.

Most FR studies of adsorption dynamics have used what we refer to as the volume-swing frequency response (VSFR) technique, in which the volume of a batch system containing the gas and adsorbent to be characterized is oscillated (typically

by a metal bellows or a piston-cylinder arrangement) and the resulting response in system pressure is measured. Naphtali and Polinski[1] first applied the VSFR technique to study the rate of adsorption of hydrogen on a nickel catalyst. Yasuda later used VSFR to study zeolite diffusion[2–4] as well as various other dynamic processes.[5–9] Sun and coworkers[10,11] studied diffusion rates of various hydrocarbons in silicalite-1 and NaX zeolite. Sun et al.[12] were also the first to suggest that the FR spectrum in a VSFR experiment could be affected by temperature changes caused by heats of adsorption. Rees and coworkers used a nontraditional square-wave VSFR technique to study rates of diffusion and adsorption of various gases in silicalite-1,[13–16] beta-zeolite,[13] zeolites A,[17,18] X,[13,18] and Y,[18] ZSM-5[16,18] and mordenite.[18] Additionally, substantial work on the development of general diffusion models for interpretation of VSFR spectra has been done by Jordi and Do[19,20] and Sun et al.[21] A review by Reyes and Iglesia[22] summarizes further examples of VSFR investigations of adsorption systems.

Besides VSFR, there exist multiple flow-through FR techniques which use changes in the concentration of flowing gas to perturb an adsorbent/gas system.[23–25] The most recent work using such flow-through techniques has been done by LeVan and coworkers, who developed the pressure-swing frequency response (PSFR)[26,27] technique and adopted the concentration-swing frequency response (CSFR) technique[28,29] pioneered by Deisler and Wilhelm.[23] In PSFR experiments, the system pressure is perturbed sinusoidally using a flow-based pressure controller and the response induced in the flow rate leaving the system is measured. In CSFR experiments, the composition of an inlet stream with constant total molar flow rate is perturbed sinusoidally and the response induced in the outlet stream composition is measured. These techniques have been used to study diffusion of pure gases and gas mixtures on silica gel and various carbon adsorbents.[27–32]

Each of these FR methods has its own advantages and disadvantages. Since

PSFR and CSFR are flow-through techniques, they allow for isothermal conditions to be maintained more easily than with batch systems due to the additional heat capacity of the flowing gas. Relatedly, PSFR and CSFR experience smaller nonisothermal effects caused by mechanical work done on the fluid. Another advantage of the CSFR technique is that it is particularly suited to studies involving gas mixtures, as the nature of the technique requires that multiple gases be used. By contrast, while mixture studies are possible using VSFR and PSFR,[31,32] data analysis is complicated and more prone to error. The greatest advantage of VSFR over PSFR and CSFR is its ability to measure FR spectra to frequencies near 10 Hz and above, whereas PSFR and CSFR have difficulty measuring spectra in the region above 0.5 Hz. Data in the high frequency region are required in order to identify fast mass transfer resistances that do not manifest at lower frequencies. In order to thoroughly and accurately characterize the dynamics of adsorbent/gas systems, the advantages of each of these FR techniques are desired.

In this work, we present a single FR apparatus that can perform VSFR, PSFR, and CSFR experiments. Noting that VSFR and PSFR can be treated mathematically in a very similar way,[33] data from these two techniques can be easily combined to yield FR spectra for pure gas systems over a wider frequency range than VSFR or PSFR alone. Additionally, using its CSFR capabilities, the apparatus also adds the ability to perform mixed-gas experiments. The expanded frequency range and mixture-study capability of this apparatus will aid in the characterization of adsorption dynamics in an expanded set of adsorbent/gas systems. As an example system, diffusion of pure CO_2 in 13X beads is considered.

2.2   New Apparatus

Because PSFR and CSFR are both flow-through methods, it is relatively simple to design a single apparatus capable of both of these techniques. Adding VSFR

capability is less straightforward, however, as a suitable volume perturbation mechanism must be identified. The new apparatus uses a simple, cost-effective metal bellows pump with the check valves removed as its volume perturbation mechanism. Such a pump has been used previously in a VSFR apparatus.[34] Figure 2.1 shows a schematic representation of the new apparatus. Flow of gas into the system is controlled by two mass flow controllers (MKS type 1479A). The outlets from each controller converge and lead into a small adsorption bed. Capillary tubing leads from this adsorption bed to a mass spectrometer (Agilent 5975C), which is used to analyze the composition of the stream leaving the bed. Downstream of the first adsorption bed is a pressure transducer (Omega custom configuration) and another (larger) adsorption bed. The metal bellows pump (Senior Aerospace MB-21) and a copper tubing coil each reside on separate side branches which can be closed off using plug valves. Downstream of the second adsorption bed are a mass flow meter (MKS type 179A) and a flow-based pressure controller (MKS type 640A). A vacuum can be drawn continuously at the end of the flow path. All controllers and sensors interface with a National Instruments PCI-6289 M Series data acquisition board installed in an HP Compaq dc7900 PC.

To perform CSFR experiments, both mass flow controllers are used simultaneously to generate an inlet stream with sinusoidally oscillating composition. This stream passes through the first adsorption bed which contains the adsorbent to be analyzed. The smaller adsorption bed is used for CSFR experiments, as keeping the system volume small helps reduce weakening of the perturbation amplitude caused by gas mixing. A sample of the gas stream leaving the adsorbent bed is drawn through the capillary tubing to the mass spectrometer, where its composition is analyzed. The dynamics of the system are characterized by comparing the input perturbation (the inlet composition) with the system response (the outlet composition).
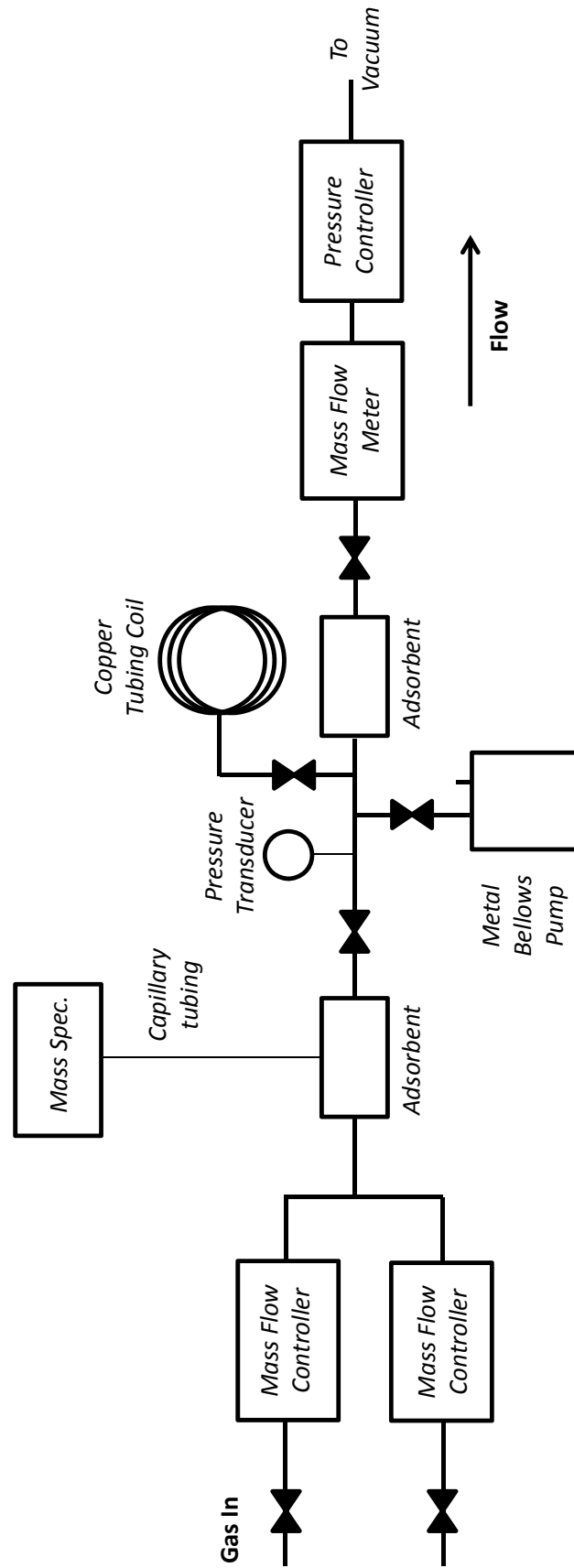
Figure 2.1 Schematic diagram of the combined-technique FR apparatus.

To perform PSFR experiments (for pure gases), only one mass flow controller is used. The capillary tubing port is capped off and gas flows through the now empty upstream adsorption bed to the second adsorption bed which contains the adsorbent to be characterized. The branches containing the tubing coil and the metal bellows pump are closed off to keep the system volume as small as possible. The pressure in the system is oscillated sinusoidally using the pressure controller and the induced response in mass flow leaving the system is measured by the mass flow meter.

For VSFR experiments, the metal bellows pump and tubing coil branches are opened and the system is filled to the desired pressure with the desired gas. The adsorbent in the larger of the two adsorbent beds is allowed to come to equilibrium with the flowing gas. Once equilibrium has been reached, plug valves are closed to produce a batch system volume containing the large adsorption bed, pressure transducer, tubing coil and metal bellows pump. The pump is used to oscillate the system volume sinusoidally and the resulting pressure response is measured using the pressure transducer. The copper tubing coil serves two purposes. First, since the magnitude of the volume perturbation is fixed by the design of the metal bellows pump, more volume is needed in the system to keep the perturbation small relative to the overall system volume. Secondly, the long section of tubing provides additional surface area for heat transfer to help reduce nonisothermal effects caused by gas compression.

Combining PSFR and VSFR experiments, the new apparatus can perform pure component studies up to 1 bar over the frequency range from 10^{-5} Hz to 10 Hz. The CSFR capability permits studies of binary gas mixtures of nearly any composition at pressures up to 1 bar over the frequency range from 10^{-5} Hz to 0.1 Hz. The large adsorption bed used for PSFR and VSFR has a volume of 7 cm^3, which is large enough to hold approximately 3 to 4 g of adsorbent particles. Depending on the isotherm slope of the material at the experimental pressure, less adsorbent than this maximum

can be used. The bed used for CSFR experiments is smaller, having a volume of approximately 0.2 cm³. The amount of adsorbent used in CSFR experiments is correspondingly lower than the amounts used for PSFR and VSFR.

2.3 Theory

Previous analyses have followed Yasuda's treatment[5] of VSFR, which expresses experimental data in the form of the in-phase and out-of-phase components of the frequency response. However, expressing FR data instead in the form of amplitude ratio and phase lag response curves simplifies the treatment of multiple simultaneous dynamic processes and can aid in the understanding of the effects of coupling between mechanisms.[22] Furthermore, amplitude ratio curves offer the added convenience of allowing graphical determination of the isotherm slope from the low-frequency asymptote of the curve.

Expressions for the amplitude ratio and phase lag response curves for PSFR and VSFR have been presented in detail in previous work by Wang and LeVan.[33] As they discuss, the amplitude ratio has been found to be useful by itself in identifying controlling mechanisms and evaluating rate parameters. For PSFR, the amplitude ratio is given by

$$\frac{A_F}{\omega A_P} = \left| M_s G_n(j\omega) + \frac{V}{RT} \right| \tag{2.1}$$

where A_F and A_P represent, respectively, the oscillation amplitudes of the mass flow rate leaving the system and the system pressure, ω is the angular frequency of oscillation, M_s is the mass of adsorbent, G_n is the adsorbed-phase transfer function, and V is the system volume. The corresponding expression for VSFR is

$$\frac{A_V}{A_P} \frac{P_0}{RT} = \left| M_s G_n(j\omega) + \frac{V_0}{RT} \right| \tag{2.2}$$

In the above expression, A_V represents the oscillation amplitude of the system vol-

ume and P_0 and V_0 represent the average system pressure and volume, respectively. The amplitude ratio in FR experiments is usually written as the ratio of the response amplitude to the perturbation amplitude. However, writing Eq. 2.2 using the inverse of the usual amplitude ratio gives equations for PSFR and VSFR having the same form and using the same adsorbed-phase transfer function G_n. For practical reasons, however, the analysis of VSFR data departs slightly from Eq. 2.2 due to a common correction used to account for system delays. Yasuda[2] gave this approximation as $A_V/V_0 = A_{P,B}/P_0$, where A_V/V_0 is the reduced volume perturbation amplitude and $A_{P,B}/P_0$ is the reduced pressure amplitude of a blank (containing no adsorbent) system. Using this approximation, Eq. 2.2 becomes

$$\frac{A_{P,B}}{A_P}\frac{V_0}{RT} = \left| M_s G_n(j\omega) + \frac{V_0}{RT} \right| \tag{2.3}$$

The adsorbed-phase transfer function contains the whole of the contribution of the occurring mass transfer mechanism to the dynamic response of the system. The work by Wang and LeVan[33] gives expressions for G_n for various mass transfer mechanisms. An additional case, the case of nonisothermal macropore diffusion control, is of interest for bidispersed adsorbent systems with significant heats of adsorption and/or slow heat transfer rates. When adsorption dynamics in a bidispersed pellet are macropore diffusion limited, the adsorbed-phase concentration in an individual zeolite crystal will be at equilibrium with the gas surrounding it in the macropore void space. For a FR system undergoing small perturbations, the adsorbed-phase concentration in a zeolite crystal can be expressed by an equilibrium expression linearized around a single equilibrium point:

$$n(c_p, T) = n(c_{p,0}, T_0) + K(c_p - c_{p,0}) + K_T(T - T_0) \tag{2.4}$$

where c_p is the gas-phase concentration in the intercrystalline voids, n is the adsorbed-

12

phase concentration, and K and K_T are the slopes of the isotherm and isobar, respectively. The macropore mass balance equation is written in spherical coordinates with the appropriate boundary conditions as

$$\rho_p \frac{\partial n}{\partial t} + \epsilon_p \frac{\partial c_p}{\partial t} = \frac{\epsilon_p D_p}{R^2} \frac{\partial}{\partial R} \left(R^2 \frac{\partial c_p}{\partial R} \right) \tag{2.5}$$

$$c_p = c \text{ at } R = R_p \tag{2.6}$$

$$\frac{\partial c_p}{\partial R} = 0 \text{ at } R = 0 \tag{2.7}$$

where ρ_p is the pellet density, ϵ_p is the pellet porosity, D_p is the macropore diffusivity, c is the gas-phase concentration in the volume outside the adsorbent pellet, and R_p is the pellet radius.

The adsorbent temperature can be linked with adsorbent loading using a simplified energy balance, expressed as[33]

$$M_s C_s \frac{dT}{dt} + M_s \lambda \frac{d\tilde{n}}{dt} = -\alpha(T - T_0) \tag{2.8}$$

where C_s represents the combined heat capacity of the solid adsorbent and the adsorbed gas, λ is the heat of adsorption (taken to be negative), $\tilde{n}$ is the adsorbed-phase concentration averaged over an entire adsorbent particle, and α is an effective heat transfer coefficient. Using Eq. 2.8, temperature can be eliminated from Eq. 2.4. After conversion to the Laplace domain, the modified equilibrium expression is substituted into Eq. 2.5, and the differential equation is solved.

The final expression for the adsorbed-phase transfer function is

$$G_n(s) = \frac{3}{RT_0} l_1 \left\{ \frac{K \left[1 - \frac{\epsilon_p \beta}{\rho_p \eta} (1 - 3l_1) \right]}{1 - K_T G_T + \frac{K\beta}{\eta}(1 - 3l_1)} + \frac{\epsilon_p}{\rho_p} \right\} \tag{2.9}$$

13

with

$$l_1 = \frac{\sqrt{\eta}\coth(\sqrt{\eta}) - 1}{\eta} \tag{2.10}$$

$$\eta = \frac{s}{D_p/R_p^2}\left(1 + \frac{\rho_p K}{\epsilon_p}\right) \tag{2.11}$$

$$\beta = \frac{\rho_p s K_T G_T}{\epsilon_p D_p/R_p^2} \tag{2.12}$$

In Eq. 2.9, G_T is the energy balance transfer function, which arises from the energy balance equation and is defined in Appendix A, where the adsorbed-phase transfer function is derived in detail.

2.4   Experiments

In this work, PSFR and VSFR experiments were performed for 8-12 mesh ($R_p = 1$ mm) 13X zeolite beads (Grace Davison) with CO_2 (99%) at pressures of 0.125 bar, 0.25 bar, 0.5 bar and 1 bar. In addition, beads from the same lot were ground with a mortar and pestle and sieved to 30-40 mesh ($R_p = 0.25$ mm). Both PSFR and VSFR experiments were performed using these particles at 0.25 and 0.5 bar. The samples were regenerated under vacuum at 350 °C for 10 hours. The sample sizes for the 8-12 mesh and the 30-40 mesh particles were 3.15 g and 3.25 g, respectively. The PSFR experiments were carried out over the frequency range from 10^{-4} Hz to 0.2 Hz and the VSFR experiments were carried out from 0.05 Hz to 10 Hz. All experiments were performed at room temperature. Because only pure CO_2 was studied in this work, CSFR was not used. We note that the CSFR section of the apparatus is identical to what we have used previously.[28–30]

2.5   Results and Discussion

Zeolite adsorbents often consist of small zeolite crystals formed into larger pellets or beads. The structure of these adsorbents results in two porous domains:

micropores in the individual zeolite crystals and macropores comprising the intercrystalline voids. Transport of pure gases in these "bidispersed" zeolite particles can be governed by a combination of diffusion in macropores, transport in individual zeolite crystals, and nonisothermal effects. In crystals of faujasite-type zeolites like 13X, mass transfer is expected to be fast[35] because of the relatively large (0.74 nm)[36] aperture dimensions of the zeolite framework. For example, Onyestyák et al.[37] and Ahn et al.[38] have each reported intracrystalline diffusivities of CO_2 in type-X zeolites that are orders of magnitude greater than intracrystalline diffusivities in type-A zeolites. Thus, provided that the constituent zeolite crystals are not too large, the effect of intracrystalline diffusion on the dynamic response of a bidispersed faujasite-type zeolite bead can be negligible, and the response will then be governed by either macropore diffusion, heat transfer, or a combination of the two. Macropore diffusion limitation of CO_2 in type-A and type-X zeolite pellets was observed by Onyestyák et al.[37] and Onyestyák,[39] which suggests that even particles formed from slower type-A zeolite crystals can be limited by macropore diffusion.

Figures 2.2a and 2.2b show the pressure-swing and volume-swing FR spectra for CO_2 on the 8-12 mesh 13X zeolite beads. At all pressures, these spectra are well described by the nonisothermal macropore diffusion model. The model parameters extracted from the experimental data are listed in Table 1. Adding either a micropore diffusion resistance or a barrier resistance[33] to the nonisothermal macropore diffusion model did not yield any advantage in the ability of the model to describe the experimental data.

The influence of macropore diffusion on the adsorption dynamics of the system is confirmed by the FR spectra of CO_2 on the 30-40 mesh zeolite particles. Figures 2.3a and 2.3b show sample PSFR and VSFR spectra for the two different particle sizes. The response of a system governed by macropore diffusion depends on the value of D_p/R_p^2 rather than just D_p, so any change in particle radius will change the macropore

Parameter	Value
D_p/R_p^2	2.3 1/s
K (0.125 bar)	0.13 m^3/kg
K (0.25 bar)	0.058 m^3/kg
K (0.5 bar)	0.025 m^3/kg
K (1 bar)	0.010 m^3/kg
λ	-32.6 kJ/mol
α_{PSFR}	0.045 J/kg·s
α_{VSFR}	0.25 J/kg·s

Table 2.1 Extracted parameters for the nonisothermal macropore diffusion model.

Figure 2.2 Frequency response of 8-12 mesh 13X beads at all pressures compared with nonisothermal macropore diffusion model predictions. a) PSFR; b) VSFR.

(b)

○ 0.125 bar
+ 0.25 bar
△ 0.5 bar
□ 1 bar
—— nonisothermal MD model

Frequency (Hz)

$AR \cdot (P_0/RT)$ (mol/bar) $\times 10^3$
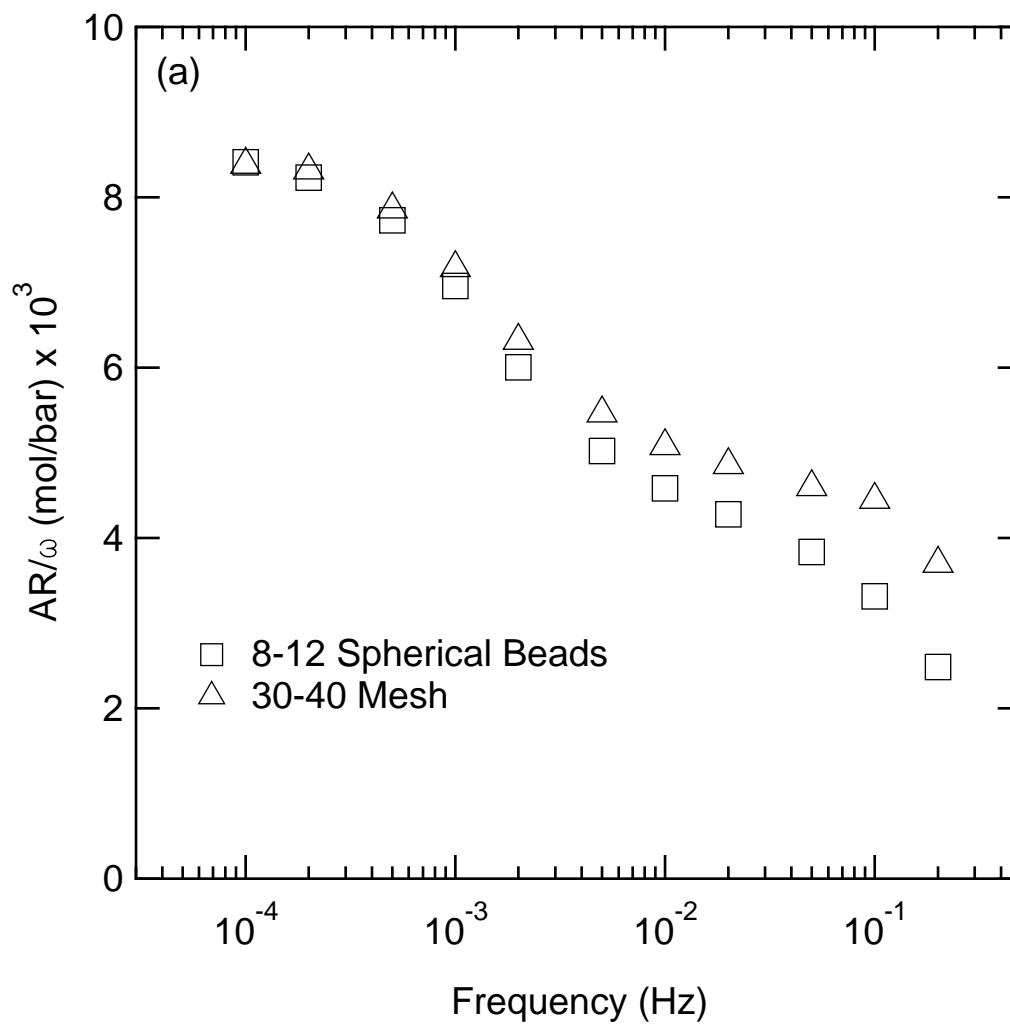
Figure 2.3 Comparison of frequency response of two particle sizes at 0.25 bar. a) PSFR; b) VSFR.

(b)

8-12 Spherical Beads
30-40 Mesh

$AR \cdot (P_0/RT)$ (mol/bar) x 10^3

Frequency (Hz)

20
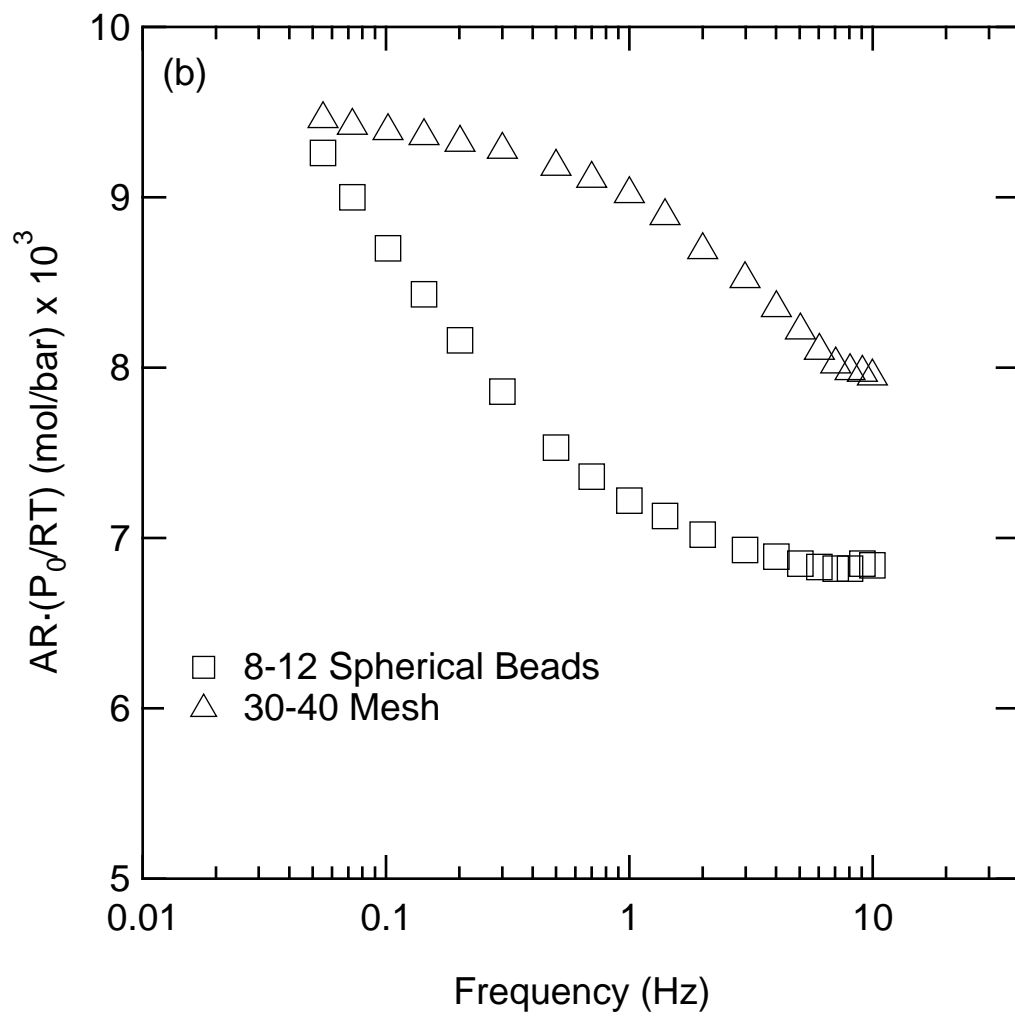
diffusion resistance, which will only affect the dynamic response of a system for which macropore diffusion is important. That the dynamic response of this system depends on particle size is a strong indication of macropore diffusion. Figures 2.4a and 2.4b compare the experimental data at 0.25 bar with the predictions of both isothermal and nonisothermal macropore diffusion models, which show clearly that temperature effects are also important to the dynamic character of the system. Futhermore, while the predictions of isothermal and nonisothermal micropore diffusion models are similar to their macropore diffusion analogs, the particle size dependence of the system response discounts these models as acceptable descriptions of the dynamic behavior of this system.

The curves predicted by the nonisothermal macropore diffusion model use a common macropore diffusion coefficient for each pressure tested. Pressure independence of macropore diffusion coefficients indicates a Knudsen-type mechanism occurring in the macropores; the other possible macropore diffusion mechanism for pure gas systems is Poiseuille flow, for which the diffusivity increases linearly with pressure.[40] Using the standard estimation of Knudsen diffusivity and assuming a typical value of tortuosity ($\tau = 3.0$) and a uniform pore size distribution yields a macropore dimension of 64 nm, which is within the defined range for macropores.[40] We note that the mean free path for CO_2 in bulk at room temperature and 1 bar is 61 nm, so our highest pressure is near the upper limit for Knudsen diffusion.

The rest of the parameters extracted from the experimental data for the nonisothermal macropore diffusion model are also reasonable. The isosteric heat is similar to the value reported by Dunne et al.[41] Because the FR spectra were measured in the region where isosteric heat is approximately independent of loading, only a single isosteric heat value was used in the model curves for all pressures. The extracted isotherm slopes, while reasonable, are slightly lower than values obtained from our measured isotherms.[42]

21
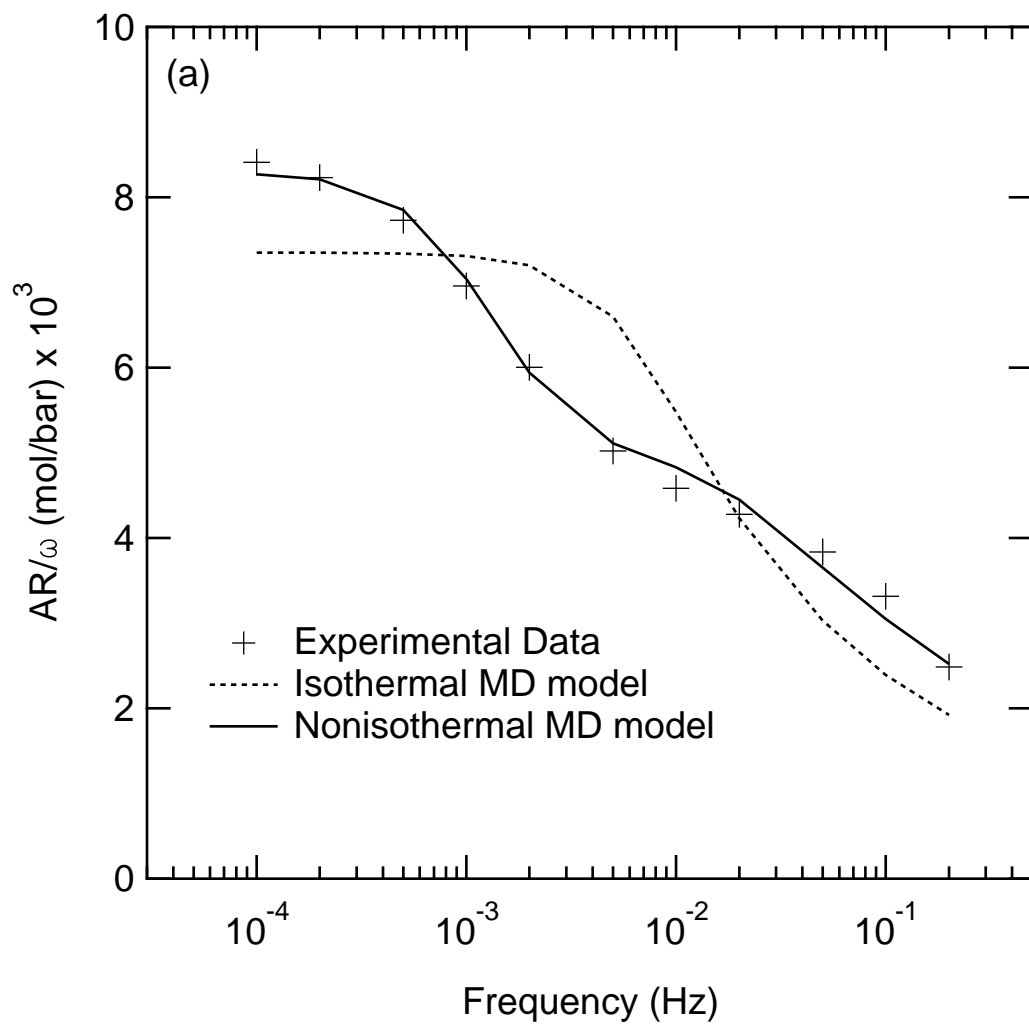
Figure 2.4 Comparison of isothermal and nonisothermal macropore diffusion models with frequency response data at 0.25 bar. a) PSFR; b) VSFR.

(b)

Frequency (Hz)

AR·(P_0/RT) (mol/bar) x 10^3

Legend:
+ Experimental Data
···· Isothermal MD model
— Nonisothermal MD model
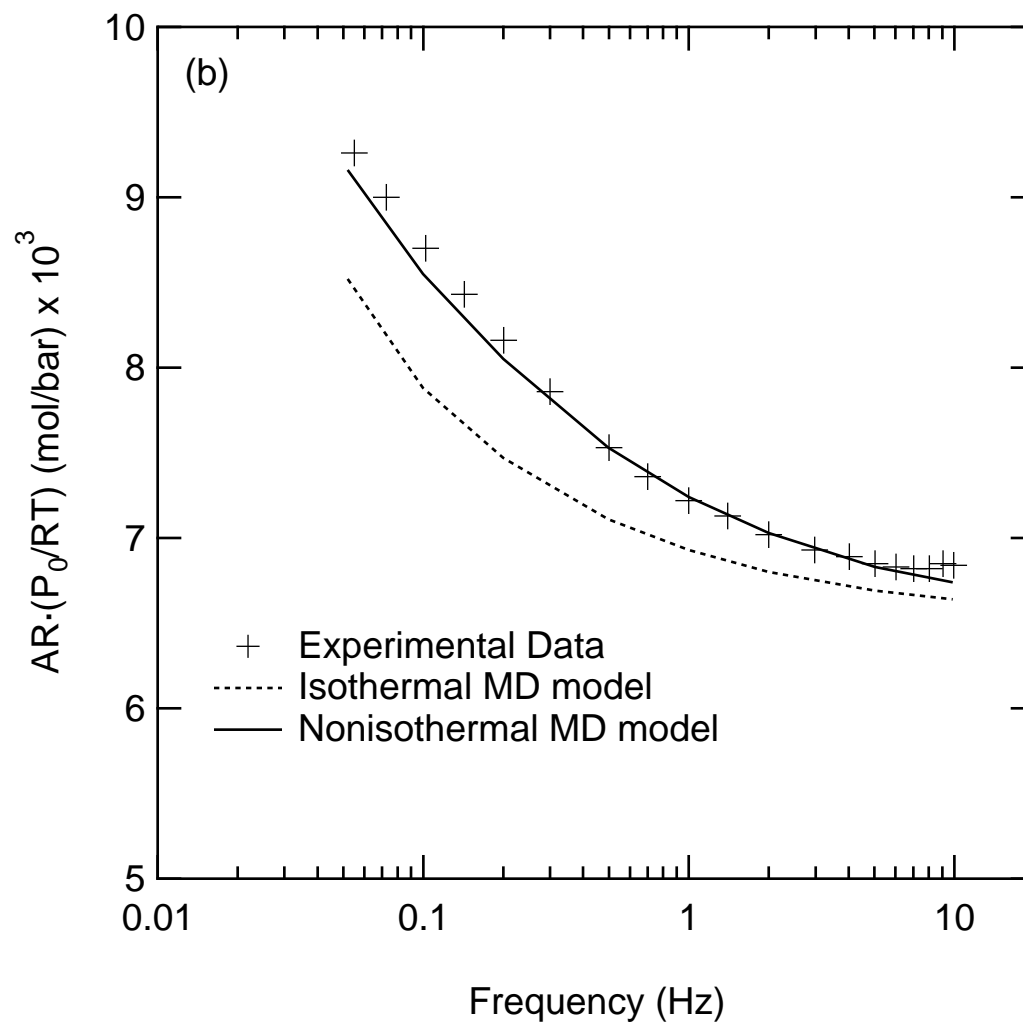
Figures 2.5a and 2.5b show the 30-40 mesh particle spectra compared with the predictions of the nonisothermal macropore diffusion model. Although the values of D_p/R_p^2 are on the order of those expected based on the response of the whole beads and the change in particle size upon grinding, the agreement of the model with the experimental data is only qualitative. Grinding the beads exposes faster dynamic mechanisms in the zeolite crystals which are masked by the slower macropore diffusion resistance in the whole beads. However, adding a micropore diffusion resistance or a surface barrier resistance to the nonisothermal macropore diffusion model did not yield an improved description of the data.

Regarding the dynamic response of the 30-40 mesh particles, there are a few interpretations. First, it is possible that adsorption dynamics are governed by mass transfer in the zeolite crystals and that the transport mechanism is more complex than either Fickian diffusion or a surface barrier mechanism. Bülow[43] discusses this possibility in detail, suggesting that chemisorbed species could influence the mobility of CO_2 in 13X crystals. Ruthven[44] notes that transport in zeolite crystals may be governed by defects in the crystal structure, which is a mechanism for which Fick's law may be an inadequate description.

Secondly, it may be the case that the nonisothermal macropore diffusion model is too idealized to capture the dynamic behavior of the small particles in a detailed way. Ruthven and Loughlin[45] noted the importance of particle shape and size distribution in the dynamic response of an adsorbent. The presented nonisothermal macropore diffusion model treats the case of spherical particles with a single particle radius. However, the grinding process leaves the 30-40 mesh particles irregularly shaped, and while sieving controls the size distribution somewhat, there is nevertheless some size variation and great shape variation in the particles. Furthermore, the heat transfer component of the model is described by a single lumped heat transfer coefficient. Such an approximation is often adequate, but it clearly does not rigor-
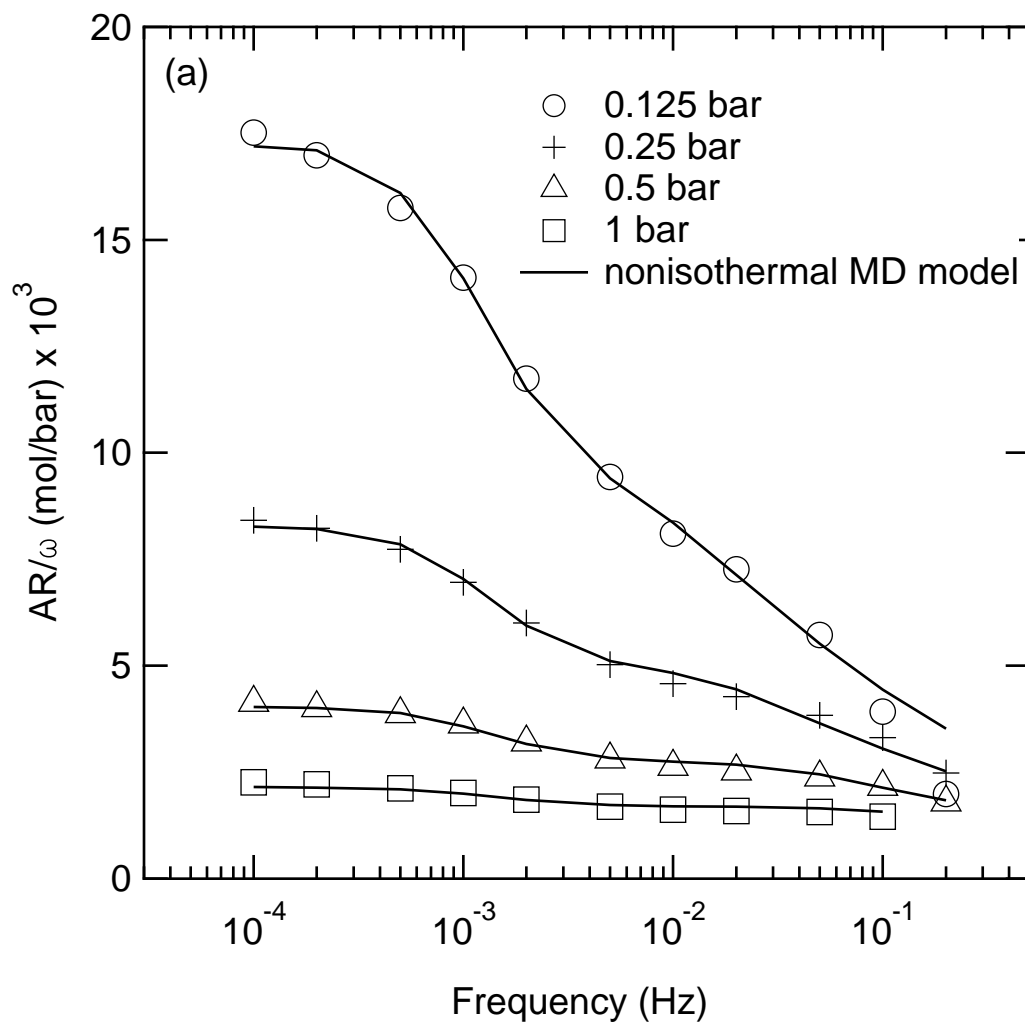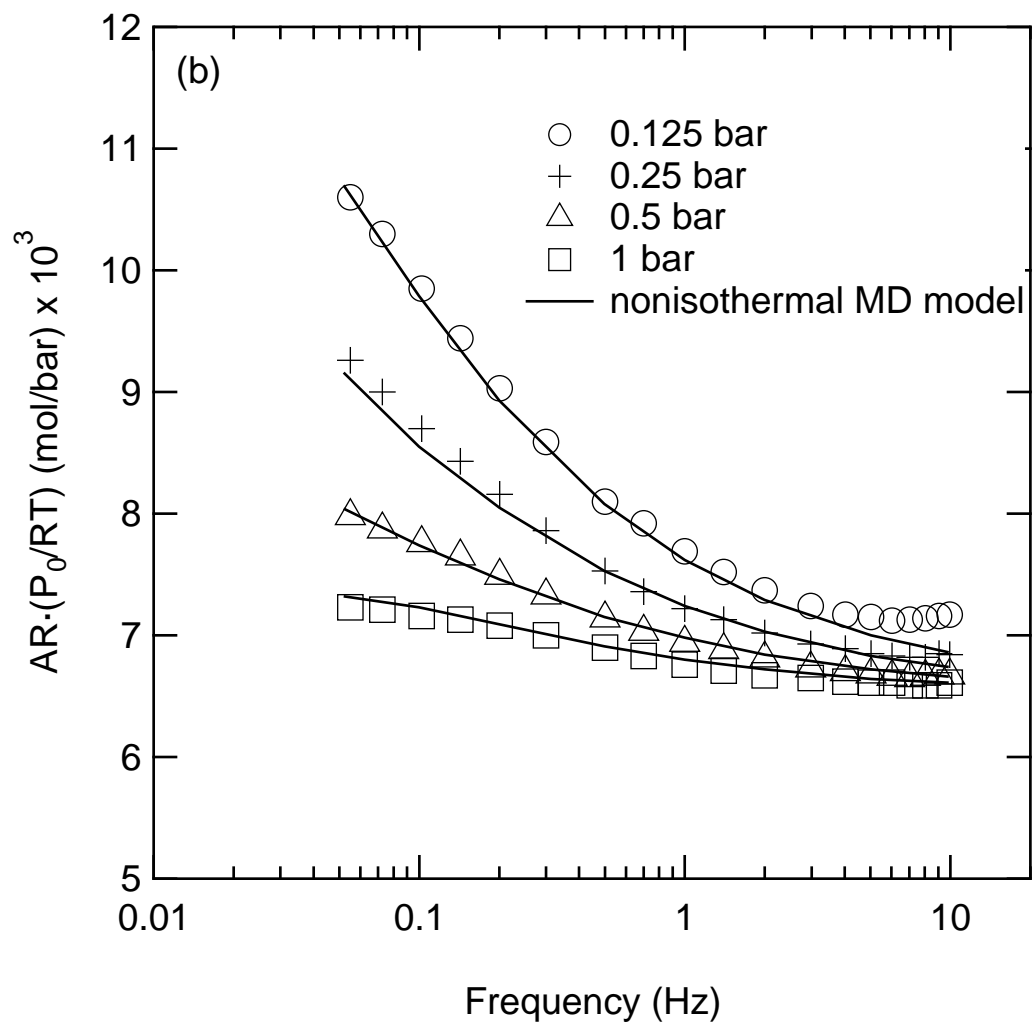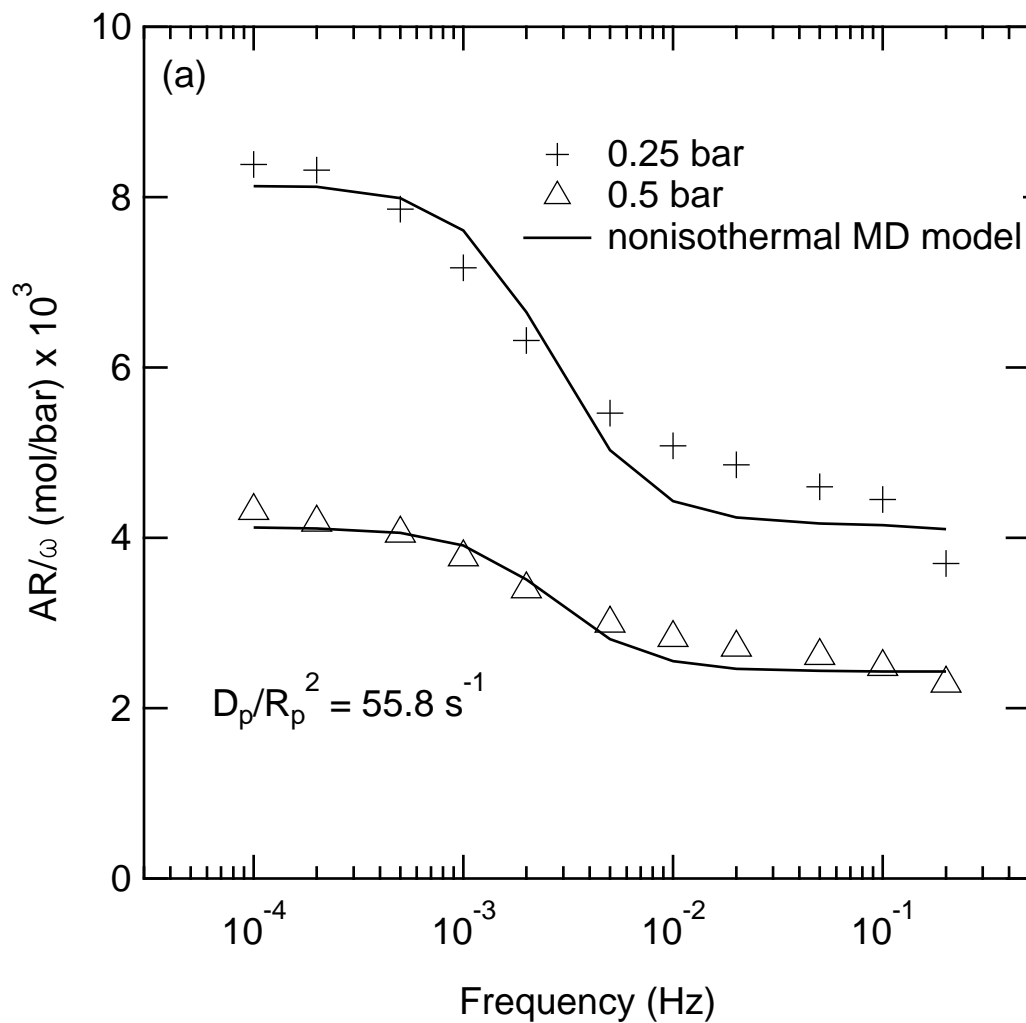
Figure 2.5 Frequency response of 30-40 mesh 13X particles at each pressure compared with nonisothermal macropore diffusion model predictions ($D_p/R_p^2 = 55.8\ s^{-1}$). a) PSFR; b) VSFR.
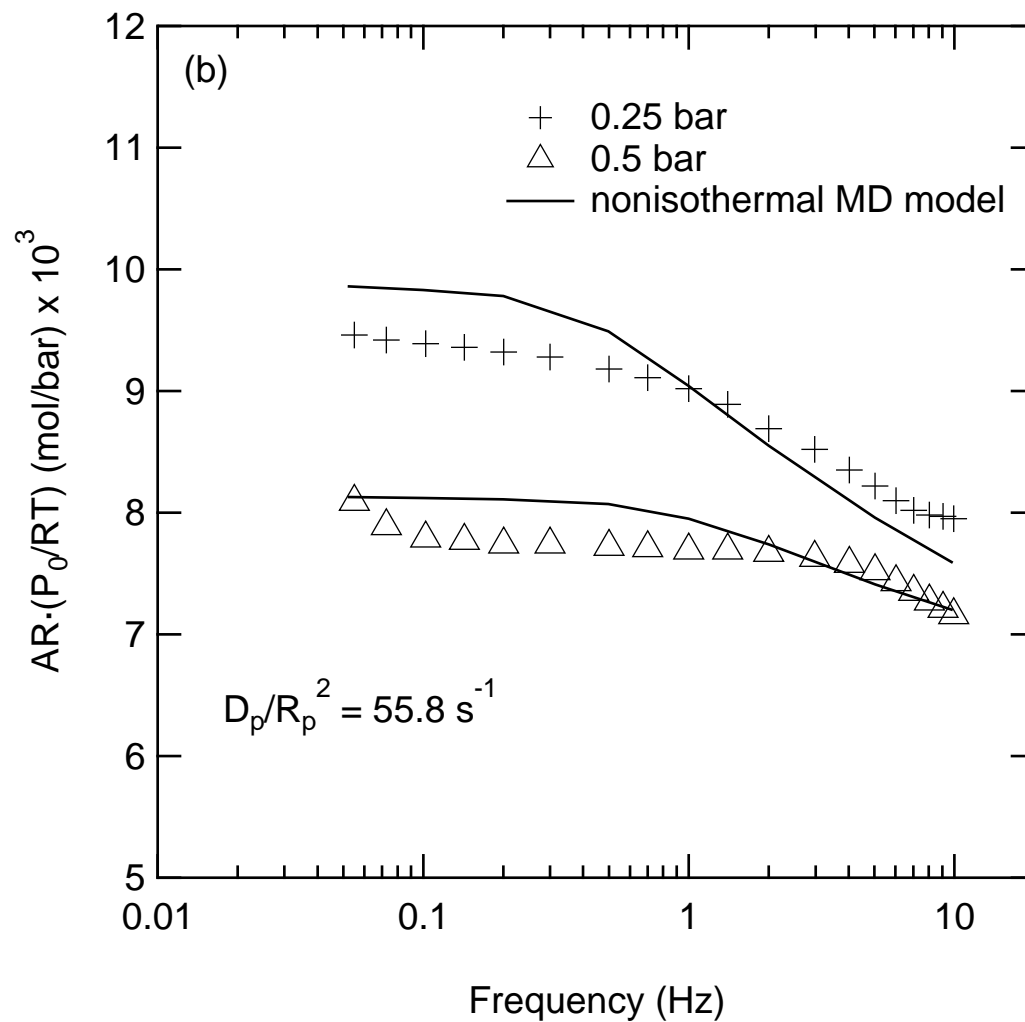
ously describe heat transfer in the system. Also, Neogi and Ruckenstein[46] noted that the validity of the "point-sink" treatment of zeolite crystals, which is implicit to the nonisothermal macropore diffusion model, becomes less valid as the ratio of crystal radius to particle radius increases. The data from the 30-40 mesh size particles may reflect such an effect.

Finally, it is possible that when adsorption dynamics are fast, transport of gas to the adsorbent particles may significantly affect the dynamic response of the system. Ruthven and Lee[35] showed that the adsorption dynamics of faujasite-type zeolite crystals depended on how thinly the particles were arranged during uptake experiments. This observation suggests that transport of at least some gases in these crystals is too fast to measure in uptake experiments, and that "bed effects" will always affect the dynamics of these systems. Similar kinds of bed effects may also be significant in systems using gram quantities of 30-40 mesh size particles.

2.6   Conclusions

A new combined-technique FR apparatus for investigation of mass transfer in adsorbents has been presented. The new apparatus combines the VSFR, PSFR, and CSFR techniques, allowing it to perform a diverse set of FR experiments. The enhanced experimental capabilities of the apparatus will permit more thorough characterization of the dynamic behavior of gas/adsorbent systems.

The capabilities of the new apparatus were demonstrated on the CO_2 on 13X system. The simultaneous use of VSFR and PSFR experiments allowed investigation of a wide frequency range, including the region in which faster dynamic mechanisms are manifested. The ability to perform CSFR studies of mixture diffusion will prove useful in future investigations. The adsorption dynamics of pure CO_2 on 8-12 mesh 13X zeolite beads are well described by a nonisothermal macropore diffusion model, where diffusion in the macropores takes place via a Knudsen-type mechanism. Macro-

27

pore diffusion control is confirmed by the existence of a substantial effect of particle size on the dynamic response of this system. For smaller (30-40 mesh) bidispersed particles in which macropore diffusion is less important, the dynamic response begins to be controlled by other mechanisms. Inclusion of a surface barrier resistance or a micropore diffusion resistance in the nonisothermal macropore diffusion model did not improve the model's ability to capture the dynamic behavior of these smaller particles. Clearly, more investigation is warranted in order to adequately characterize the faster transport mechanisms which are uncovered by decreasing the macropore diffusion resistance using smaller particle sizes.

Notation

A_F = amplitude of mass flow oscillation, mol/s

A_P = amplitude of pressure oscillation in system with adsorbent, bar

$A_{P,B}$ = amplitude of pressure oscillation in system with no adsorbent, bar

A_V = amplitude of volume oscillation, m^3

c = extraparticle fluid-phase concentration, mol/m^3

c_p = fluid-phase concentration in macropores, mol/m^3

C_s = combined heat capacity of adsorbent and adsorbate, J/(kg K)

D_p = macropore diffusivity, m^2/s

G_n = adsorbed-phase transfer function

G_T = energy balance transfer function

K = local isotherm slope, m^3/kg

K_T = local isobar slope, mol/(kg K)

l_1 = lumped parameter

M_s = mass of adsorbent, kg

n = adsorbed-phase concentration, mol/kg

$\tilde{n}$ = adsorbed-phase concentration averaged over adsorbent particle, mol/kg

$\hat{n}$ = average adsorbate concentration including gas in macropores, mol/kg

P = pressure, bar

R = distance along macroparticle radius, m

R_p = macroparticle radius, m

T = temperature, K

V = volume of pressure-controlled region, m^3

x_p = dimensionless macroparticle radial coordinate

Greek Letters

α = lumped heat transfer coefficient, W/K

β = lumped parameter

ϵ_p =   macropore porosity

η =   lumped parameter

λ =   heat of adsorption, J/mol

ρ_p =   density of adsorbent particle, kg/m^3

ω =   angular frequency of oscillation, rad/s

Superscripts

$'$ =   deviation variable

$^-$ =   Laplace domain

Subscripts

$_0$ =   equilibrium (mean) state

References

[1] Naphtali, L. M.; Polinski, L. M. A novel technique for characterization of adsorption rates on heterogeneous surfaces. *J. Phys. Chem.* **1963**, *67*, 369.

[2] Yasuda, Y. Determination of vapor diffusion coefficients in zeolite by the frequency response method. *J. Phys. Chem.* **1982**, *86*, 1913.

[3] Yasuda, Y. A frequency response technique to study zeolitic diffusion of gases. *J. Catal.* **1984**, *88*, 530.

[4] Yasuda, Y.; Yamamoto, A. Zeolitic diffusivities of hydrocarbons by the frequency response method. *J. Catal.* **1985**, *93*, 176.

[5] Yasuda, Y. Frequency response method for study of the kinetic behavior of a gas-surface system. 1. Theoretical treatment. *J. Phys. Chem.* **1976**, *80*, 1867.

[6] Yasuda, Y. Frequency response method for study of the kinetic behavior of a gas surface system. 2. An ethylene-on-zinc oxide system. *J. Phys. Chem.* **1976**, *80*, 1870.

[7] Yasuda, Y.; Suzuki, Y.; Fukada, H. Kinetic details of a gas/porous adsorbent system by the frequency response method. *J. Phys. Chem.* **1991**, *95*, 2486.

[8] Yasuda, Y. Frequency response method for study of kinetic details of a heterogeneous catalytic reaction of gases. 1. Theoretical treatment. *J. Phys. Chem.* **1993**, *97*, 3314.

[9] Yasuda, Y.; Nomura, K. Frequency response method for study of kinetic details of a heterogeneous catalytic reaction of gases. 2. A methanol conversion to olefins. *J. Phys. Chem.* **1993**, *97*, 3319.

[10] Sun, L. M.; Bourdin, V. Measurement of intracrystalline diffusion by the frequency response method: analysis and interpretation of bimodal response curves. *Chem. Eng. Sci.* **1993**, *48*, 3783.

[11] Giermanska-Kahn, J.; Cartigny, J.; Cohen De Lara, E.; Sun, L. M. Heat effect and intercrystalline diffusion of light n-alkanes in zeolite NaX measured by frequency response method. *Zeolites* **1996**, *17*, 365.

[12] Sun, L. M.; Meunier, F.; Kärger, J. On the heat effect in measurements of sorption kinetics by the frequency response method. *Chem. Eng. Sci.* **1993**, *48*, 715.

[13] Shen, D.; Rees, L. V. C. Study of fast diffusion in zeolites using a higher harmonic frequency response method. *J. Chem. Soc. Faraday T.* **1994**, *90*, 3011.

[14] Shen, D.; Rees, L. V. C. Analysis of bimodal frequency-response behaviour of p-xylene diffusion in silicalite-1. *J. Chem. Soc. Faraday T.* **1995**, *91*, 2027.

[15] Song, L.; Rees, L. V. C. Adsorption and transport of n-hexane in silicalite-1 by the frequency response technique. *J. Chem. Soc. Faraday T.* **1997**, *93*, 649.

[16] Song, L.; Rees, L. V. C. Adsorption and diffusion of cyclic hydrocarbon in MFI-type zeolites studied by gravimetric and frequency-response techniques. *Micropor. Mesopor. Mat.* **2000**, *35-36*, 301.

[17] Onyestyák, G.; Shen, D.; Rees, L. V. C. Frequency-response studies of CO_2 diffusion in commercial 5A powders and pellets. *Microporous Mater.* **1996**, *5*, 279.

[18] Valyon, J.; Onyestyák, G.; Rees, L. V. C. A frequency-response study of the diffusion and sorption dynamics of ammonia in zeolites. *Langmuir* **2000**, *16*, 1331.

[19] Jordi, R. G.; Do, D. D. Analysis of the frequency response method for sorption kinetics in bidispersed structured sorbents. *Chem. Eng. Sci.* **1993**, *48*, 1103.

[20] Jordi, R. G.; Do, D. D. Analysis of the frequency response method applied to non-isothermal sorption studies. *Chem. Eng. Sci.* **1994**, *49*, 957.

[21] Sun, L. M.; Meunier, F.; Grenier, P.; Ruthven, D. M. Frequency response for nonisothermal adsorption in biporous pellets. *Chem. Eng. Sci.* **1994**, *49*, 373.

[22] Reyes, S. C.; Iglesia, E. Frequency response techniques for characterization of porous catalytic solids. *Catalysis* **1994**, *11*, 51.

[23] Deisler, P. F.; Wilhelm, R. H. Diffusion in beds of porous solids. Measurement by frequency response techniques. *Ind. Eng. Chem.* **1953**, *45*, 1219.

[24] Gunn, D. J.; England, R. Dispersion and diffusion in beds of porous particles. *Chem. Eng. Sci.* **1971**, *26*, 1413.

[25] Boniface, H. A.; Ruthven, D. M. Chromatographic adsorption with sinusoidal input. *Chem. Eng. Sci.* **1985**, *40*, 2053.

[26] Sward, B. K.; LeVan, M. D. Frequency response method for measuring mass transfer rates in adsorbents via pressure perturbation. *Adsorption* **2003**, *9*, 37.

[27] Wang, Y.; Sward, B. K.; LeVan, M. D. New frequency response method for measuring adsorption rates via pressure modulation: Application to oxygen and nitrogen in a carbon molecular sieve. *Ind. Eng. Chem. Res.* **2003**, *42*, 4213.

[28] Glover, T. G.; Wang, Y.; LeVan, M. D. Diffusion of condensable vapors in single adsorbent particles measured via concentration-swing frequency response. *Langmuir* **2008**, *24*, 13406.

[29] Wang, Y.; LeVan, M. D. Nanopore diffusion rates for adsorption determined by pressure-swing and concentration-swing frequency response and comparison with Darken's equation. *Ind. Eng. Chem. Res.* **2008**, *47*, 3121.

[30] Wang, Y.; LeVan, M. D. Mixture diffusion in nanoporous adsorbents: Development of Fickian flux relationship and concentration-swing frequency response method. *Ind. Eng. Chem. Res.* **2007**, *46*, 2141.

[31] Wang, Y.; LeVan, M. D. Investigation of mixture diffusion in nanoporous adsorbents via the pressure-swing frequency response method. 1. Theoretical treatment. *Ind. Eng. Chem. Res.* **2005**, *44*, 3692.

[32] Wang, Y.; LeVan, M. D. Investigation of mixture diffusion in nanoporous adsorbents via the pressure-swing frequency response method. 2. Oxygen and nitrogen in a carbon molecular sieve. *Ind. Eng. Chem. Res.* **2005**, *44*, 4745.

[33] Wang, Y.; LeVan, M. D. Master curves for mass transfer in bidisperse adsorbents for pressure-swing and volume-swing frequency response methods. *AIChE J.* **2011**, *57*, 2054.

[34] Turner, M. D.; Capron, L.; Laurence, R. L.; Conner, W. C.; The design and construction of a frequency response apparatus to investigate diffusion in zeolites. *Rev. Sci. Instrum.* **2001**, *72*, 4424.

[35] Ruthven, D. M.; Lee, L. K. Kinetics of nonisothermal sorption: Systems with bed diffusion control. *AIChE J.* **1981**, *27*, 654.

[36] Rouquerol, F.; Rouquerol, J.; Sing, K. *Adsorption by powders and porous solids: Principles, methodology and applications*; Academic Press: San Diego, 1999.

[37] Onyestyák, G.; Shen, D.; Rees, L. V. C. Frequency-response study of micro- and macro-pore diffusion in manufactured zeolite pellets. *J. Chem. Soc. Faraday T.* **1995**, *91*, 1399.

[38] Ahn, H.; Moon, J. H.; Hyun, S. H.; Lee, C. H. Diffusion mechanism of carbon dioxide in zeolite 4A and CaX pellets. *Adsorption* **2004**, *10*, 111.

[39] Onyestyák, G. Comparison of dinitrogen, methane, carbon monoxide, and carbon dioxide mass-transport dynamics in carbon and zeolite molecular sieves. *Helv. Chim. Acta* **2011**, *94*, 206.

[40] Kärger, J.; Ruthven, D. M. *Diffusion in zeolites and other microporous solids*; Wiley-Interscience Publications: New York, 1992.

[41] Dunne, J. A.; Rao, M.; Sircar, S.; Gorte, R. J.; Myers, A. L. Calorimetric heats of adsorption and adsorption isotherms. 2. O_2, N_2, Ar, CO_2, CH_4, C_2H_6, and SF_6 on NaX, H-ZSM-5, and Na-ZSM-5 zeolites. *Langmuir* **1996**, *12*, 5896.

[42] Wang, Y.; LeVan, M. D. Adsorption equilibrium of carbon dioxide and water vapor on zeolites 5A and 13X and silica gel: Pure components. *J. Chem. Eng. Data* **2009**, *54*, 2839.

[43] Bülow, M. Complex sorption kinetics of carbon dioxide in NaX-zeolite crystals. *Adsorption* **2002**, *8*, 9.

[44] Ruthven D. M. Diffusion in zeolites-a continuing saga. *Adsorption* **2010**, *16*, 511.

[45] Ruthven, D. M.; Loughlin, K. F. The effect of crystallite shape and size distribution on diffusion measurements in molecular sieves. *Chem. Eng. Sci.* **1971**, *26*, 577.

[46] Neogi, P.; Ruckenstein, E. Transport phenomena in solids with bidispersed pores. *AIChE J.* **1980**, *26*, 787.

CHAPTER III

MASS TRANSFER RATES OF OXYGEN, NITROGEN, AND ARGON IN
CARBON MOLECULAR SIEVES DETERMINED BY PRESSURE-SWING
FREQUENCY RESPONSE

3.1   Introduction

Knowledge of adsorption rates is essential for the design of adsorption-based gas separation processes. Adsorption rates are generally limited by mass transfer, which can occur by one or more of a variety of possible mechanisms including micropore diffusion, macropore diffusion (ordinary diffusion, Knudsen diffusion, or Poiseuille flow), transport across a surface barrier, and external mass transfer. As each of these mechanisms differs in its dynamic behavior, the study of adsorption rates includes both the identification of the occurring mass transfer mechanisms and the measurement of relevant model parameters.

Frequency response (FR) methods have proven useful in studies of mass transfer in adsorbents due to their ability to discriminate between similar mass transfer mechanisms (Grzegorczyk and Carta, 1997; Hsu and Pigford, 1991; Sun et al., 1993; Wang et al., 2003). In FR experiments, some system variable is perturbed, typically sinusoidally, around an equilibrium point, and the induced response in some other system variable is used to characterize the dynamics of the system. In applying FR to studies of adsorption systems, the frequency of perturbation is thus introduced as an additional degree of freedom by which similar mass transfer mechanisms may be differentiated.

One adsorption system that is of particular interest is the PSA-based separation of air by a carbon molecular sieve (CMS). CMS materials have a narrow pore size distribution with pores on the order of molecular dimensions (Braymer et al.,

36

1994; Verma and Walker, 1992). As a result, these materials achieve a "sieving" effect, whereby small differences in molecular size can result in vastly different rates of adsorption, regardless of the equilibrium characteristics of the adsorbing gases (Cabrera et al., 1993; Seaton et al., 1997). This feature of CMS has proven useful for air separation due to the different molecular dimensions of O_2 (3.46 Å) (Cabrera et al., 1993) and N_2 (3.64 Å) (Cabrera et al., 1993), which allow O_2 to adsorb up to 30 times faster than N_2 (Seaton et al., 1997).

Since N_2 adsorbs more slowly than O_2, PSA processes using CMS to separate air have usually been designed to produce a purified N_2 product (Ruthven, 1992; Ruthven et al., 1986; Yang, 1997). However, interest has recently been generated in the use of CMS (alone or paired with a zeolite) to produce high-purity O_2 by PSA (Hayashi et al., 1996, Jee et al., 2005b). The sieving ability that allows CMS to separate O_2 and N_2 kinetically can also be used to separate O_2 from Ar, which has been a difficult separation in traditional zeolite-based PSA processes due to the similar equilibrium characteristics of O_2 and Ar on many zeolites (Hayashi et al., 1996; Jee et al., 2005a, 2005b; Jin et al., 2006; Rege and Yang, 2000). Separation of O_2 from Ar is important in order to overcome the purity limit in PSA-generated O_2, which is caused by the Ar naturally present in air remaining with the O_2 during the separation (Hayashi et al., 1996; Jee et al., 2005b).

Because of the potential of CMS for air separation, there have been many studies devoted to understanding adsorption rates of O_2 and N_2, the major constituents of air, on these materials. The majority of the work done on $O_2/N_2/CMS$ systems has treated adsorption rates using either a micropore (Fickian) diffusion model (Chagger et al., 1995; Chen and Yang, 1994; Chen et al., 1994; Chihara et al., 1978; Kawazoe et al., 1974; Liu and Ruthven, 1996; Ruthven, 1992; Ruthven et al., 1986) or a linear driving force (LDF) model (Chagger et al., 1995; Dominguez et al., 1988; Fitch et al., 1994; LaCava et al., 1989; Koresh and Soffer, 1980, 1981; Reid et al., 1998; Rynders et

al., 1997; Srinivasan et al., 1995), which Kärger and Caro (1977) suggested could be associated with a barrier resistance at the surface of a microporous region. A model that treats a surface barrier resistance in series with a micropore diffusion resistance has also been applied (Loughlin et al., 1993; Qinglin et al., 2003, 2004). Diffusion of O_2 and N_2 in the macropores of CMS pellets has been found to be insignificant for system response, with no dependence or only very weak dependence observed for mass transfer rates on the size of the pellets (Wang et al., 2003).

Despite the volume of work performed regarding air separation by CMS, further study of these systems is warranted. Determinations of limiting mass transfer mechanisms in CMS have varied widely, and Huang et al. (2004) have noted that the observed mechanism in a CMS system cannot be linked to either the adsorbent manufacturer or to the adsorbing gas. Furthermore, despite the importance of CMS for O_2/Ar separation, there is little Ar/CMS rate data available in the literature (Bae and Lee, 2005; Liu and Ruthven, 1996; Nguyen and Do, 2000; Reid et al., 1998). In this work, we apply the pressure-swing frequency response (PSFR) technique (Sward and LeVan, 2003; Wang et al., 2003) to study adsorption rates of pure O_2, N_2, and Ar on two commercially available CMS materials that, to our knowledge, have not been used in O_2/N_2/Ar rate studies in the literature. The use of frequency response will facilitate correct identification of the rate mechanisms occurring in these systems. This work also provides important, up-to-date adsorption rate data for use in the development of PSA processes, especially those for which the Ar adsorption rate is important.

3.2   Theory

The FR apparatus used in this work, shown in Fig. 3.1, has been described previously (Giesy et al., 2012). In PSFR experiments, gas flows into the system containing the adsorbent at a constant rate. The system pressure (the input variable

in PSFR experiments) is perturbed sinusoidally around an equilibrium point using the flow-based pressure controller, and the sinusoidal response in the flow rate out of the system (the output variable) is measured using the mass flow meter. The pressure perturbation is kept small ($<3\%$ of the equilibrium pressure) so that the system is appropriately linearized.

For the mathematical treatment of FR data, we follow the recommendation of Reyes and Iglesia (1994) in analyzing experimental data in the form of amplitude ratio (AR) and phase lag measurements. For PSFR, the AR response curves are given by (Giesy et al., 2012; Wang and LeVan, 2011)

$$\frac{A_F}{\omega A_P} = \left| M_s G_n(j\omega) + \frac{V}{RT} \right| \tag{3.1}$$

where A_F and A_P represent, respectively, the oscillation amplitudes of the mass flow rate leaving the system and the system pressure, ω is the angular frequency of oscillation, M_s is the mass of adsorbent, G_n is the adsorbed-phase transfer function, and V is the system volume.

PSFR systems can be characterized using amplitude ratio measurements by themselves (Giesy et al., 2012; Wang and LeVan, 2011). However, the phase lag between the input and output variable oscillations offers additional data for the characterization of PSFR systems. We have sometimes found our phase angle measurements to include more experimental error than our amplitude ratio measurements, so amplitude ratios are favored in this work for the characterization of adsorption dynamics.

Nevertheless, the phase angle for a PSFR system is still of interest and can be expressed by

$$\phi = \tan^{-1} \left[\frac{M_s \text{Re}[G_n(j\omega)] + V/RT}{M_s \text{Im}[G_n(j\omega)]} \right] \tag{3.2}$$
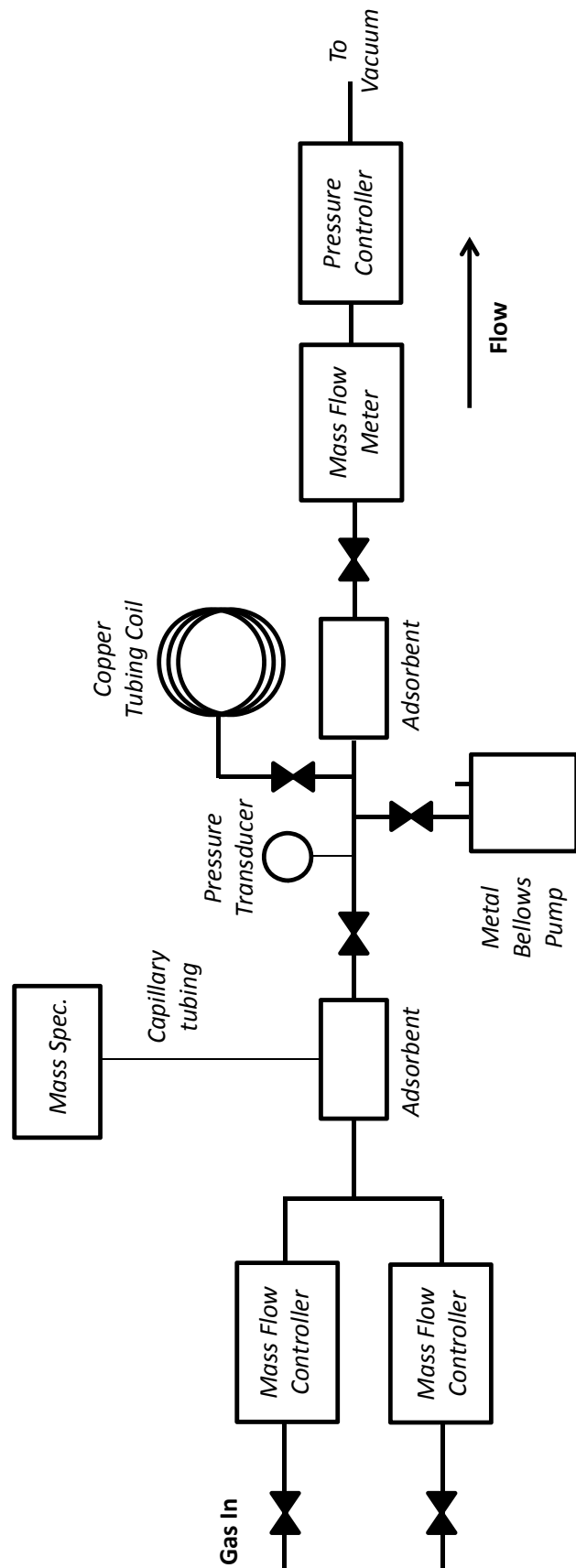
Figure 3.1 Schematic diagram of the FR apparatus.

where $\text{Re}[G_n(j\omega)]$ and $\text{Im}[G_n(j\omega)]$ signify, respectively, the real and imaginary components of the adsorbed phase transfer function evaluated at $s = j\omega$.

The adsorbed-phase transfer function G_n contains the entire contribution of the mass transfer mechanism to the dynamic character of the PSFR system. An extensive list of analytical expressions for G_n for various mass transfer mechanisms has been given by Wang and LeVan (2011). The mass transfer mechanisms of primary interest in this work are transport across a surface barrier (described by the LDF rate equation), micropore diffusion, and the combined resistance mechanism (barrier + micropore diffusion).

The LDF model is defined by

$$\frac{dn}{dt} = k(n^* - n) \tag{3.3}$$

where n is the adsorbed-phase concentration in the micropore region of the adsorbent, n^* is the adsorbed-phase concentration that would exist in equilibrium with the fluid-phase concentration surrounding the micropore region, and k is the rate coefficient. Expressing Eq. 3.3 in terms of deviation variables and taking the Laplace transform gives

$$\bar{n} = \frac{k\bar{n}^*}{s + k} \tag{3.4}$$

Introducing a linearized isotherm $\bar{n}^* = K\bar{c}$ and integrating over the entire adsorbent particle yields the expression (Wang and LeVan, 2011)

$$G_n(s) = \frac{\bar{\bar{n}}}{\bar{P}} = \frac{Kk}{RT(s + k)} + \frac{\epsilon_p}{\rho_p RT} \tag{3.5}$$

where K is the local isotherm slope, ϵ_p is the macropore porosity, and ρ_p is the particle density.

When micropore diffusion is controlling, adsorption rates can be described in

41

spherical geometry by

$$\frac{\partial n}{\partial t} = \frac{D_s}{r^2}\frac{\partial}{\partial r}\left(r^2\frac{\partial n}{\partial r}\right) \tag{3.6}$$

$$n = n^* \quad \text{at} \quad r = r_s \tag{3.7}$$

$$\frac{\partial n}{\partial r} = 0 \quad \text{at} \quad r = 0 \tag{3.8}$$

Converting to the Laplace domain and solving the differential equation leads to the solution

$$\bar{n}(s,x) = \frac{\bar{n}^*}{x}\frac{\sinh\left(x\sqrt{s/\eta}\right)}{\sinh\left(\sqrt{s/\eta}\right)} \tag{3.9}$$

where $x = r/r_s$ and $\eta = D_s/r_s^2$. Again introducing a linearized isotherm and integrating over an entire adsorbent particle yields (Wang and LeVan, 2011)

$$G_n(s) = \frac{\bar{\bar{n}}}{\bar{P}} = \frac{3K}{RTs/\eta}\left[\sqrt{s/\eta}\coth\left(\sqrt{s/\eta}\right) - 1\right] + \frac{\epsilon_p}{\rho_p RT} \tag{3.10}$$

The governing equation for the combined resistance model is the same as that for the micropore diffusion model, but the boundary condition at the microparticle surface is replaced with

$$D_s\frac{\partial n}{\partial r} = k_b(n^* - n) \quad \text{at} \quad r = r_s \tag{3.11}$$

where k_b is the barrier resistance coefficient. Solving in the Laplace domain with the new boundary condition leads to

$$\bar{n}(s,x) = \frac{\beta_{bm}\bar{n}^*}{x}\frac{\sinh\left(x\sqrt{s/\eta}\right)}{(\beta_{bm} - 1)\sinh\left(\sqrt{s/\eta}\right) + \sqrt{s/\eta}\cosh\left(\sqrt{s/\eta}\right)} \tag{3.12}$$

with $\beta_{bm} = k_b r_s/D_s$. Introducing the linearized isotherm and integrating over an

entire adsorbent particle yields (Wang and LeVan, 2011)

$$G_n(s) = \frac{\bar{\bar{n}}}{\bar{P}} = \frac{3K\beta_{bm}}{RTs/\eta} \frac{\sqrt{s/\eta}\coth\left(\sqrt{s/\eta}\right) - 1}{\sqrt{s/\eta}\coth\left(\sqrt{s/\eta}\right) + \beta_{bm} - 1} + \frac{\epsilon_p}{\rho_p RT} \qquad (3.13)$$

While the models developed in Eqs. 3.3–3.13 assume isothermal conditions, temperature changes caused by heats of adsorption can significantly affect the dynamic response of an adsorption system (Sun et al. 1993). Temperature effects are generally not observed, however, in systems similar to those investigated in this work (Chagger et al., 1995; Wang and LeVan, 2005). Nevertheless, frequency response methods are sensitive enough to detect thermal effects should they occur; equations for various non-isothermal transport models have been given previously (Sun et al. 1994; Wang and LeVan, 2011).

3.3   Experiments

In this work, PSFR experiments were performed using pure O_2 (99.994%), N_2 (99%), and Ar (99.999%) for two different CMS materials, Shirasagi MSC-3R types 162 and 172, in the form of 1.8 mm diameter cylindrical pellets supplied by Japan EnviroChemicals. The sample size of each type of CMS was 3.02 g. Before measuring experimental data, the CMS samples were regenerated under vacuum at 90 °C for 1 hour, after which the regeneration temperature was increased to 150 °C, with the sample held for 8 additional hours. For each gas/adsorbent pair, the system response was investigated over the frequency range from 5×10^{-5} Hz to 0.2 Hz and at pressures from 0.125 bar to 1 bar. All experiments were performed at room temperature (23 °C).

3.4   Results and Discussion

A primary goal of studies of adsorption rates and a main reason for using FR techniques in adsorption studies is to correctly identify the transport mechanism.

Figure 3.2 shows amplitude ratio plots for O_2, N_2, and Ar measured at 0.5 bar on Shirasagi MSC-3R type 162. These data are representative of those measured at other pressures and on type 172. All of the experimental data in this figure are compared with best-fit descriptions of both the LDF and micropore diffusion models, and the O_2 data are also compared with the combined resistance model description. From these figures, it is clear that the transport of Ar and N_2 in this system is described by the LDF model and not by the micropore diffusion model. For transport of O_2, however, the combined resistance model offers the best description of the experimental data. It is nevertheless worth noting that for O_2 the LDF model is similar to the combined resistance model in its ability to describe the experimental data. This suggests that the contribution of micropore diffusion to O_2 adsorption dynamics in these materials is small.

In fitting the combined resistance model to the O_2 experimental data, the data from all four pressures on one material were analyzed simultaneously using a single corrected diffusivity, which was converted into micropore diffusivity values for each pressure according to the following equation (Do, 1998; Qinglin et al., 2004; Srinivasan et al., 1995):

$$D_s = D_{s0}(1 + bP) \qquad (3.14)$$

where $(1 + bP)$ is the form of the Darken-type thermodynamic correction factor assuming adsorption follows the Langmuir isotherm $n = NbP/(1 + bP)$. For type 162, we determined $D_{s0}/r_s^2 = 6.4 \times 10^{-3}$ s^{-1}, and for type 172, $D_{s0}/r_s^2 = 1.1 \times 10^{-2}$ s^{-1}. Introducing only the one additional parameter, the corrected diffusivity, for all the experimental data from a single material strengthens the case that this parameter is significant, and that the enhanced ability of the combined resistance model to describe the experimental data is not simply the result of excessive fitting parameters.

Figure 3.3 compares amplitude ratio data for all three gases at 0.5 bar on Shirasagi MSC-3R type 162 and type 172. For each material, O_2 transport is much
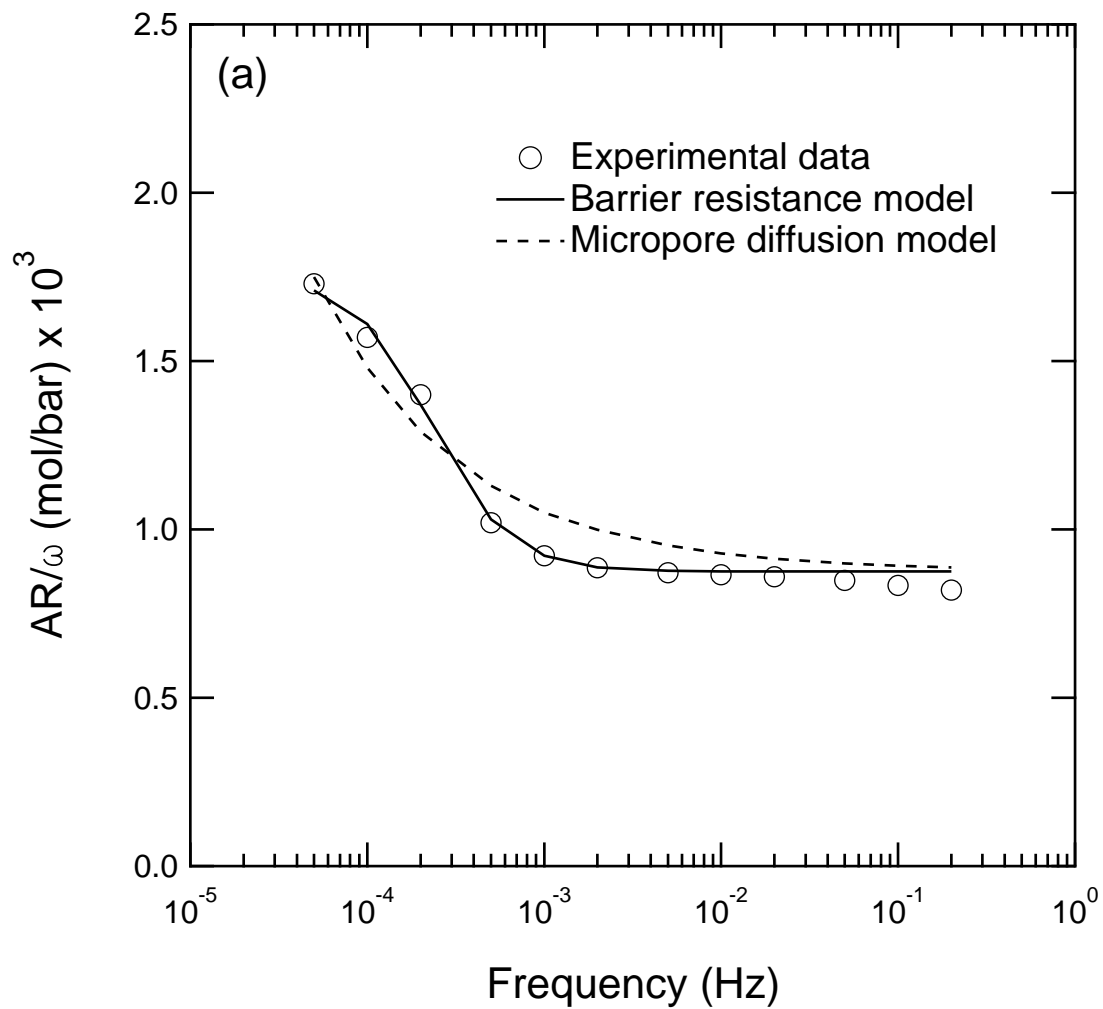
Figure 3.2 Single-gas amplitude ratio curves and model descriptions on Shirasagi MSC-3R type 162 at 0.5 bar. a) Argon; b) Nitrogen; c) Oxygen.

Figure (b): Plot of AR/ω (mol/bar) $\times 10^3$ versus Frequency (Hz), comparing Experimental data, Barrier resistance model, and Micropore diffusion model.

47
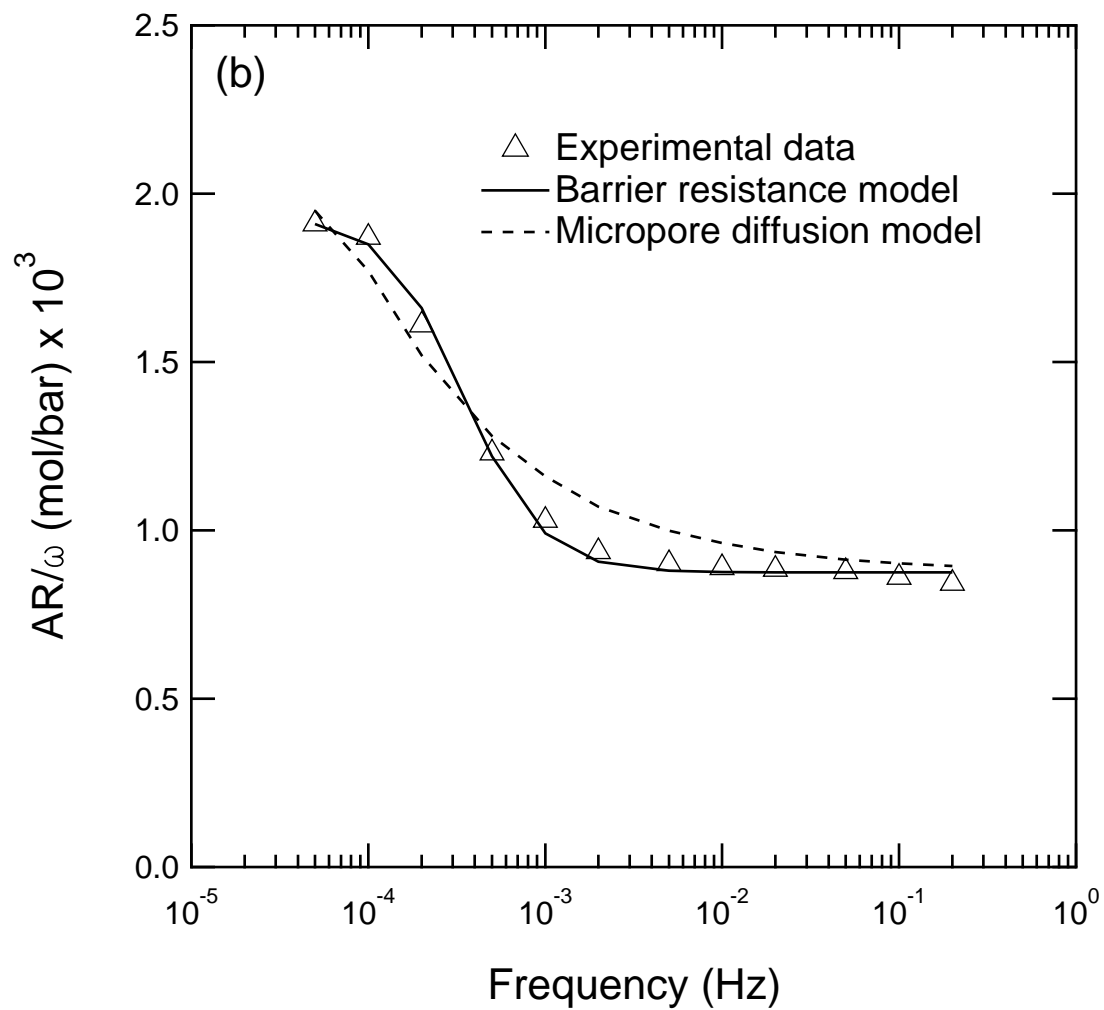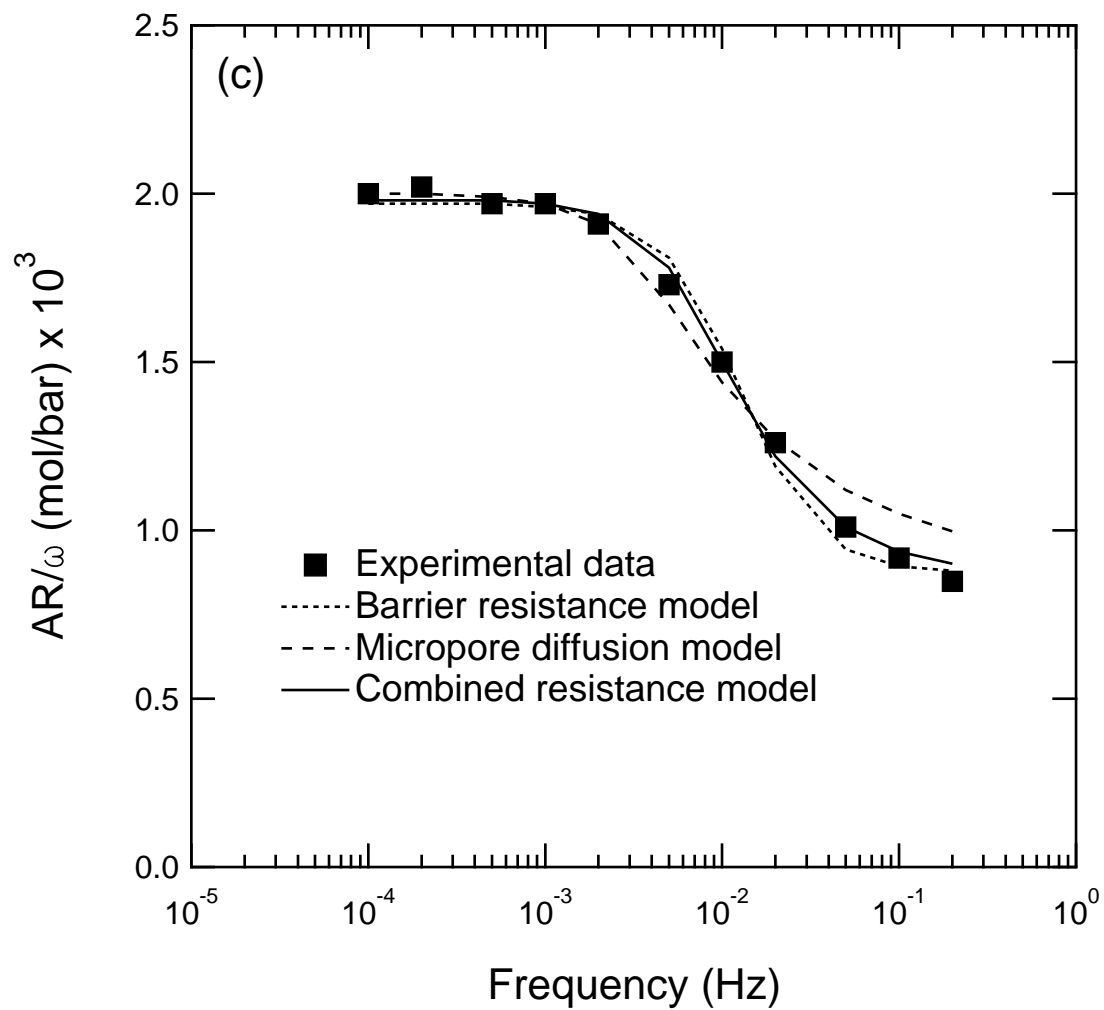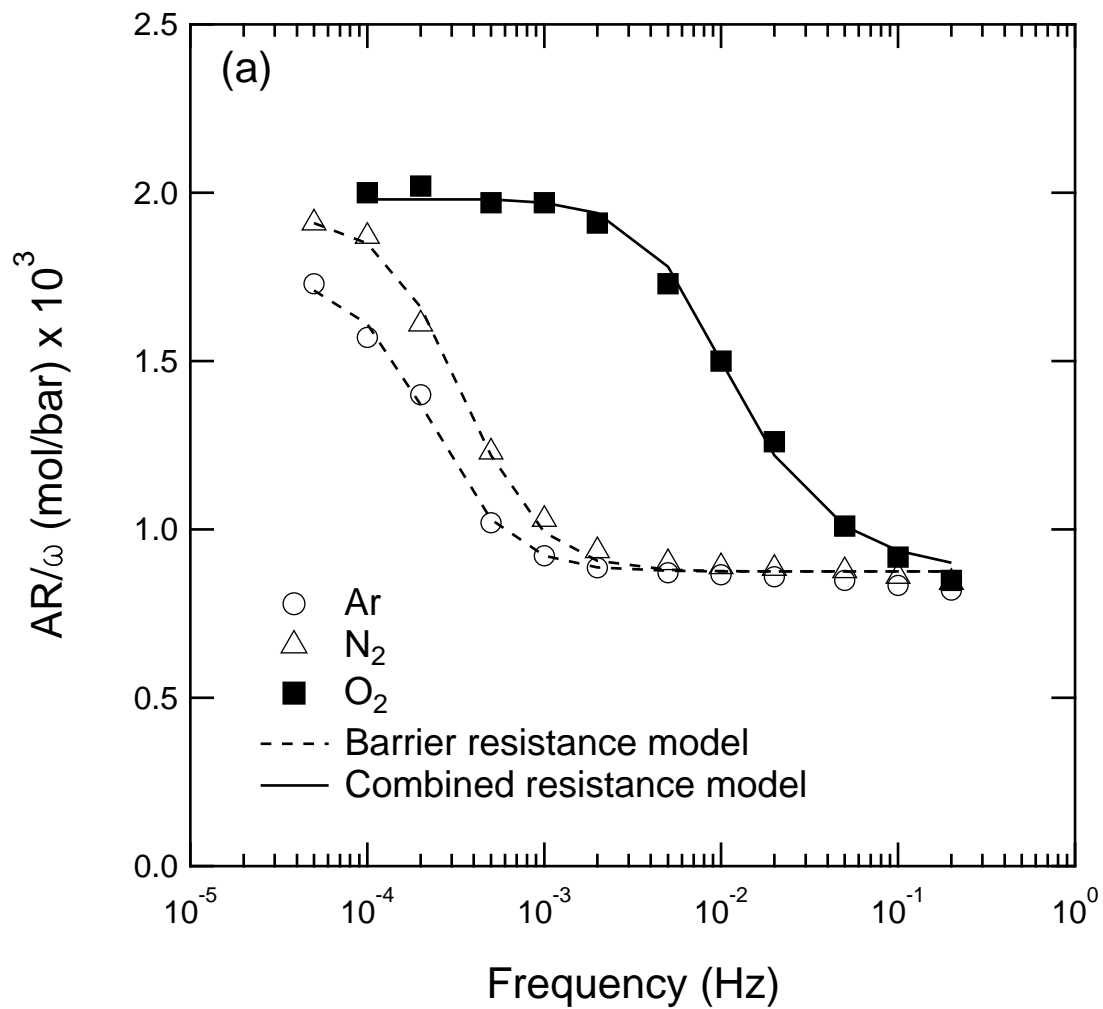
Figure 3.3 Amplitude ratio curves and corresponding best model descriptions compared for each gas at 0.5 bar. a) Type 162; b) Type 172.
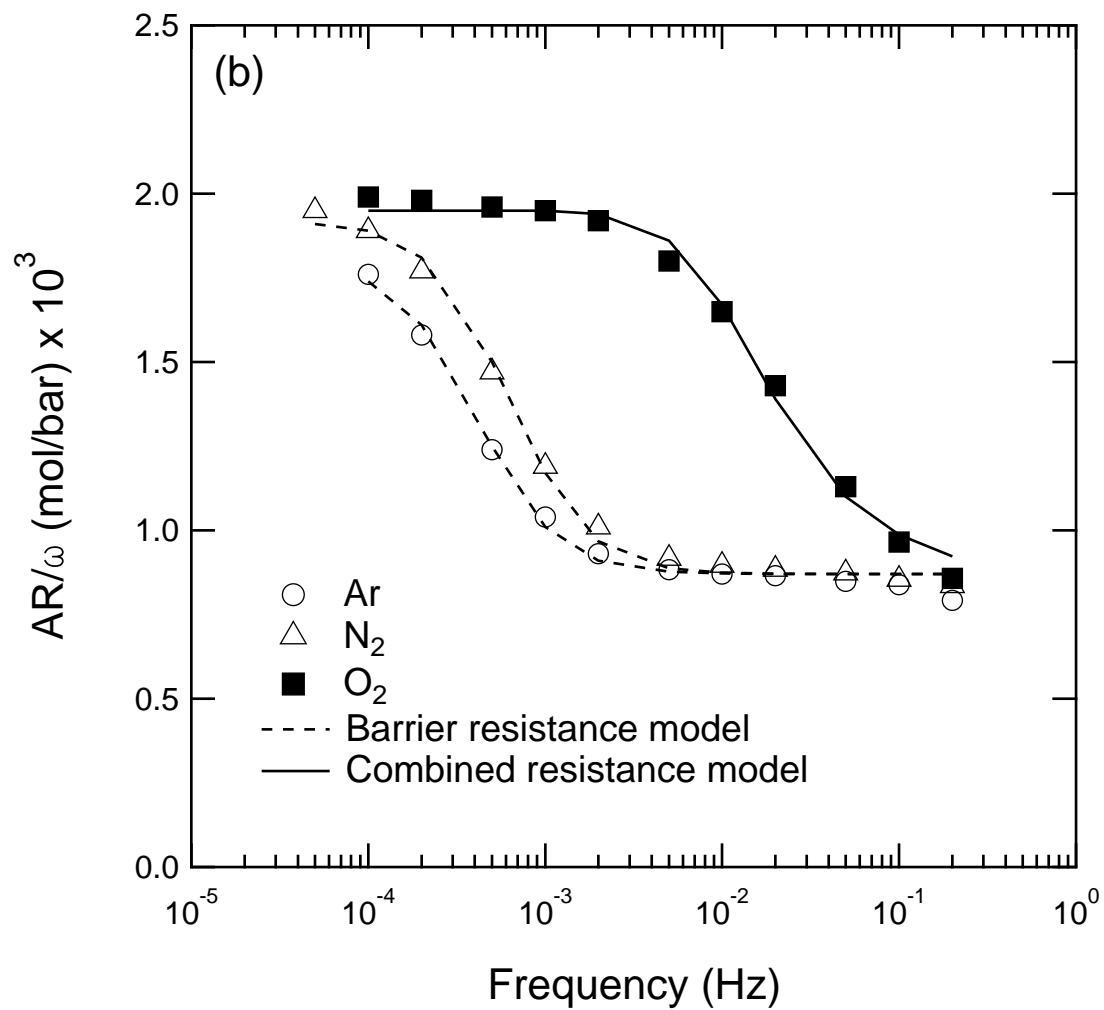
faster than transport of both Ar and N_2, with Ar being the slowest of the three. This observation is represented graphically by the fact that the predominant change in the amplitude ratio curve for O_2 occurs at higher frequencies than that of the other curves. The differences in transport rates result in a high kinetic selectivity for O_2 in each material. On average, over the investigated pressure range, for type 162 we found $k'_{O2}/k_{Ar} = 45$ and $k'_{O2}/k_{N2} = 25$, and for type 172 $k'_{O2}/k_{Ar} = 32$ and $k'_{O2}/k_{N2} = 23$, where $k' \equiv k_b/r_s$ with k_b given by Eq. 3.11, the boundary condition for the combined resistance model, and k is the LDF coefficient in Eq. 3.3.

Figure 3.4 shows phase angle plots for N_2 at four different pressures on type 172. The experimental data are compared with phase angle curves generated using the barrier coefficient and isotherm slope values extracted from the corresponding amplitude ratio data. There is reasonable agreement between the phase angle and amplitude ratio data, which supports the characterization of these systems based on amplitude ratio. It can be noted that the accuracy of phase angle measurements is lowest at the extreme values of perturbation frequency.

Though the LDF model has been traditionally used as an approximation to a more complex micropore diffusion model (Sircar and Hufton, 2000), for this system the LDF model is used as an exact representation of a different transport model. CMS manufacture often involves carbon deposition at the mouths of pores in a non-selective carbon material in order to impart kinetic selectivity (Cabrera et al., 1993; Freitas and Figueiredo, 2001). This deposition process has been confirmed by Paredes et al. (2003) and Villar-Rodil et al. (2005) using scanning tunneling microscopy. LDF-type rate behavior indicates that these carbon deposits are confined to the outermost region of a CMS particle, forming what is referred to as a surface barrier resistance (Srinivasan et al., 1995). Transport through the surface barrier in CMS is associated with two main mechanistic interpretations in the literature, both of which can be described using the LDF rate equation. The first interpretation of the barrier mecha-
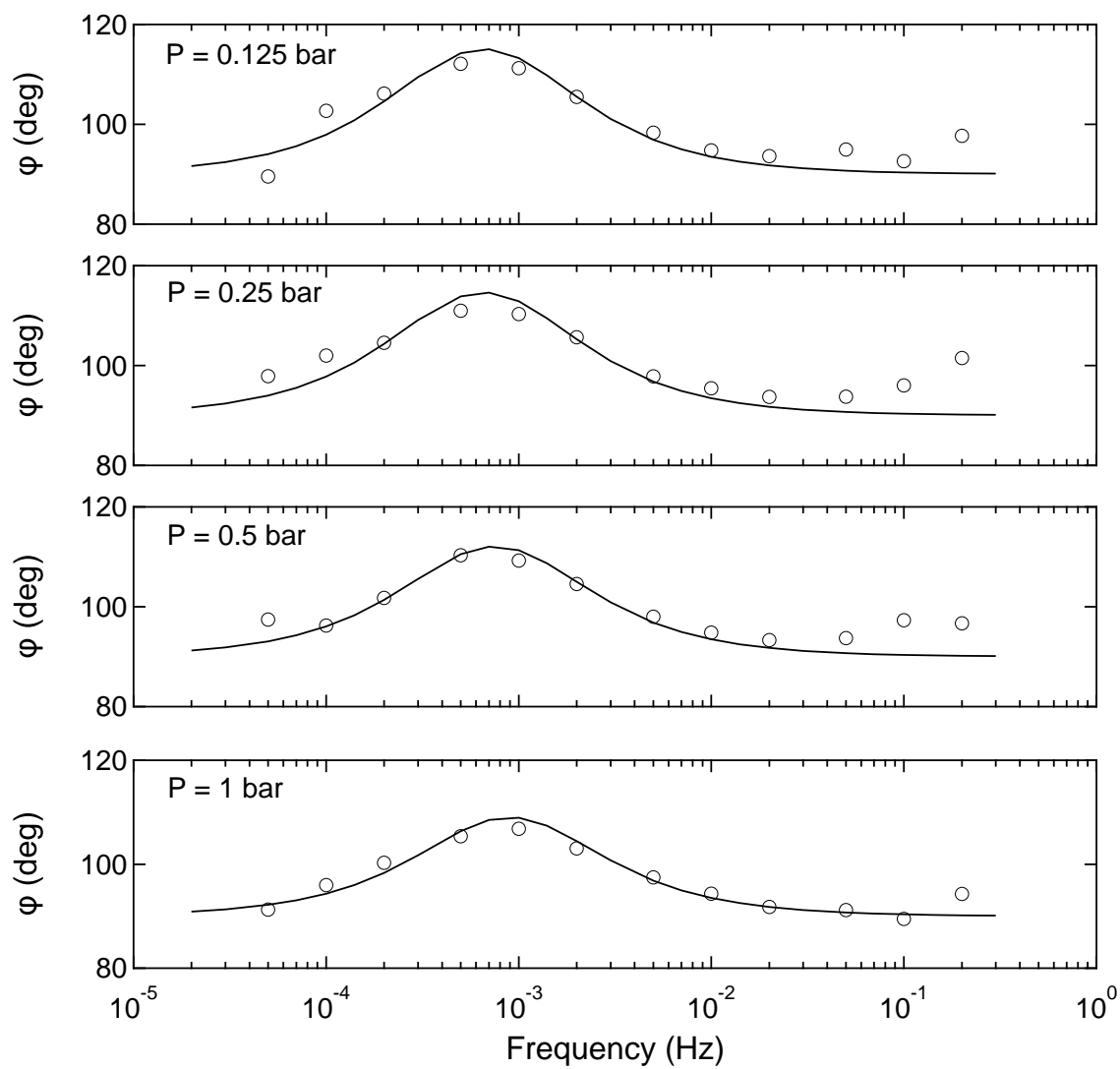
Figure 3.4 Phase angle plots for N_2 on Shirasagi MSC-3R type 172.

51

nism in CMS visualizes mass exchange between the gas phase and the adsorbed phase to occur by a kinetic process at the particle surface (Dominguez et al., 1988; Fitch et al., 1994; LaCava et al., 1989; Liu and Ruthven, 1996). This kinetic process is commonly treated using a Langmuir-type kinetic expression. The second interpretation visualizes the barrier as a thin shell at the outermost part of a CMS particle in which micropore diffusivities are drastically reduced compared with micropore diffusivities in the core of the particle (Srinivasan et al., 1995). If adsorption rates are assumed to obey Langmuir kinetics, it can be shown (Do and Wang, 1998; Liu and Ruthven, 1996; Qinglin et al., 2003, 2004) that the LDF model will exactly represent the dynamic response of the system for a differential step, but that the LDF coefficient will depend on pressure as given by

$$k = k_0(1 + bP) \tag{3.15}$$

where k_0 is the barrier coefficient in the Henry's law region. An equivalent expression was derived by Srinivasan et al. (1995) for the shell diffusion model, assuming that the diffusivity in the shell depends on adsorbate loading according to the Darken relation and that adsorption equilibrium follows the Langmuir isotherm. The dependence of barrier coefficient on pressure given by Eq. 3.15 was observed by Liu and Ruthven (1996) and Shen et al. (2003) at pressures below 100 torr. An empirical modification was given by Huang et al. (2003) to explain an observed pressure dependence of the barrier coefficient that was stronger than that predicted by Eq. 3.15; expressed as

$$k_0 = k_0^* \left(1 + \beta_b \frac{\theta}{1 - \theta}\right) \tag{3.16}$$

this modification was postulated on the grounds that each pore size likely has a distinctive value of k_0 and that pores fill in the order of increasing size.

The predicted trends in barrier coefficient given by Eqs. 3.15 and 3.16 are

compared in Figure 3.5 with the barrier coefficient values across all pressures for each gas on both materials. As is evident from the graph, there is indeed a slight increase in the barrier coefficient with increasing pressure for each adsorbent/gas pair. As was similarly observed by Huang et al. (2003, 2004), the observed pressure dependence is stronger than that predicted by Eq. 3.15 alone, but inclusion of the empirical correction described in Eq. 3.16 allows Eq. 3.15 to describe the experimental data well.

The Langmuir b parameter values used to plot Eq. 3.15 in Figure 3.5 were found using isotherm slope values from the transport model descriptions of the amplitude ratio data. Thus, in fitting the barrier coefficient data to Eq. 3.15, the only fitting parameter is k_0. Making the Langmuir b an additional fitting parameter, however, allows Eq. 3.15 to adequately capture the pressure dependence of the barrier coeffcient, as demonstrated by Figure 3.6. Using b as a fitting parameter to better describe pressure dependence of barrier coefficients necessarily results in a disparity between b values determined from barrier coefficients and those determined from isotherm slope data. This disparity can be justified by assuming that the shell diffusion model is an accurate portrayal of the transport phenomena in these systems. If this is the case, b in Eq. 3.15 corresponds with the Langmuir isotherm description of adsorption equilibrium only in the thin shell at the outer region of a CMS particle. It is well-established that pore size has a significant effect on adsorption isotherms; this effect is even the basis for the determination of micropore size distribution in porosimetry (Rouquerol et al., 1999). Due to the deposition of carbon in the thin shell during CMS manufacture and the associated change in pore size, it is reasonable to expect equilibrium characteristics of this thin shell to differ from those in the core of the particle. Since the core of a particle will contain the majority of the adsorbate at equilibrium, isotherm slope data will be heavily influenced by the character of the core material and not the thin shell. The difference in adsorption isotherms in the
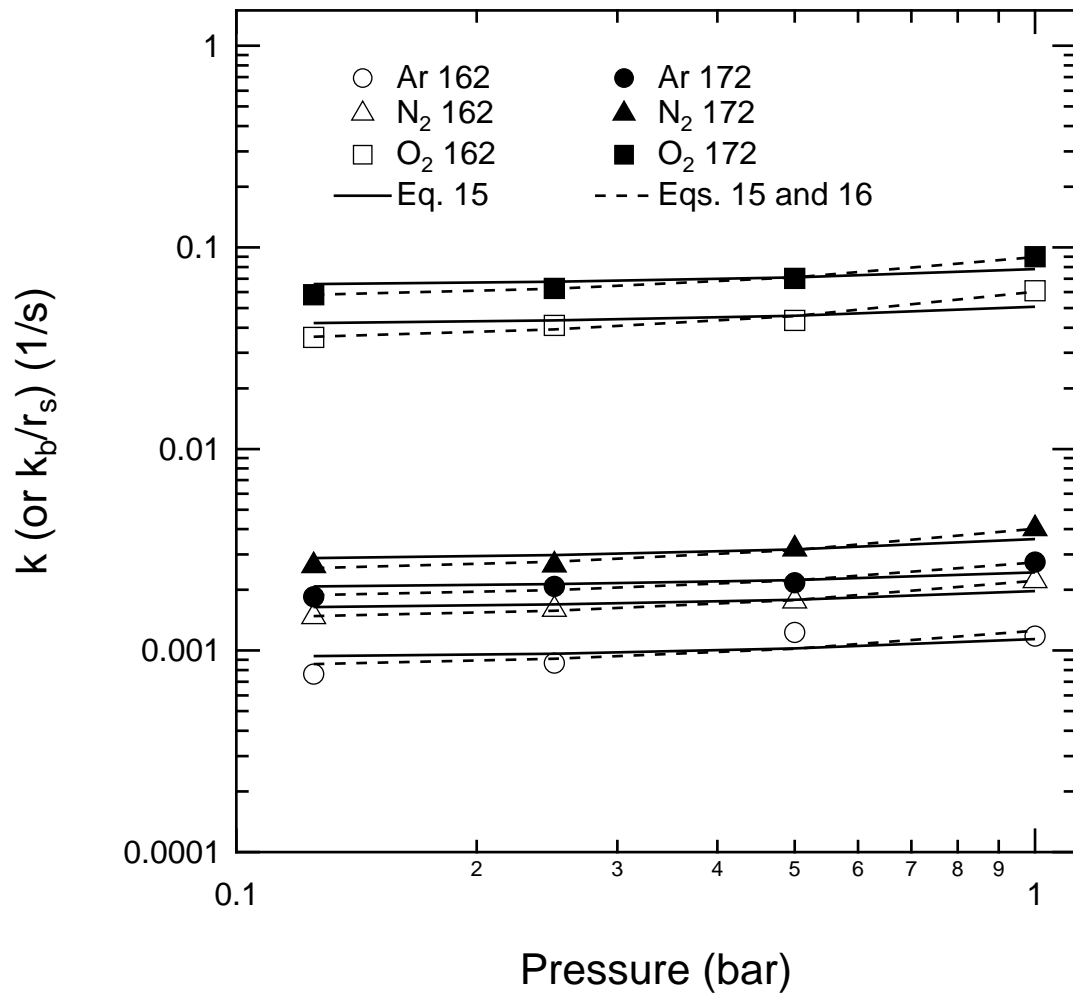
Figure 3.5 Pressure dependence of barrier coefficients. Solid lines correspond with the trend in Eq. 3.15, while dotted lines also include the empirical correction in Eq. 3.16.
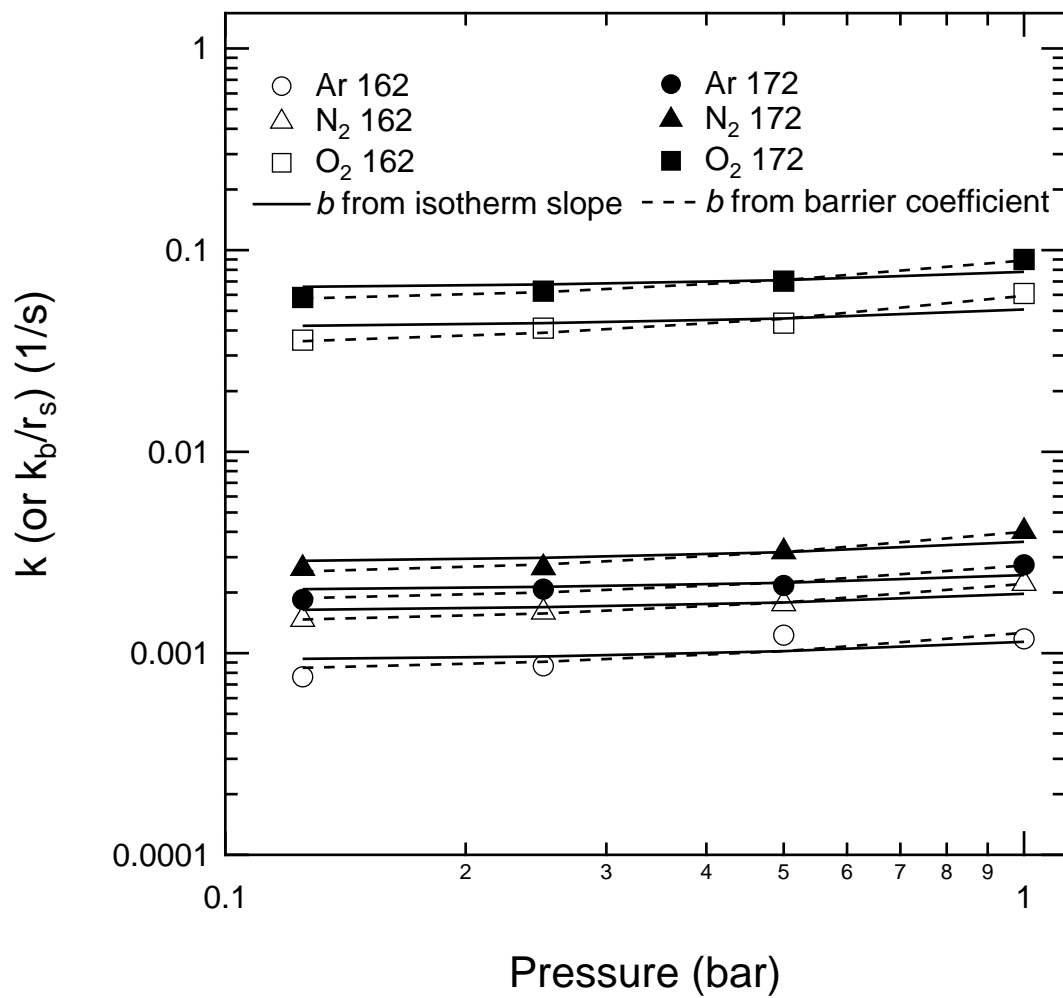
Figure 3.6 Pressure dependence of barrier coefficients. All lines correspond with the trend in Eq. 3.15. For solid lines, b is constrained by isotherm slope data, while for dotted lines, b is used as a fitting parameter for barrier coefficients.

shell and core of a particle is illustrated in Figure 3.7, which compares theoretical Langmuir isotherms for Ar on type 162 using two different b values, one determined from isotherm slope values and one determined by fitting barrier coefficients.

The Langmuir kinetics model is not as accomodating to the existence of two different values of the Langmuir b. Liu and Ruthven (1996) gave the Langmuir kinetics expression for adsorption rates in CMS as

$$\frac{d\bar{q}}{dt} = \frac{3}{R} \left[kc(1 - \theta) - k^{\dagger}\theta \right] \tag{3.17}$$

The authors noted that as $t \to \infty$, this expression reduces to a Langmuir isotherm with $b = k/k^{\dagger}$. However, if the b used to describe barrier coefficients is allowed to differ from the b used to describe adsorption equilibrium, this advantage of the Langmuir kinetics interpretation of the barrier resistance is negated; as $t \to \infty$ the expression reduces to an isotherm that incorrectly describes adsorption equilibrium.

The dependence of the barrier coefficient on pressure can be described well according to either of two depictions of the CMS barrier. However, the shell diffusion model with loading-dependent diffusivity offers a reasonable interpretation of the transport phenomena in this system without the introduction of an empirical correction to describe the pressure dependence of the barrier coefficient. Both methods require two fitting parameters, but for the shell diffusion model, the fitting parameters each have a simple physical interpretation. The difference in b values calculated from rate and equilibrium data can be explained by the change in equilibrium characteristics of a carbon material upon deposition of carbon in the shell during CMS manufacture.
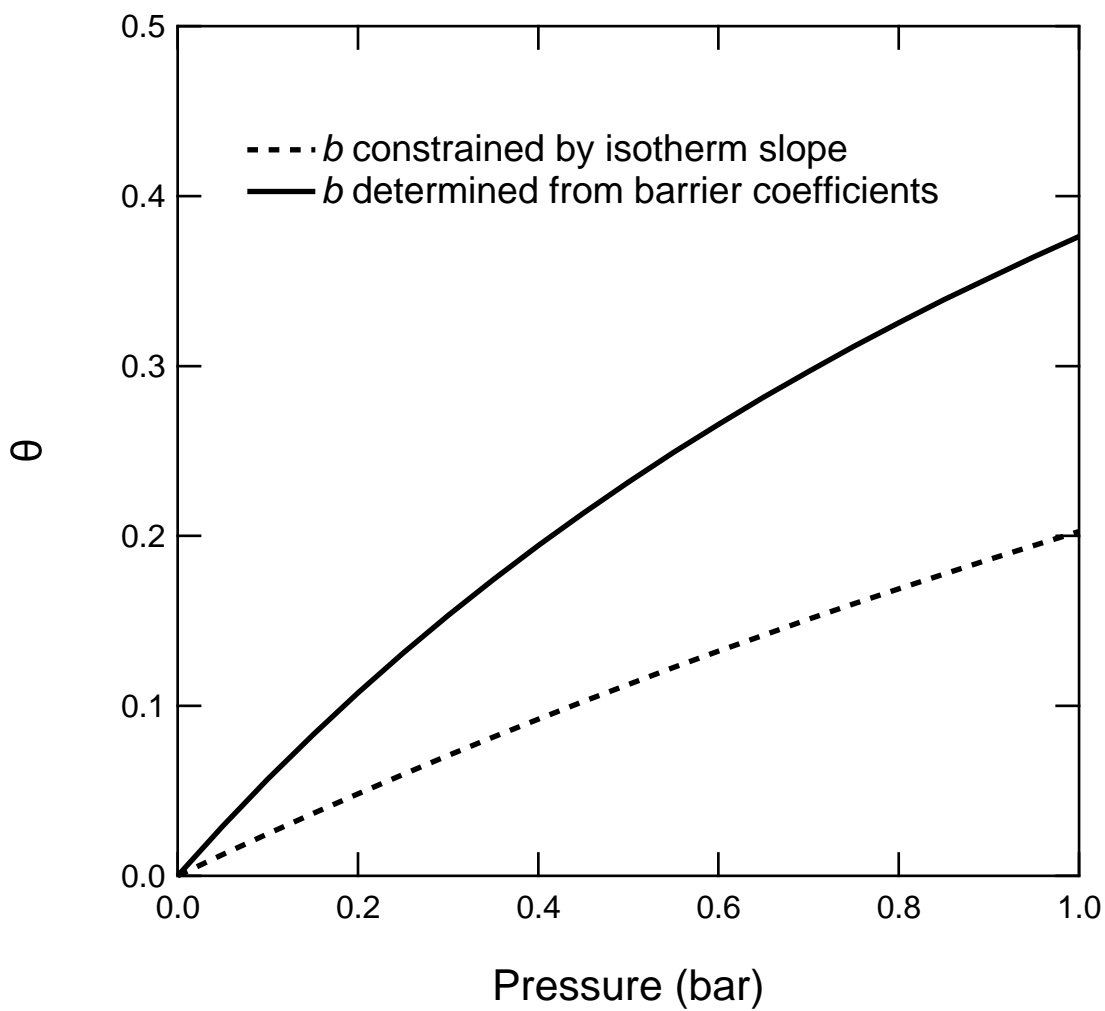
Figure 3.7 Comparison of Langmuir isotherms generated using two different b values found from isotherm slope ($b = 0.254$ bar^{-1}) and barrier coefficient ($b = 0.603$ bar^{-1}) data for Ar on type 162.

3.5 Conclusions

Adsorption rates of O_2, N_2 and Ar have been studied on two carbon molecular sieves. In both materials, O_2 adsorbs the fastest, and Ar adsorbs the slowest. The kinetic selectivity for O_2 in both materials is high. The adsorption rates of N_2 and Ar obey the LDF rate model, indicating that a barrier resistance is limiting. The rate of O_2 adsorption is governed by a barrier resistance in series with a micropore diffusion resistance, with the contribution of micropore diffusion to the adsorption dynamics of O_2 being only slight. The barrier resistance coefficients for each gas increase slightly with pressure. The observed pressure dependence of the barrier coefficient can be interpreted according to the single trend predicted by both the Langmuir kinetics and shell diffusion models, but if the Langmuir b is constrained to the value which best describes adsorption equilibrium, an empirical correction allowing for different values of k_0 for each pore size must be used. If b is not constrained, transport in this system can be simply interpreted according to the shell diffusion model where b in the particle shell differs from b in the core due to the deposition of carbon in the shell.

Notation

A_F = amplitude of mass flow oscillation, mol/s

A_P = amplitude of pressure oscillation in system with adsorbent, bar

b = Langmuir isotherm parameter, 1/bar

D_s = micropore diffusivity, m^2/s

D_{s0} = corrected micropore diffusivity, m^2/s

G_n = adsorbed-phase transfer function

k = barrier (LDF) transport coefficient, 1/s

k_b = barrier transport coefficient in combined resistance model, m/s

k_0 = limiting barrier transport coefficient, 1/s

k_0^* = empirical parameter for correlation of barrier transport coefficients, 1/s

K = local isotherm slope, m^3/kg

M_s = mass of adsorbent, kg

n = adsorbed-phase concentration, mol/kg

n^* = fictional adsorbed-phase concentration, mol/kg

$\hat{n}$ = average adsorbate concentration including gas in macropores, mol/kg

P = pressure, bar

r = distance along microparticle radius, m

r_s = microparticle radius, m

T = temperature, K

V = volume of pressure-controlled region, m^3

x = dimensionless microparticle radial coordinate

Greek Letters

β_b = dimensionless parameter for correlation of barrier transport coefficients

β_{bm} = dimensionless transport parameter, $k_b r_s / D_s$

ϵ_p = macropore porosity

η = dimensionless diffusion parameter, D_s / r_s^2

θ = fractional surface coverage

ρ_p = density of adsorbent particle, kg/m^3

ϕ = phase angle, deg

ω = angular frequency of oscillation, rad/s

Superscripts

$^-$ = Laplace domain

References

Bae, Y.-S., Lee, C.-H., 2005. Sorption kinetics of eight gases on a carbon molecular sieve at elevated pressure. Carbon 43, 95-107.

Braymer, T.A., Coe, C.G., Farris, T.S., Gaffney, T.R., Schork, J.M., Armor, J.N., 1994. Granular carbon molecular sieves. Carbon 32, 445-452.

Cabrera, A.L., Zehner, J.E., Coe, C.G., Gaffney, T.R., Farris, T.S., Armor, J.N., 1993. Preparation of carbon molecular sieves, I. Two-step hydrocarbon deposition with a single hydrocarbon. Carbon 31, 969-976.

Chagger, H.K., Ndaji, F.E., Sykes, M.L., Thomas, K.M., 1995. Kinetics of adsorption and diffusional characteristics of carbon molecular sieves. Carbon 33, 1405-1411.

Chen, Y.D., Yang, R.T., 1994. Preparation of carbon molecular sieve membrane and diffusion of binary mixtures in the membrane. Ind. Eng. Chem. Res. 33, 3146-3153.

Chen, Y.D., Yang, R.T., Uawithya, P., 1994. Diffusion of oxygen, nitrogen and their mixtures in carbon molecular sieve. AIChE J. 40, 577-585.

Chihara, K., Suzuki, M., Kawazoe, K., 1978. Adsorption rate on molecular sieving carbon by chromatography. AIChE J. 24, 237-246.

Do, D.D., 1998. Adsorption analysis: Equilibria and kinetics. Imperial College Press, London.

Do, D.D., Wang, K., 1998. Dual diffusion and finite mass exchange model for adsorption kinetics in activated carbon. AIChE J. 44, 68-82.

Dominguez, J.A., Psaris, D., LaCava, A.I., 1988. Langmuir kinetics as an accurate simulation of the rate of adsorption of oxygen and nitrogen mixtures on non-Fickian carbon molecular sieves. AIChE Symp. Ser. 84, 73-82.

Fitch, F.R., Bülow, M., LaCava, A.I., 1994. Investigation of the mechanism for the separation of nitrogen-oxygen mixtures on carbon molecular sieves. Gas Sep. Purif. 8, 45-51.

Freitas, M.M.A., Figueiredo, J.L., 2001. Preparation of carbon molecular sieves for gas separations by modification of the pore sizes of activated carbons. Fuel 80, 1-6.

Giesy, T.J., Wang, Y., LeVan, M.D., 2012. Measurement of mass transfer rates in adsorbents: New combined-technique frequency response apparatus and application to CO_2 in 13X zeolite. Ind. Eng. Chem. Res. 51, 11509-11517.

Grzegorczyk, D.S., Carta, G., 1997. Frequency response of liquid-phase adsorption on polymeric adsorbents. Chem. Eng. Sci. 52, 1589-1608.

Hayashi, S., Kawai, M., Kaneko, T., 1996. Dynamics of high purity oxygen PSA. Gas Sep. Purif. 10, 19-23.

Hsu, T.-B., Pigford, R.L., 1991. Mass transfer in a thermally regenerable ion-exchange resin by continuous cycling. Ind. Eng. Chem. Res. 30, 1067-1075.

Jee, J.-G., Kim, M.-B., Lee, C.-H., 2005a. Pressure swing adsorption processes to purify oxygen using a carbon molecular sieve. Chem. Eng. Sci. 60, 869-882.

Jee, J.-G., Lee, S.-J., Kim, M.-B., Lee, C.-H., 2005b. Three-bed PVSA process for high-purity O_2 generation from ambient air. AIChE J. 51, 2988-2999.

Jin, X., Malek, A., Farooq, S., 2006. Production of argon from an oxygen-argon mixture by pressure swing adsorption. Ind. Eng. Chem. Res. 45, 5775-5787.

Kärger J., Caro, J., 1977. Interpretation and correlation of zeolitic diffusivities obtained from nuclear magnetic resonance and sorption experiments. J. Chem. Soc., Faraday Trans. I. 73, 1363-1376.

Kawazoe, K., Suzuki, M., Chihara, K., 1974. Chromatographic study of diffusion in molecular sieve carbon. J. Chem. Eng. Japan 7, 151-157.

Koresh, J., Soffer, A., 1980. Study of molecular sieve carbons. Part 1. Pore structure, gradual pore opening and mechanism of molecular sieving. J. Chem. Soc., Faraday Trans. I 76, 2457-2471.

Koresh, J., Soffer, A., 1981. Molecular sieve carbons. Part 3. Adsorption kinetics according to a surface-barrier model. J. Chem. Soc., Faraday Trans. I. 77, 3005-3018.

LaCava, A.I., Koss, V.A., Wickens, D., 1989. Non-Fickian adsorption rate behaviour of some carbon molecular sieves. Gas Sep. Purif. 3, 180-186.

Liu, H., Ruthven, D.M., 1996. Diffusion in carbon molecular sieves, in: LeVan, M.D. (Ed.), Proceedings of the 5th International Conference on the Fundamentals of Adsorption. Kluwer Academic Publishers, Norwell, pp. 529-536.

Loughlin, K F., Hassan, M.M., Fatehi, A.I., Zahur, M., 1993. Rate and equilibrium sorption parameters for nitrogen and methane on carbon molecular sieve. Gas Sep. Purif. 7, 264-273.

Nguyen, C., Do, D.D., 2000. Dual Langmuir kinetic model for adsorption in carbon molecular sieve materials. Langmuir 16, 1868-1873.

Paredes, J.I., Villar-Rodil, S., Martínez-Alonso, A., Tascón, J.M.D., 2003. A scanning tunnelling microscopy insight into the preparation of carbon molecular sieves by chemical vapour deposition. J. Mater. Chem. 13, 1513-1516.

Qinglin, H., Farooq, S., Karimi, I.A., 2004. Prediction of binary gas diffusion in carbon molecular sieves at high pressure. AIChE J. 50, 351-367.

Qinglin, H., Sundaram, S.M., Farooq, S., 2003. Revisiting transport of gases in the micropores of carbon molecular sieves. Langmuir 19, 393-405.

Rege, S.U., Yang, R.T., 2000. Kinetic separation of oxygen and argon using molecular sieve carbon. Adsorption 6, 15-22.

Reid, C.R., O'koye, I.P., Thomas, K.M., 1998. Adsorption of gases on carbon molecular sieves used for air separation. Spherical adsorptives as probes for kinetic selectivity. Langmuir 14, 2415-2425.

Reyes, S.C., Iglesia, E., 1994. Frequency response techniques for the characterization of porous catalytic solids. Catalysis 11, 51-92.

Rouquerol, F., Rouquerol, J., Sing, K., 1999. Adsorption by powders and porous solids: Principles, methodology and applications. Academic Press, San Diego.

Ruthven, D.M., 1992. Diffusion of oxygen and nitrogen in carbon molecular sieve. Chem. Eng. Sci. 47, 4305-4308.

Ruthven, D.M., Raghavan, N.S., Hassan, M.M., 1986. Adsorption and diffusion of nitrogen and oxygen in a carbon molecular sieve. Chem. Eng. Sci. 41, 1325-1332.

Rynders, R.M., Rao, M.B., Sircar, S., 1997. Isotope exchange technique for measurement of gas adsorption equilibria and kinetics. AIChE J. 43, 2456-2470.

Seaton, N.A., Friedman, S.P., MacElroy, J.M.D., Murphy, B.J., 1997. The molecular sieving mechanism in carbon molecular sieves: A molecular dynamics and critical path analysis. Langmuir 13, 1199-1204.

Shen, D., Bülow, M., Lemcoff, N.O., 2003. Mechanisms of molecular mobility of oxygen and nitrogen in carbon molecular sieves. Adsorption 9, 295-302.

Sircar, S., Hufton, J.R., 2000. Why does the linear driving force model for adsorption kinetics work? Adsorption 6, 137-147.

Srinivasan, R., Auvil, S.R., Schork, J.M., 1995. Mass transfer in carbon molecular sieves - an interpretation of Langmuir kinetics. Chem. Eng. J. 57, 137-144.

Sun, L.M., Meunier, F., Grenier, Ph., Ruthven, D.M., 1994. Frequency response for nonisothermal adsorption in biporous pellets. Chem. Eng. Sci. 49, 373-381.

Sun, L.M., Meunier, F., Kärger, J., 1993. On the heat effect in measurements of sorption kinetics by the frequency response method. Chem. Eng. Sci. 48, 715-722.

Sward, B.K., LeVan, M.D., 2003. Frequency response method for measuring mass transfer rates in adsorbents via pressure perturbation. Adsorption 9, 37-54.

Verma, S.K., Walker, P.L., 1992. Preparation of carbon molecular sieves by propylene pyrolysis over microporous carbons. Carbon 30, 829-836.

Villar-Rodil, S., Navarrete, R., Denoyel, R., Albiniak, A., Paredes, J.I., Martínez-Alonso, A., Tascón, J.M.D., 2005. Carbon molecular sieve cloths prepared by chemical vapour deposition of methane for separation of gas mixtures. Micropor. Mesopor. Mat. 77, 109-118.

Wang, Y., LeVan, M.D., 2005. Investigation of mixture diffusion in nanoporous adsorbents via the pressure-swing frequency response method. 2. Oxygen and nitrogen in a carbon molecular sieve. Ind. Eng. Chem. Res. 44, 4745-4752.

Wang, Y., LeVan, M.D., 2011. Master curves for mass transfer in bidisperse adsorbents for pressure-swing and volume-swing frequency response methods. AIChE

J. 57, 2054-2069.

Wang, Y., Sward, B.K., LeVan, M.D., 2003. New frequency response method for measuring adsorption rates via pressure modulation: application to oxygen and nitrogen in a carbon molecular sieve. Ind. Eng. Chem. Res. 42, 4213-4222.

Yang, R.T., 1997. Gas separation by adsorption processes. Imperial College Press, London.

CHAPTER IV

MASS TRANSFER OF BINARY MIXTURES OF OXYGEN AND ARGON IN A

CARBON MOLECULAR SIEVE

4.1 Introduction

Carbon molecular sieve (CMS) materials have received attention as potential adsorbents for the production of high-purity (>99%) O_2 from air by PSA.[1–14] In traditional zeolite-based PSA processes, the O_2 product is often limited to 94-95% purity, as the similar adsorption behavior of O_2 and Ar on many zeolites results in a substantial Ar impurity in the product.[1,2] In CMS, however, O_2 adsorbs much more rapidly than Ar, allowing separation of these two gases to be effected by the difference in their adsorption rates.

In order to rigorously design a PSA process utilizing CMS or any other adsorbent, accurate knowledge of the adsorption rate behavior of the relevant adsorbent/gas system is desirable. Adsorption rates are generally limited by mass transfer, which can occur by one or more of a variety of possible mechanisms including micropore diffusion, macropore diffusion (ordinary diffusion, Knudsen diffusion, or Poiseuille flow), transport across a surface barrier, and external mass transfer. The existence of cross-coefficients introduced by multicomponent transport models can further complicate adsorption rate behavior. As a result, adsorption rates are an important and nontrivial subject worthy of thorough investigation.

As CMS has long been recognized for its ability to produce purified N_2 from air, many of the studies of adsorption rates of atmospheric gases on CMS have been focused on O_2 and N_2.[15–28] However, with the exception of a few studies,[24,25,29] adsorption rates of Ar have been largely ignored. Moreover, though adsorption rates of pure gases are generally presumed to differ from those of gases in multicomponent

67

mixtures, studies of adsorption rates in such mixtures have been infrequent.[26] We thus conclude that there remains a need for further study, especially regarding adsorption rates of mixtures of O_2 and Ar.

In a recent work,[30] we studied pure component adsorption rates of O_2, N_2, and Ar on two varieties of CMS. In the present work, we study adsorption rates of binary O_2/Ar mixtures on one of the CMS varieties from the first study with the view that transport behavior of each gas in the mixture could differ compared with the behavior of the pure gas. To allow for the best possible characterization of this system, we employ the concentration-swing frequency response (CSFR) technique,[31–35] which, like other FR techniques,[28,36,37] has the ability to distinguish between different mass transfer mechanisms. CSFR is intended to study transport in mixtures, and we have used it previously to measure main-term and cross-term transport coefficients in CO_2/CH_4 binary mixtures on CMS.[33]

This study will provide insight into the transport behavior of O_2 and Ar in CMS, which will be useful for the rigorous design of PSA air separation processes, especially those designed to produce high-purity O_2. Furthermore, the CMS surface barrier has seen multiple physical interpretations in the literature,[19,21,22,27] and as a result, the behavior of binary mixtures in CMS systems governed by a surface barrier resistance remains a matter of speculation. This study will aid in the characterization of transport of gas mixtures in CMS systems governed by a surface barrier resistance, and in so doing, will help lead to a proper physical interpretation of the CMS surface barrier. A proper physical interpretation of the CMS surface barrier and the knowledge of the transport of gas mixtures in such barriers will further enhance the ability to rigorously design PSA processes utilizing CMS.

4.2 Theory

The FR apparatus used in this work, the relevant components of which are shown in Fig. 4.1, has been described previously.[38] To perform CSFR experiments, each of the two mass flow controllers at the system inlet fixes a sinusoidally oscillating molar flow rate of a different gas into the system. The oscillations of the mass flow controllers are π out of phase, resulting in a constant total molar flow rate into the system with sinusoidally oscillating composition. This gas mixture flows through the adsorbent to be analyzed, and the mass spectrometer measures the composition of the effluent.

To model the system, an overall material balance is written for the adsorption bed, which assumes the region can be well-represented by a single well-mixed volume. More complicated two-volume models have been given[33,34] but were found to be unnecessary for this work. Noting that the pressure in the system is constant, this material balance is expressed as

$$M_b \frac{dn_{tot}}{dt} = c_0 \left(F_{in} - F_{out} \right) \tag{4.1}$$

where M_b is the adsorbent mass, n_{tot} is the combined loading of both gases, c_0 is the total gas concentration, and F_{in} and F_{out} are the volumetric flow rates in and out of the adsorption region, respectively. As the total loading will respond to the oscillations in inlet gas composition, F_{out} will differ from F_{in}. Rearranging Eq. 4.1 allows this difference to be written as

$$F_{out} = F_{in} - \left[\frac{M_b}{c_0} \frac{dn_{tot}}{dt} \right] \tag{4.2}$$

A material balance can also be written for a single component in the binary
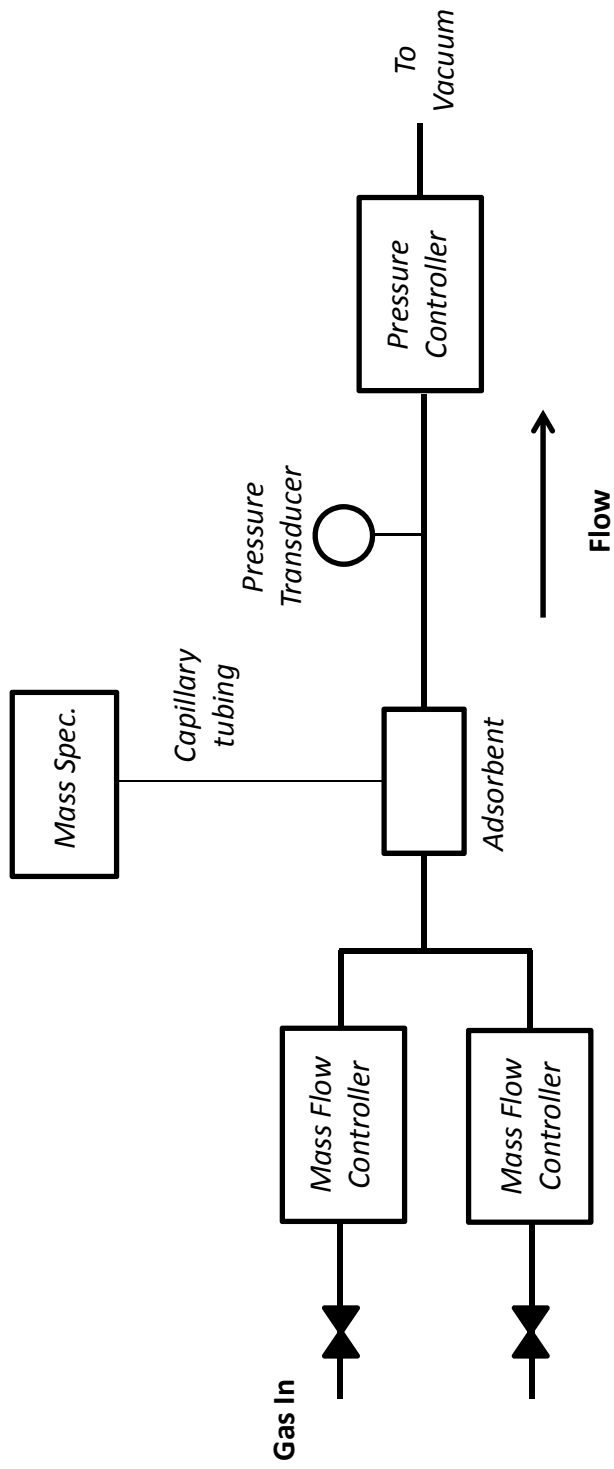
Figure 4.1 A schematic representation of the key components of the CSFR apparatus. The full apparatus allows for multiple frequency response techniques.[38]

gas mixture:

$$\frac{M_b}{c_0}\frac{dn_i}{dt} + V_b\frac{dy_{i,out}}{dt} = F_{in}\,y_{i,in} - F_{out}\,y_{i,out} \tag{4.3}$$

where V_b represents the volume of the adsorption region and the y_i terms represent the gas-phase mole fractions of component i entering and leaving the adsorption region. Substituting in Eq. 4.2 yields

$$\frac{M_b}{V_b c_0}\frac{dn_i}{dt} + \frac{dy_{i,out}}{dt} = \frac{F_{in}}{V_b}\left(y_{i,in} - y_{i,out}\right) + \frac{M_b}{V_b c_0}y_{i,out}\frac{dn_{tot}}{dt} \tag{4.4}$$

Introducing the deviation variables

$$y_i' = y_i - y_{i,0} \tag{4.5}$$

$$n_i' = n_i - n_{i,0} \tag{4.6}$$

and noting that $n_{tot} = n_i + n_j$, where j denotes the component in the binary mixture that is not component i, allows the single-component mass balance to be written as

$$\frac{M_b}{V_b c_0}\frac{dn_i'}{dt} + \frac{dy_{i,out}'}{dt} = \frac{F_{in}}{V_b}\left(y_{i,in}' - y_{i,out}'\right) + \frac{M_b}{V_b c_0}\left(y_{i,out}' + y_{i,0}\right)\frac{d\left(n_i' + n_j'\right)}{dt} \tag{4.7}$$

Perturbations in CSFR experiments are kept small, meaning that $y_{i,out}'$ will be small with respect to $y_{i,0}$. Eq. 4.7 can thus be rewritten as

$$\frac{M_b}{V_b c_0}\frac{dn_i'}{dt} + \frac{dy_{i,out}'}{dt} = \frac{F_{in}}{V_b}\left(y_{i,in}' - y_{i,out}'\right) + \frac{M_b}{V_b c_0}y_{i,0}\frac{d\left(n_i' + n_j'\right)}{dt} \tag{4.8}$$

Converting Eq. 4.8 to the Laplace domain and rearranging yields the overall system transfer function

$$G_{tot} = \frac{\bar{y}_{i,out}}{\bar{y}_{i,in}} = \frac{F_{in}/V_b}{s + F_{in}/V_b + \left[M_b s/\left(V_b c_0\right)\right]\left[(1 - y_{i,0})G_{n,i} + y_{i,0}G_{n,j}\right]} \tag{4.9}$$

In Eq. 4.9, the terms $G_{n,i}$ and $G_{n,j}$ are the adsorbed-phase transfer functions, which contain the whole of the contributions of the gas adsorption rates to the overall system dynamics. Expressions for $G_{n,i}$ can be derived for a variety of mass transfer mechanisms[39, 40] including multicomponent models with cross coefficients.[33] Adsorbed-phase transfer functions are given here only for simple systems with no cross-coefficients. For a surface barrier resistance, the equation takes the form[40]

$$G_{n,i} = \frac{\bar{n}_i}{\bar{y}_{i,out}} = \frac{3K_i'' k_{b,i}/r_s}{s + 3k_{b,i}/r_s} \tag{4.10}$$

where r_s is the microparticle radius, $k_{b,i}$ is the barrier coefficient, and $K_i'' = P\, \partial n_i/\partial P_i$.

For a combined resistance model, treating a barrier resistance in series with a micropore diffusion resistance, the adsorbed-phase transfer function is[40]

$$G_{n,i} = \frac{\bar{n}_i}{\bar{y}_{i,out}} = \frac{3K_i'' \beta_{bm}}{s/\eta} \frac{\sqrt{s/\eta}\coth\left(\sqrt{s/\eta}\right) - 1}{\sqrt{s/\eta}\coth\left(\sqrt{s/\eta}\right) + \beta_{bm} - 1} \tag{4.11}$$

where $\beta_{bm} = k_b r_s/D_s$ and $\eta = D_s/r_s^2$.

Experimental results for CSFR are interpreted in terms of the ratio of the oscillation amplitudes of the outlet and inlet mole fractions. This amplitude ratio is related to the overall transfer function (with $s = j\omega$) as follows:

$$\text{AR} = |G_{tot}\left(j\omega\right)| = \sqrt{\left(\text{Re}\left[G_{tot}\left(j\omega\right)\right]\right)^2 + \left(\text{Im}\left[G_{tot}\left(j\omega\right)\right]\right)^2} \tag{4.12}$$

4.3   Experiments

In this work, CSFR experiments were performed using Shirasagi MSC-3R type 172 CMS with pure He (99.99%), O_2 (99.994%) and Ar (99.999%). A full characterization including a pore size distribution for a similar CMS from the same manufacturer, Shirasagi MSC-3K type 162, has been performed by Campo et al.[41] Micropores were in two primary groupings, a small set centered at about 0.38 nm and a much larger

set centered near 0.63 nm.

At total pressures of 0.5 and 1 bar, the frequency response of this system was measured at molar compositions of 80% He + 20% O_2, 50% He + 50% O_2, 80% Ar + 20% O_2, and 50% Ar + 50% O_2. In each experiment, the system response was measured over the frequency range from 0.0001 Hz to 0.05 Hz. Perturbation amplitudes were kept small ($< 5\%$ of the average mole fraction) to keep the system appropriately linearized.

At each pressure/composition combination, the adsorbent used was 0.13 g of 1.8 mm diameter cylindrical CMS pellets. The experiments at 1 bar were also repeated using 0.12 g of crushed pellets that had been sieved to 30-40 mesh.

All CMS samples were regenerated prior to experimentation by heating under vacuum to 90 °C for 1 h, after which the temperature was increased to 150 °C, where the sample was held for 8 additional hours under vacuum. All experiments were performed at room temperature (23 °C).

4.4 Results and Discussion

In the CSFR experiments using mixtures of He and O_2, He is expected to be nonadsorbing and is not expected to affect the transport of O_2 in the CMS. There are possible exceptions to this rule; the presence of a nonadsorbing gas could still introduce additional transport resistances associated with ordinary diffusion in the gas phase (e.g., film resistance or macropore diffusion resistance), which would not exist in a system with only one gas (i.e., a concentration gradient in a pure gas is a pressure gradient, which results in bulk flow).

In performing CSFR experiments with He and O_2, we wish to establish a basis for comparison of the CSFR data with the pure component data measured using a different frequency response technique in our earlier work.[30] Figure 4.2 shows CSFR
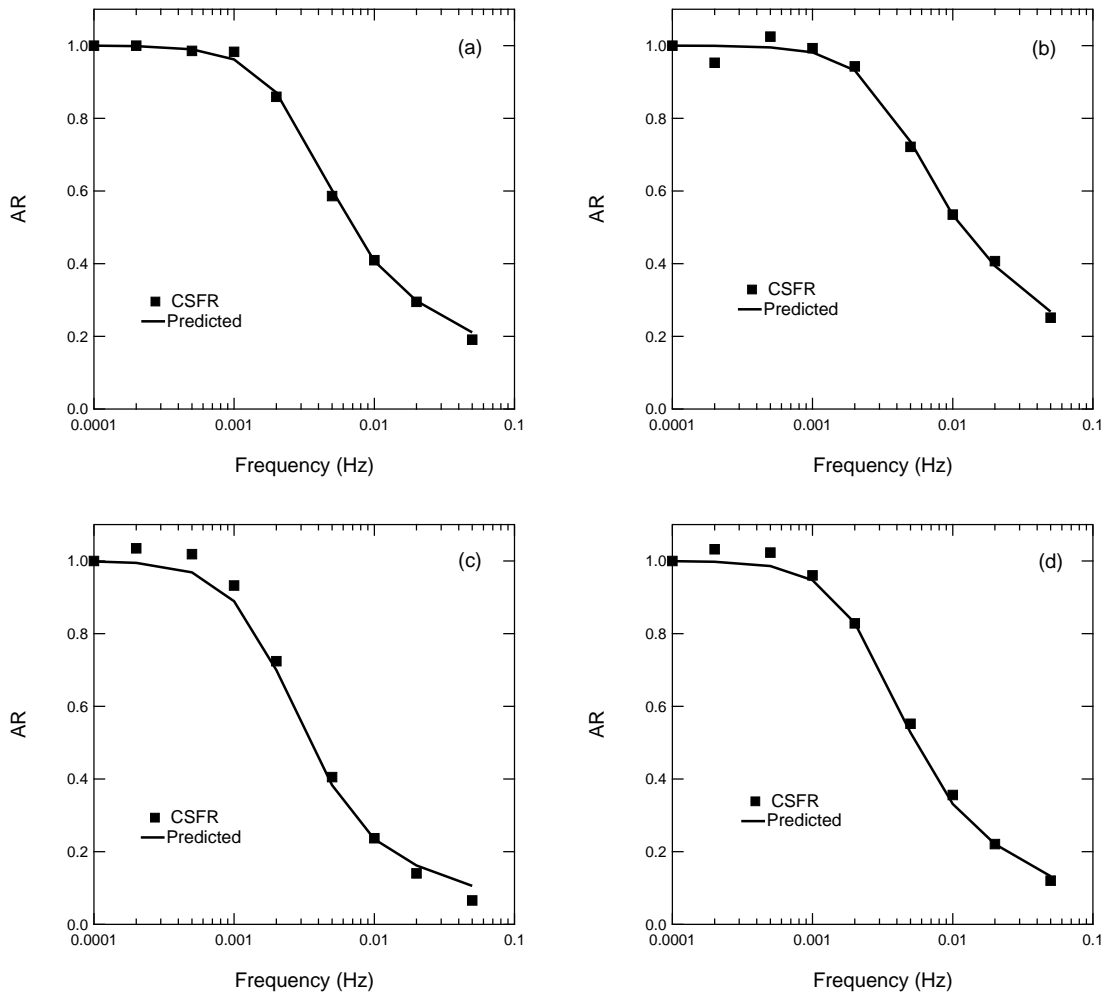
Figure 4.2 CSFR data measured with O_2/He mixtures compared with theoretical CSFR curves using pure component transport models. (a) 20% O_2 + 80% He at 0.5 bar; (b) 50% O_2 + 50% He at 0.5 bar; (c) 20% O_2 + 80% He at 1 bar; (d) 50% O_2 + 50% He at 1 bar.

data at all pressures and compositions compared with theoretical CSFR response curves generated using the O_2 transport model (barrier resistance and micropore diffusion in series) and parameter values from our earlier work[30] that were found to best describe pure O_2 transport in this system. Helium is treated as nonadsorbing, and no other transport resistances are introduced. The transport parameters and models from the pure component experiments agree well with the binary O_2/He data measured using CSFR, which strongly suggests that the two frequency response techniques are comparable and that no additional transport resistances have been introduced; the existence of another transport resistance in the system would alter the system's frequency response, causing the experimental data points in Figure 4.2 to deviate from the solid curves.

This conclusion is strengthened by the plots in Figure 4.3, which compare O_2/He and O_2/Ar CSFR data at 1 bar with data from identical experiments using smaller 30-40 mesh CMS particles ground from the whole pellets. That the response of the two CMS particle sizes are very similar suggests a very weak or nonexistent macropore diffusion effect on the system response. Moreover, analysis of a similar CSFR system[35] found the film resistance to be negligible.

In performing the O_2/Ar mixture experiments, we wish to ascertain how transport of each gas in the CMS is affected by the presence of the other gas. However, in this system there is a large difference in the transport rates of the two gases. As a result, while the adsorbed-phase concentration of O_2 is strongly oscillating in response to the change in gas-phase composition, the adsorbed-phase concentration of Ar is oscillating much more weakly. Thus, the adsorption of O_2 contributes the majority of the character of the CSFR curves in this work, and the data are much more sensitive to the O_2 transport parameters than to those of Ar. This observation is shown graphically in Figure 4.4, which compares a theoretical CSFR curve showing both O_2 and Ar adsorption with one showing only O_2 adsorption. The two curves in this fig-
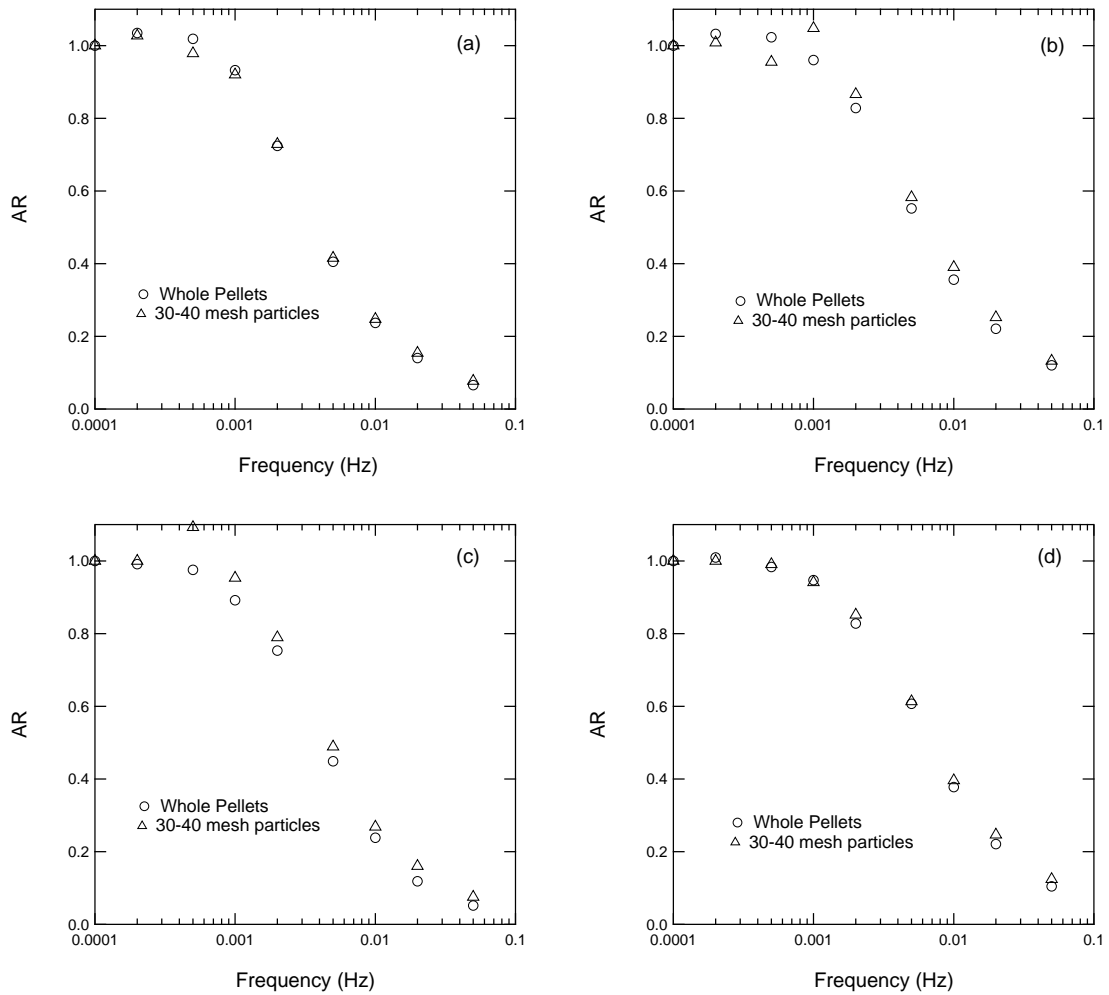
Figure 4.3 Comparison of CSFR experiments at 1 bar using 8-16 mesh pellets and 30-40 mesh particles. (a) 20% O_2 + 80% He; (b) 50% O_2 + 50% He; (c) 20% O_2 + 80% Ar; (d) 50% O_2 + 50% Ar.
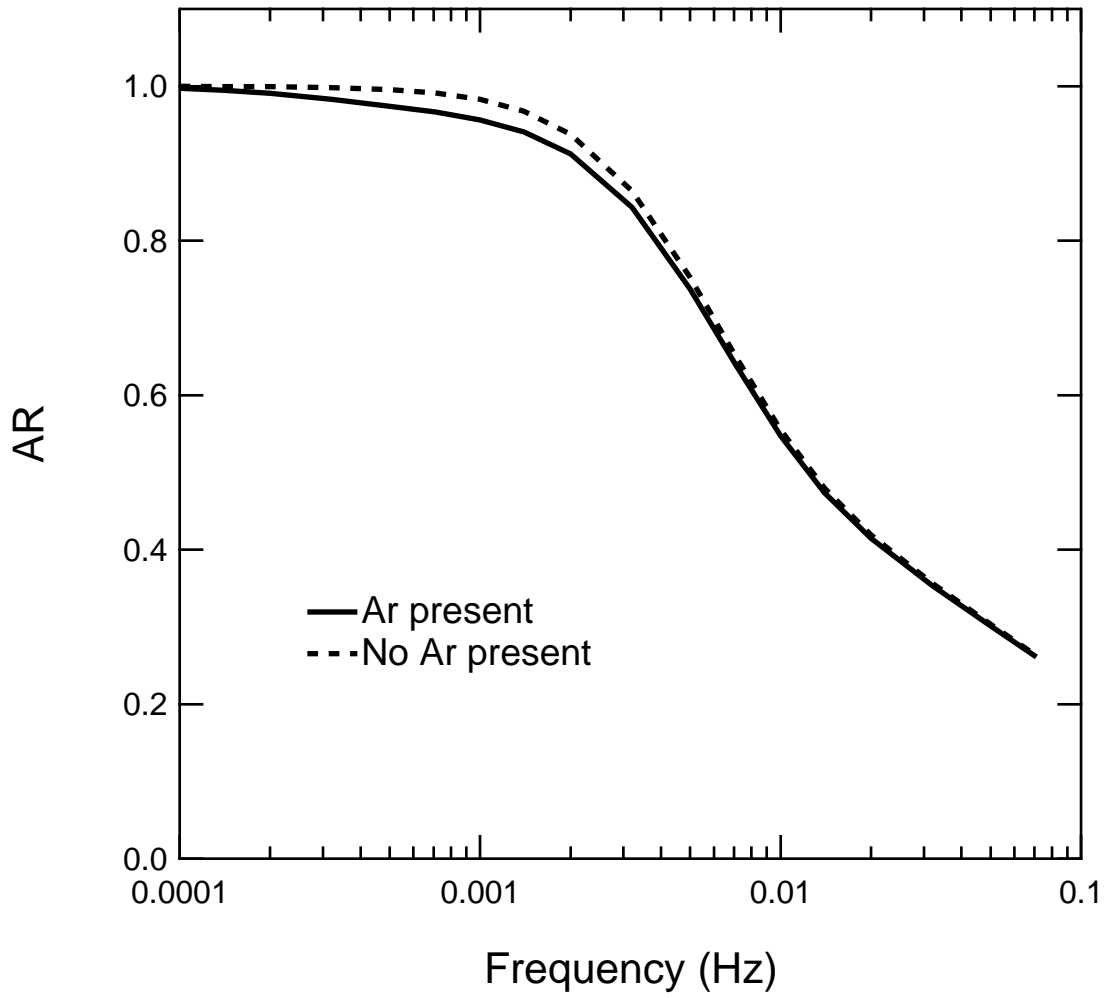
Figure 4.4 Comparison of theoretical CSFR curves showing the effect of Ar adsorption on the system response.

ure are similar, which indicates that the effect of Ar transport on the frequency response of this system is small.

Given the lack of sensitivity of the CSFR data in this system to Ar transport coefficients, our main focus in analysis of the O_2/Ar data is the effect that Ar has on the transport of O_2. Figure 4.5 shows the O_2/Ar response curves at all pressures and compositions compared with three sets of theoretical CSFR curves. The first set of curves represents independent O_2 and Ar transport using the pure component transport coefficients from our earlier work. The mechanisms used to describe O_2 (surface barrier and micropore diffusion in series) and Ar (surface barrier) transport were those determined to describe the pure component data best. Numerical values for these pure component transport parameters are given in our earlier work.[30] The second set of curves is similar to the first, except that the O_2 transport coefficients are increased by a factor of ten. The third set of curves shows the analogous decrease in O_2 transport coefficients by a factor of ten. The curves generated using pure component transport coefficients and those representing faster transport coefficients are each in reasonable agreement with the experimental data, and neither set of curves offers a better description of the experimental data than the other. By contrast, the curves generated using the slower transport coefficients depart significantly from the observed behavior. These plots suggest that Ar does not significantly impede transport of O_2 in this variety of CMS. However, given that the agreement between the experimental data and the theoretical curves is not as consistently close as has been previously observed[33–35] and that increasing the O_2 transport coefficients has only a slight effect on the response curve, these data still allow for the possibility of small transport cross coefficients or an increase in the O_2 main-term transport coefficients caused by the presence of Ar.

In work related to our frequency response experiments, we have also measured isotherms for O_2 and Ar on this variety of CMS materials. Isotherms were measured

Figure 4.5 CSFR data measured with O_2/Ar mixtures compared with theoretical CSFR curves using pure component transport models. (a) 20% O_2 + 80% Ar at 0.5 bar; (b) 50% O_2 + 50% Ar at 0.5 bar; (c) 20% O_2 + 80% Ar at 1 bar; (d) 50% O_2 + 50% Ar at 1 bar.
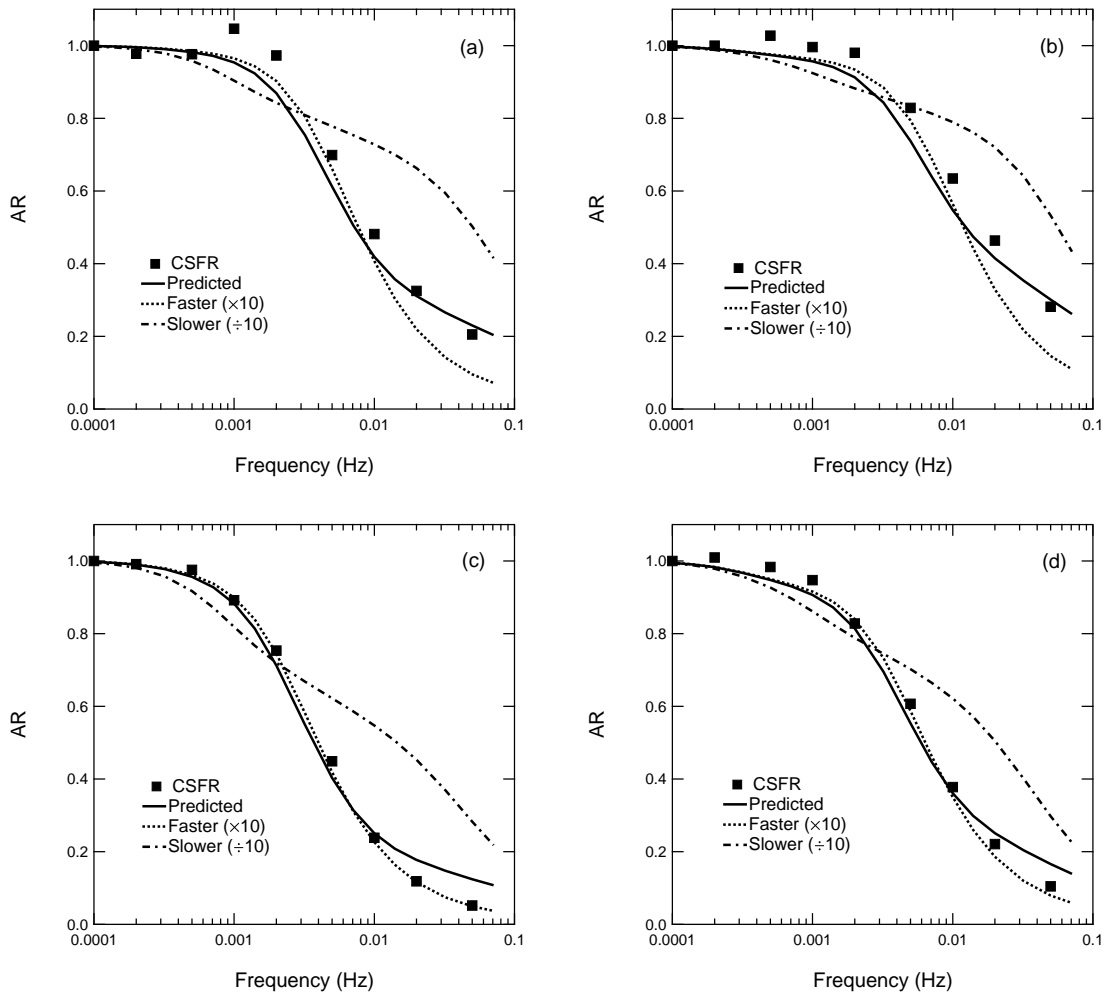
over a range of temperatures, the lowest being 25 °C, and the experimental data were described well by the temperature-dependent Toth equation. Figure 4.6 shows a plot of the temperature-dependent Toth fit for O_2, extrapolated slightly to 23 °C, the temperature at which the CSFR experiments were conducted. The corresponding curve for Ar is nearly identical. The isotherms are linear up to pressures higher than those at which the CSFR experiments were performed.

The implications of these linear isotherms on the transport of O_2 and Ar in this CMS will depend on the physical interpretation of the surface barrier resistance to which these gases owe the majority of their transport character. In our earlier work, we discussed the interpretation of the CMS surface barrier as a thin shell at the outermost region of a CMS microparticle that has a drastically reduced diffusivity compared with the core of the material caused when carbon is deposited around the pore openings of a nonselective base carbon material.[42, 43] We also suggested that due to the effect of pore size on adsorption isotherms, this interpretation of the surface barrier could allow for different isotherm behavior in this thin shell compared with the core of the material. As the core of the material, being a much larger region than the shell, will contain most of the adsorbate at equilibrium, a measured isotherm will not necessarily reflect the isotherm behavior of the surface barrier region. Thus, while isotherm linearity suggests a lack of intermolecular interaction in the adsorbed phase, this lack of interaction can only be said to apply to the adsorbate in the core of the CMS. Since micropore diffusion (which takes place in the core of a microparticle) is also important to O_2 transport in this system, the measured isotherms would suggest that diffusion of O_2 in the CMS core is unaffected by the presence of Ar. This conclusion is consistent with the CSFR data, which are described well by transport models and parameters which do not allow for any effect of Ar on the micropore diffusion component of O_2 transport. By contrast, with such an interpretation of the surface barrier, the linear isotherms cannot be used to say anything definitive regard-

80
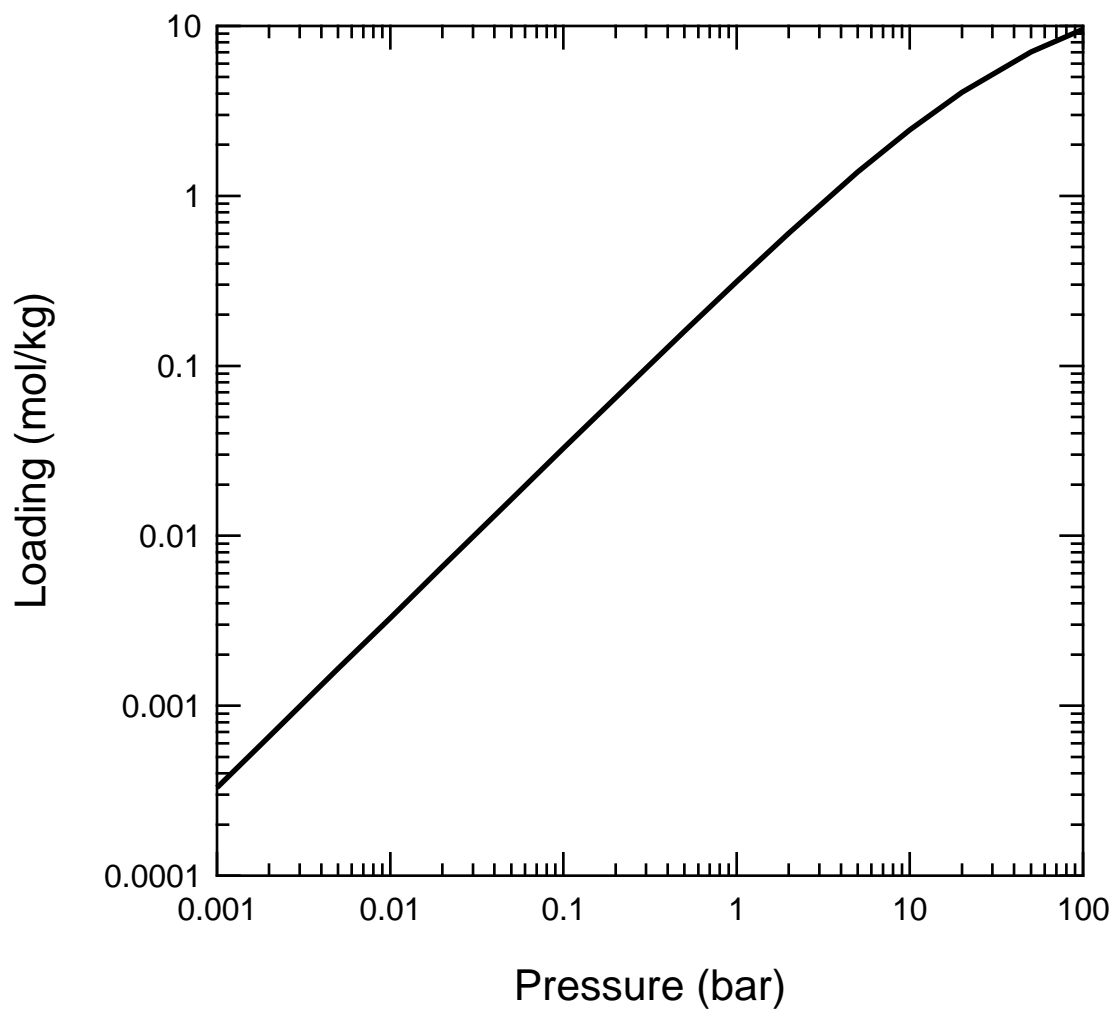
Figure 4.6 Temperature-dependent Toth equation fit of O_2/CMS equilibrium data extrapolated slightly to 23 °C.

ing the existence of intermolecular interactions in the adsorbed phase within the surface barrier. However, isotherm linearity within the surface barrier region would serve to explain why the CSFR data are well described using transport models with no interaction between O_2 and Ar.

4.5 Conclusions

The transport of binary O_2/Ar gas mixtures in Shirasagi MSC-3R type 172 CMS has been studied using CSFR at pressures up to 1 bar. The experimental data can be described well using the pure component transport models and coefficients with no additional cross coefficients. The data suggest that transport of O_2 is not inhibited by the presence of Ar at the gas concentrations investigated. However, the CSFR data for this system are not sensitive enough to rule out the possibility of some enhancement of the O_2 transport due to the presence of Ar. Nevertheless, the linear character of the O_2 and Ar isotherms on this material suggest that loadings at the experimental conditions are small enough that the adsorbed gases can be treated as noninteracting, at least within the core of a CMS microparticle.

References

[1] Hayashi, S.; Kawai, M.; Kaneko, T. Dynamics of high purity oxygen PSA. *Gas Sep. Purif.* **1996**, *10*, 19.

[2] Jee, J.-G.; Lee, S.-J.; Kim, M.-B.; Lee, C.-H. Three-bed PVSA process for high-purity O$_2$ generation from ambient air. *AIChE J.* **2005**, *51*, 2988.

[3] Jee, J.-G.; Kim, M.-B.; Lee, C.-H. Pressure swing adsorption processes to purify oxygen using a carbon molecular sieve. *Chem. Eng. Sci.* **2005**, *60*, 869.

[4] Jin, X.; Malek, A.; Farooq, S. Production of argon from an oxygen-argon mixture by pressure swing adsorption. *Ind. Eng. Chem. Res.* **2006**, *45*, 5775.

[5] Ma, Y. H.; Sun, W.; Bhandarkar, M.; Wang, J.; Miller, G. W. Adsorption and diffusion of nitrogen, oxygen, argon, and methane in molecular sieve carbon at elevated pressures. *Separ. Technol.* **1991**, *1*, 90.

[6] Rege, S. U.; Yang., R. T. Kinetic separation of oxygen and argon using molecular sieve carbon. *Adsorption* **2000**, *6*, 15.

[7] Armond, J. W.; Webber, D. A.; Smith, K. C. Gas separation. U.S. Patent 4,190,424, 1980.

[8] Richter, E.; Knoblauch, K.; Schlegel, R.; Körbächer, W. Process and apparatus for producing oxygen with a low proportion of argon from air. U.S. Patent 4,566,881, 1986.

[9] Haruna, K.; Hayashi, S. Process for producing high concentration oxygen by a pressure-swing-adsorption method. U.S. Patent 4,661,128, 1987.

[10] Miller, G. W.; Theis, C. F. Secondary oxygen purifier for molecular sieve oxygen concentrator. U.S. Patent 4,813,979, 1989.

[11] Miller, G. W.; Theis, C. F. Molecular sieve oxygen concentrator with secondary oxygen purifier. U.S. Patent 4,880,443, 1989.

[12] Bansal, R. K. Pressure swing adsorption process and system for gas separation. U.S. Patent 4,973,339, 1990.

[13] Garrett, M. E. Separation of gas mixtures. U.S. Patent 4,959,083, 1990.

[14] Haruna, K.; Ueda, K.; Inoue, M.; Someda, H. Process for producing high purity oxygen from air. U.S. Patent 4,985,052, 1991.

[15] Ruthven, D. M. Diffusion of oxygen and nitrogen in carbon molecular sieve. *Chem. Eng. Sci.* **1992**, *47*, 4305.

[16] Ruthven, D. M.; Raghavan, N. S.; Hassan, M. M. Adsorption and diffusion of nitrogen and oxygen in a carbon molecular sieve. *Chem. Eng. Sci.* **1986**, *41*, 1325.

[17] Chagger, H. K.; Ndaji, F. E.; Sykes, M. L.; Thomas, K. M. Kinetics of adsorption and diffusional characteristics of carbon molecular sieves. *Carbon* **1995**, *33*, 1405.

[18] Chen, Y. D.; Yang, R. T.; Uawithya, P. Diffusion of oxygen, nitrogen and their mixtures in carbon molecular sieve. *AIChE J.* **1994**, *40*, 577.

[19] Dominguez, J. A.; Psaris, D.; LaCava, A. I. Langmuir kinetics as an accurate simulation of the rate of adsorption of oxygen and nitrogen mixtures on non-Fickian carbon molecular sieves. *AIChE Symp. Ser.* **1988**, *84*, 73.

[20] Kawazoe, K.; Suzuki, M.; Chihara, K. Chromatographic study of diffusion in molecular-sieving carbon. *J. Chem. Eng. Jpn.* **1974**, *7*, 151.

[21] Fitch, F. R.; Bülow, M.; LaCava, A. I. Investigation of the mechanism for the separation of nitrogen-oxygen mixtures on carbon molecular sieves. *Gas Sep. Purif.* **1994**, *8*, 45.

[22] LaCava, A. I.; Koss, V. A.; Wickens, D. Non-Fickian adsorption rate behavior of some carbon molecular sieves: I. Slit-potential rate model. *Gas Sep. Purif.* **1989**, *3*, 180.

[23] Koresh, J.; Soffer, A. Study of molecular sieve carbons. Part 1. Pores structure, gradual pore opening and mechanism of molecular sieving. *J. Chem. Soc. Faraday Trans. I* **1980**, *76*, 2457.

[24] Liu, H.; Ruthven, D. M. Diffusion in carbon molecular sieves. In *Proceedings of the 5th International Conference on the Fundamentals of Adsorption*; LeVan, M. D., Ed.; Kluwer Academic Publishers: Norwell, MA, 1996.

[25] Reid, C. R.; O'koye, I. P.; Thomas, K. M. Adsorption of gases on carbon molecular sieves used for air separation. Spherical adsorptives as probes for kinetic selectivity. *Langmuir* **1998**, *14*, 2415.

[26] Rynders, R. M.; Rao, M. B.; Sircar, S. Isotope exchange technique for measurement of gas adsorption equilibria and kinetics. *AIChE J.* **1997**, *43*, 2456.

[27] Srinivasan, R.; Auvil, S. R.; Schork, J. M. Mass transfer in carbon molecular sieves - an interpretation of Langmuir kinetics. *Chem. Eng. J.* **1995**, *57*, 137.

[28] Wang, Y.; Sward, B. K.; LeVan, M. D. New frequency response method for measuring adsorption rates via pressure modulation: Application to oxygen and nitrogen in a carbon molecular sieve. *Ind. Eng. Chem. Res.* **2003**, *42*, 4213.

[29] Chihara, K.; Suzuki, M.; Kawazoe, K. Adsorption rate on molecular sieving carbon by chromatography. *AIChE J.* **1978**, *24*, 237.

[30] Giesy, T. J.; LeVan, M. D. Mass transfer rates of oxygen, nitrogen, and argon in carbon molecular sieves determined by pressure-swing frequency response. *Chem. Eng. Sci.* **2013**, *90*, 250.

[31] Deisler, P. F.; Wilhelm, R. H. Diffusion in beds of porous solids. Measurement by frequency response techniques. *Ind. Eng. Chem.* **1953**, *45*, 1219.

[32] Boniface, H. A.; Ruthven, D. M. Chromatographic adsorption with sinusoidal input. *Chem. Eng. Sci.* **1985**, *40*, 2053.

[33] Wang, Y.; LeVan, M. D. Mixture diffusion in nanoporous adsorbents: Development of Fickian flux relationship and concentration-swing frequency response method. *Ind. Eng. Chem. Res.* **2007**, *46*, 2141.

[34] Wang, Y.; LeVan, M. D. Nanopore diffusion rates for adsorption determined by pressure-swing and concentration-swing frequency response and comparison with Darken's equation. *Ind. Eng. Chem. Res.* **2008**, *47*, 3121.

[35] Glover, T. G.; Wang, Y.; LeVan, M. D. Diffusion of condensable vapors in single adsorbent particles measured via concentration-swing frequency response. *Langmuir* **2008**, *24*, 13406.

[36] Naphtali, L. M.; Polinski, L. M. A novel technique for characterization of adsorption rates on heterogeneous surfaces. *J. Phys. Chem.* **1963**, *67*, 369.

[37] Yasuda, Y. Freuqency response method for study of the kinetic behavior of a gas-surface system. 1. Theoretical treatment. *J. Phys. Chem.* **1976**, *80*, 1870.

[38] Giesy, T. J.; Wang, Y.; LeVan, M. D. Measurement of mass transfer rates in adsorbents: New combined-technique frequency response apparatus and application to CO_2 in 13X zeolite. *Ind. Eng. Chem. Res.* **2012**, *51*, 11509.

[39] Sun, L. M.; Meunier, F.; Grenier, P.; Ruthven, D. M. Frequency response for nonisothermal adsorption in biporous pellets. *Chem. Eng. Sci.* **1994**, *49*, 373.

[40] Wang, Y.; LeVan, M. D. Master curves for mass transfer in bidisperse adsorbents for pressure-swing and volume-swing frequency response methods. *AIChE J.* **2011**, *57*, 2054.

[41] Campo, M. C.; Magalhães, A.; Mendes, A. Comparative study between a CMS membrane and a CMS adsorbent: Part 1 - Morphology, adsorption equilibrium and kinetics. *J. Membrane Sci.* **2010**, *346*, 15.

[42] Braymer, T. A.; Coe, C. G.; Farris, T. S.; Gaffney, T. R.; Schork, J. M.; Armor, J. N. Granular carbon molecular sieves. *Carbon* **1994**, *32*, 445.

[43] Verma, S. K.; Walker, P. L. Preparation of carbon molecular sieves by propylene pyrolysis over microporous carbons. *Carbon* **1992**, *30*, 829.

CHAPTER V

FREQUENCY RESPONSE MODELS OF ADSORPTION RATES: TRANSPORT
INVOLVING A BARRIER RESISTANCE

5.1   Introduction

Over the past few decades, frequency response (FR) methods have proven
useful for characterizing transport of gases in adsorbent materials. One of the main
benefits of FR techniques is that they can easily distinguish among mass transfer
mechanisms due to their high sensitivity to the form of the governing transport equa-
tions (Sun et al., 1994). In FR experiments, one of the system variables is perturbed
periodically, typically sinusoidally, around an equilibrium point, and the resulting
periodic response in another system variable is measured to characterize the system.
For example, in volume-swing frequency response (VSFR), the volume of a batch sys-
tem containing the gas and adsorbent to be analyzed can be perturbed sinusoidally
with measurement of the resulting response in the system pressure. The dynamics of
the system are characterized by the amplitude of the response variable relative to the
amplitude of the perturbation and by the phase angle between the perturbation and
the response.

The effective use of FR techniques depends upon the availability of mathe-
matical models to describe the frequency response of all transport mechanisms that
could occur in the system under investigation. In order to use FR data to determine
the governing transport mechanism(s) in a gas/adsorbent system, the amplitude and
phase angle data over a wide range of perturbation frequencies are compared with
mathematical models describing each of the possible transport mechanisms. As each
mathematical model will behave differently across the frequency range, only the model
corresponding to the correct transport mechanism will accurately describe the data.

As with other experimental techniques, particle size and other parameters can be varied to aid in the discrimination process.

Possible transport mechanisms in pure gas adsorption systems include micropore diffusion, macropore diffusion (Knudsen diffusion or Poiseuille flow), and transport across a surface barrier. Nonisothermal effects, heat transfer resistances, and the combination of resistances can further complicate transport behavior for gas/adsorbent systems.

Throughout the history of the application of frequency response techniques to adsorption systems, mathematical models have been developed to describe the frequency response behavior of many of the aforementioned possible transport cases. Deisler and Wilhelm (1953) first presented a model treating Fickian diffusion in homogenous spheres. A simpler linear driving force (LDF) rate model was later developed by Naphtali and Polinski (Naphtali and Polinski, 1963). Other early models include diffusion in parallelepiped (Gunn, 1970) and spherical (Gunn, 1970; Yasuda, 1982) particles, as well as diffusion in an infinite sheet (Evnochides and Henley, 1970; Yasuda, 1982). Boniface and Ruthven (1985) gave a more complicated model combining the effects of macropore and micropore diffusion. The most comprehensive models are those of Sun and coworkers (1987; 1993; 1994) and Jordi and Do (1993; 1994), who have each combined the effects of micropore and macropore diffusion with surface barrier and film resistances, as well as including temperature and particle shape/size effects. A summary of models for commonly encountered resistances and combinations of resistances has been given by Wang and LeVan (2010), who include adsorbed-phase transfer functions that can be used for analysis of data from multiple frequency response techniques.

In this paper, we present additional mathematical models for the interpretation of frequency response data for adsorption of pure gases. First, as a supplement to the earlier work by Wang and LeVan, we present a general model for pure gas transport

incorporating the effects of macropore diffusion, micropore diffusion, a surface barrier, and temperature effects caused by the heat of adsorption. Existing similar models (Jordi and Do, 1993, 1994; Sun and Meunier, 1987; Sun et al., 1993; Sun et al., 1994) have not been cast as adsorbed-phase transfer functions, and a version of the general model in this form should be useful in investigations. We also present two new models describing the "shell and core" interpretation (Srinivasan et al., 1995) of the CMS barrier resistance with different degrees of complexity. These two models are a continuation of our efforts in a recent paper (Giesy and LeVan, 2013) to use the shell and core model to explain gas transport behavior in CMS.

In our recent paper (Giesy and LeVan, 2013), we suggest that different isotherm characteristics between the shell and core regions in this model could be used to explain observed pressure dependence of the surface barrier transport coefficient in CMS. The two shell and core models presented here more fully explore the implications of having different shell and core isotherms as it regards the pressure dependence of the surface barrier coefficient, the physical significance of the model parameters, and the suitability of this kind of model for explaining LDF-type rate behavior. These models should be useful for the critical assessment of the shell and core view of the CMS surface barrier and for interpretation of frequency response data in a variety of systems.

5.2   Mathematical Models

To use frequency response to extract information about adsorption rates, a material balance is written for the experimental apparatus containing the gas and adsorbent. The material balance is then transformed into the Laplace domain and rearranged to give an overall system transfer function, which gives the ratio of the response and perturbation variables in the Laplace domain. For a flow-through pressure-swing frequency response (PSFR) system (Wang et al., 2003), the overall transfer function

is (Wang and LeVan, 2010)

$$G(s) = \frac{\bar{F}}{\bar{P}} = -s \left[M_s G_n\left(s\right) + \frac{V}{RT} \right] \tag{5.1}$$

where $G_n = \bar{\hat{n}}/\bar{P}$ is the adsorbed-phase transfer function, which contains the whole of the contribution of gas adsorption to the dynamic response of the system. For a batch VSFR system, the overall transfer function is (Wang and LeVan, 2010)

$$G(s) = \frac{\bar{V}}{\bar{P}} = -\frac{RT}{P_0} \left[M_s G_n\left(s\right) + \frac{V_0}{RT} \right] \tag{5.2}$$

We note that in this treatment of a batch system, the overall system transfer function is written in terms of the ratio of the perturbation variable to the response variable, which is the inverse of what is typical for a transfer function. However, writing the equation in such a way results in a convenient similarity to the overall transfer function for a PSFR system, which allows data from both techniques to be analyzed using the same adsorbed-phase transfer function (Wang and LeVan, 2010). The amplitude ratio and the phase angle can be found using the overall transfer function according to

$$AR = |G\left(j\omega\right)| \tag{5.3}$$

$$\phi = \tan^{-1} \left[\frac{\text{Im}\left[G\left(j\omega\right)\right]}{\text{Re}\left[G\left(j\omega\right)\right]} \right] \tag{5.4}$$

Experimental amplitude ratio and phase angle data can be described by Eqs. 5.3 and 5.4 by substituting in the specific adsorbed-phase transfer function that corresponds to the desired transport model. The remainder of this section is devoted to deriving expressions for G_n for different transport mechanisms.

General Model

First, we wish to develop an expression for G_n that includes contributions from micropore and macropore diffusion, a surface barrier resistance, and nonisothermal effects. For this model, we treat a spherical macroporous particle comprising smaller agglomerated spherical microporous particles. In developing the model, a material balance is first written for a spherical microparticle.

$$\frac{\partial n}{\partial t} = \frac{D_s}{r^2} \frac{\partial}{\partial r} \left(r^2 \frac{\partial n}{\partial r} \right) \tag{5.5}$$

$$D_s \frac{\partial n}{\partial r} \bigg|_{r=r_s} = k_b \left(n^* - n \right)|_{r=r_s} \tag{5.6}$$

$$\frac{\partial n}{\partial r} = 0 \ \text{ at } \ r = 0 \tag{5.7}$$

where n is the adsorbed phase loading, n^* is the adsorbed phase loading that would exist in equilibrium with the gas concentration surrounding the microparticle, k_b is the surface barrier transport coefficient, D_s is the micropore diffusivity, and r_s is the microparticle radius. The boundary condition given by Eq. 5.6 captures the contribution of the surface barrier resistance to the overall adsorption rate and establishes flux continuity at the microparticle surface. Converting to the Laplace domain and solving the differential equation yields

$$\bar{n} = \frac{\beta_{bm} \bar{n}^*}{x} \frac{\sinh \left(x \sqrt{s/\eta} \right)}{(\beta_{bm} - 1) \sinh \left(\sqrt{s/\eta} \right) + \sqrt{s/\eta} \cosh \left(\sqrt{s/\eta} \right)} \tag{5.8}$$

where $x = r/r_s$, $\eta = D_s/r_s^2$, and $\beta_{bm} = k_b r_s/D_s$.

The next step in developing the model is to incorporate the macroparticle material balance, which can be written

$$\frac{\epsilon_p D_p}{R^2} \frac{\partial}{\partial R} \left(R^2 \frac{\partial c_p}{\partial R} \right) = \epsilon_p \frac{\partial c_p}{\partial t} + \frac{3}{r_s} \rho_p k_b \left(n^* - n \right)|_{r=r_s} \tag{5.9}$$

$$c_p = c \text{ at } R = R_p \tag{5.10}$$

$$\frac{\partial c_p}{\partial R} = 0 \text{ at } R = 0 \tag{5.11}$$

where c_p is the gas phase concentration in the macropores, R_p is the particle radius, and D_p is the macropore diffusivity. Converting to the Laplace domain and substituting in Eq. 5.8 evaluated at $r = r_s$ yields

$$\frac{\epsilon_p D_p}{R^2} \frac{\partial}{\partial R} \left(R^2 \frac{\partial \bar{c}_p}{\partial R} \right) = \epsilon_p s \bar{c}_p + \frac{3\rho_p k_b}{r_s} \bar{n}^* \left[\frac{\sqrt{s/\eta} \coth\left(\sqrt{s/\eta}\right) - 1}{\beta_{bm} + \sqrt{s/\eta} \coth\left(\sqrt{s/\eta}\right) - 1} \right] \tag{5.12}$$

Accounting for possible temperature changes in the equilibrium loading due to the heat of adsorption results in the following expression for $\bar{n}^*$ (Sward and LeVan, 2003):

$$\bar{n}^* = K\bar{c}_p + K_T G_T \bar{\bar{n}} \tag{5.13}$$

$$G_T = \frac{\bar{T}}{\bar{\bar{n}}} = \frac{-M_s \lambda s}{M_s C_s s + \alpha} \tag{5.14}$$

In the above equations, K and K_T are, respectively, the local isotherm and isobar slopes, $\bar{\bar{n}}$ is the adsorbed phase loading averaged over an entire adsorbent pellet, λ is the heat of adsorption (taken to be negative), and $\alpha = hA$ for VSFR (or $\alpha = F_{in}C_p + hA$ for PSFR) is a lumped heat transfer coefficient. Substituting Eq. 5.13 into Eq. 5.12 and rearranging gives

$$\frac{1}{x_p^2} \frac{\partial}{\partial x_p} \left(x_p^2 \frac{\partial \bar{c}_p}{\partial x_p} \right) = \eta_m \bar{c}_p + \beta \bar{\bar{n}} \tag{5.15}$$

with

$$x_p = R/R_p \tag{5.16}$$

$$\eta_m = \frac{s}{D_p/R_p^2} + \frac{3\rho_p k_b l_1 K}{\epsilon_p r_s D_p/R_p^2} \tag{5.17}$$

93

$$\beta = \frac{3\rho_p k_b K_T G_T l_1}{\epsilon_p r_s D_p / R_p^2} \tag{5.18}$$

$$l_1 = \frac{\sqrt{s/\eta}\coth\left(\sqrt{s/\eta}\right) - 1}{\beta_{bm} + \sqrt{s/\eta}\coth\left(\sqrt{s/\eta}\right) - 1} \tag{5.19}$$

Equation 15 can be solved by first solving the homogeneous equation and then assuming a constant for the particular solution. After applying the boundary conditions, the solution is

$$\bar{c}_p = \left(\bar{c} + \frac{\beta\bar{\tilde{n}}}{\eta_m}\right)\frac{1}{x_p}\frac{\sinh\left(x_p\sqrt{\eta_m}\right)}{\sinh\left(\sqrt{\eta_m}\right)} - \frac{\beta\bar{\tilde{n}}}{\eta_m} \tag{5.20}$$

The average loading in an adsorbent pellet can be found by integrating according to

$$\bar{\tilde{n}} = 3\int_0^1\left[3\int_0^1 \bar{n}x^2 dx\right]x_p^2 dx_p = 3\int_0^1\left[\frac{3\beta_{bm}l_1}{s/\eta}\left(K\bar{c}_p + K_T G_T \bar{\tilde{n}}\right)\right]x_p^2 dx_p \tag{5.21}$$

Noting that $\bar{\tilde{n}}$ is not itself a function of the macroparticle radial coordinate, Eq. 5.21 can be integrated to yield

$$\bar{\tilde{n}} = \frac{9\beta_{bm}l_1 l_2 K\bar{c}}{s/\eta - 3\beta_{bm}l_1 K_T G_T + (3\beta_{bm}l_1 K\beta/\eta_m)(1 - 3l_2)} \tag{5.22}$$

with

$$l_2 = \frac{\sqrt{\eta_m}\coth\left(\sqrt{\eta_m}\right) - 1}{\eta_m} \tag{5.23}$$

Gas present in the macropores is added by

$$\bar{\hat{n}} = \bar{\tilde{n}} + 3\int_0^1\left(\frac{\epsilon_p}{\rho_p}\bar{c}_p\right)x_p^2 dx_p \tag{5.24}$$

where $\bar{\hat{n}}$ is the total loading including the gas present in the macropores. Integration

94

and rearrangement yields the final expression for the adsorbed-phase transfer function:

$$G_n = \frac{\bar{\hat{n}}}{\bar{\bar{P}}} = \frac{3}{RT} l_2 \left[\frac{3\beta_{bm} l_1 K \left[1 - (\epsilon_p \beta / \rho_p \eta_m) (1 - 3l_2) \right]}{s/\eta - 3\beta_{bm} l_1 K_T G_T + 3\beta_{bm} l_1 K \beta / \eta_m} + \frac{\epsilon_p}{\rho_p} \right] \tag{5.25}$$

Equation 25 can be inserted into an overall transfer function for a FR system (e.g., Eq. 5.1), which when evaluated with $s = j\omega$ can be used to extract transport parameter values from experimental amplitude ratio and phase angle data. Furthermore, while Eq. 5.25 is general, it will reduce to simpler models with the appropriate substitutions.

Surface Barrier in CMS

In certain gas/CMS systems, adsorption rates have been found to follow a surface barrier rate model (equivalent to a linear driving force) rather than a micropore diffusion model (Dominguez et al., 1988; LaCava et al., 1989; LaCava et al., 1994; Koresh and Soffer, 1981). In CMS, kinetic selectivity is commonly imparted by carbon deposition on a non-rate-selective base carbon material, which results in constricted pores with openings on the order of molecular dimensions (Braymer et al., 1994; Verma and Walker, 1992). The existence of such pore constrictions has led to two major explanations of surface barrier rate behavior in CMS. First, the pore constrictions may constitute an energy barrier between the gas and adsorbed phases, with adsorption taking place according to a mass action or Langmuir kinetics type mechanism (Dominguez et al., 1988; LaCava et al., 1989; LaCava et al., 1994). Alternatively, the pore constrictions may be confined to the outermost region of a spherical microparticle and constitute a thin shell with a drastically reduced diffusivity compared to the particle core (Srinivasan et al., 1995). If curvature in this shell is ignored and the concentration profile in the shell is assumed to reach steady-state instantaneously, the equation describing micropore diffusion through this shell will reduce to a simple LDF-equivalent surface barrier model (Srinivasan et al., 1995).

In the shell and core interpretation, the surface barrier transport coefficient is a function of the micropore diffusivity within this shell. If this interpretation is correct, then the barrier coefficient can be expected to exhibit a loading dependence in accordance with the loading dependence of the shell diffusivity (Srinivasan et al., 1995). As the loading dependence of micropore diffusivities is expected to be described via non-equilibrium thermodynamics, such as by the Darken relation (Do, 1998), the loading dependence of the barrier coefficient should be predictable. However, the loading dependence of the barrier coefficient in CMS has been observed to deviate from this expected behavior in numerous instances (Giesy and LeVan, 2013; Huang et al., 2003, 2004). In a recent paper (Giesy and LeVan, 2013), we hypothesized that this unexpected behavior could be explained by the thin shell having a different isotherm than the particle core caused by a difference in pore sizes between the two regions. This is a logical supposition, as adsorption isotherms have a well established connection with pore size: this connection is even the basis for porosimetry (Rouquerol et al., 1999). A different isotherm in the shell would result in a different thermodynamic correction factor for the Darken relation and thus, a different loading dependence.

In this section, we present frequency response solutions for two different models describing transport through a thin shell at the outermost region of a spherical microparticle. First, we present a revised consideration of the simple CMS surface barrier model that allows for the existence of different isotherms in the shell compared with the particle core. We discuss the implications of this model regarding the physical significance of the rate parameters and their dependence on loading. Finally, we present a concentric sphere model that more rigorously describes the shell and core interpretation of the surface barrier. This model will aid in the critical assessment of the shell and core interpretation of surface barrier rate behavior in CMS.

Case 1: Simple surface barrier - equivalent to LDF

Figure 5.1 shows a simple visualization of the shell and core interpretation of the CMS surface barrier. Surrounding the much larger core of a CMS microparticle is a thin shell of thickness δ in which gas diffusivities are much lower than they are in the core. Diffusion through this shell is the limiting resistance and thus governs the rate of adsorption. At the outer edge of the shell, the adsorbed phase loading is assumed to be always in equilbrium with the surrounding gas.

To formulate an adsorption rate model, we follow the method of Srinivasan et al. (1995), i.e., the shell is treated a flat sheet, and Fick's law is written for the shell region in the form

$$J = -D_s \rho_s \frac{dn_s}{dx} \tag{5.26}$$

where J is the molar flux through the shell, D_s is the adsorbate diffusivity, ρ_s is the shell density, and n_s is the adsorbate loading. If the shell is thin and diffusion through it reaches a steady-state condition quickly, Eq. 5.26 can be written using the shell thickness as (Srinivasan et al., 1995)

$$J = \frac{D_s \rho_s}{\delta} \left(n^* - n_{s,i} \right) \tag{5.27}$$

where n^* is the shell loading that exists at equilibrium with the surrounding gas and $n_{s,i}$ denotes the shell loading at the shell-core interface.

Assuming that the shell is thin enough that it contributes negligibly to the overall loading and that diffusion in the core is fast, such that no gradient exists in the core, the particle material balance can be written as

$$\rho_c \frac{\partial n_c}{\partial t} = \frac{3}{r_c} \frac{D_s \rho_s}{\delta} \left(n^* - n_{s,i} \right) \tag{5.28}$$

where ρ_c is the density of the core, n_c is the core loading, and r_c is the core radius.

We note two deviations from the method of Srinivasan et al. (1995). First,
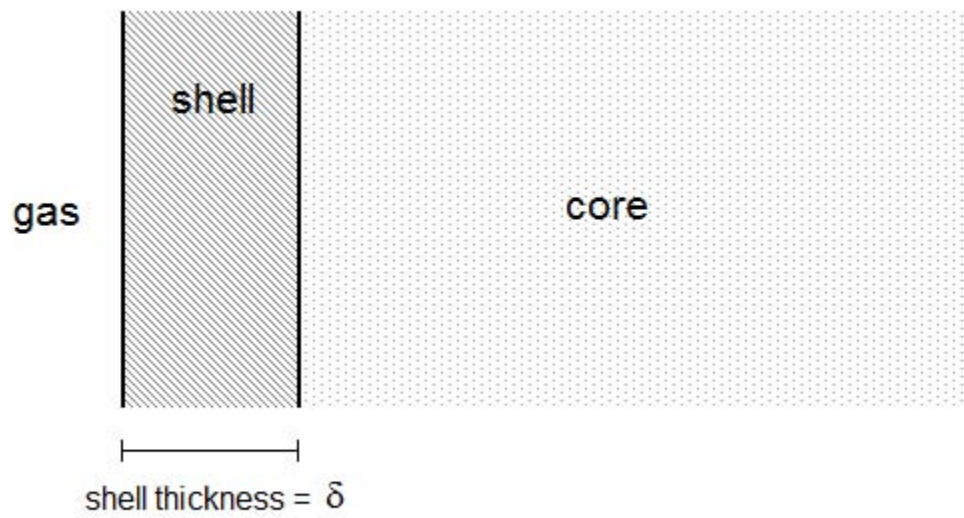
Figure 5.1 Visual representation of the shell and core interpretation of the CMS surface barrier.

we have allowed for the possibility that the adsorbent densities in the shell and core may differ from one another. This is a sensible assumption given that the shell is understood to be created by the deposition of carbon in the pores. Second, in the model of Srinivasan et al. (1995), $n_{s,i}$ is taken to signify the overall adsorbent loading, as the shell and core are described by a single isotherm and there will be no gradient in the core if the barrier is rate-limiting. However, in consideration of the possibility of the shell and core having different isotherms, we instead impose an equilibrium condition at the shell-core interface.

We express this equilibrium condition by writing

$$\mu_{s,i} = \mu_{c,i} \tag{5.29}$$

where $\mu_{s,i}$ and $\mu_{c,i}$ signify the chemical potentials of the adsorbate at the shell-side and core-side of the interface, respectively. Eq. 5.29 leads to an equality in hypothetical gas pressures that would exist in equilibrium with the shell and core loadings, namely

$$P_{s,i} = P_{c,i} \tag{5.30}$$

Using an isotherm linearized around an equilibrium point allows the condition at the interface to be stated as

$$\frac{n_{s,i} - n_{s,0}}{K_s} = \frac{n_{c,i} - n_{c,0}}{K_c} \tag{5.31}$$

where K_s and K_c are the localized isotherm slopes of the shell and core, respectively.

By introducing the deviation variables

$$n_c' = n_c - n_{c,0} \tag{5.32}$$

$$n_{s,i}' = n_{s,i} - n_{s,0} \tag{5.33}$$

$$n^{*\prime} = n^* - n_{s,0} \tag{5.34}$$

and noting that $n_c = n_{c,i}$ in the absence of a loading gradient in the particle core, the material balance given by Eq. 28 becomes

$$\frac{\partial n_c'}{\partial t} = \frac{3}{r_c} \frac{D_s \rho_s}{\delta \rho_c} \left(n^{*\prime} - \frac{K_s}{K_c} n_c' \right) \tag{5.35}$$

Converting to the Laplace domain and rearranging yields the adsorbed-phase transfer function

$$G_n = \frac{\bar{n}_c}{\bar{P}} = \frac{3\lambda \eta_\delta K_c}{RT \left(s + 3\lambda \eta_\delta \right)} \tag{5.36}$$

with

$$\lambda = \frac{\rho_s}{\rho_c} \frac{K_s}{K_c} \frac{\delta}{r_c} \tag{5.37}$$

and $\eta_\delta = D_s/\delta^2$.

Case 2: Nonsteady concentric spheres

If the curvature of the thin shell is to be accounted for, the material balance in the shell can be written in spherical geometry as

$$\frac{\partial n_s}{\partial t} = \frac{D_s}{r^2} \frac{\partial}{\partial r} \left(r^2 \frac{\partial n_s}{\partial r} \right) \tag{5.38}$$

$$n_s - n_{s,0} = \frac{K_s}{K_c} \left(n_c - n_{c,0} \right) \text{ at } r = r_c \tag{5.39}$$

$$n_s = n^* \text{ at } r = r_s \tag{5.40}$$

We again introduce deviation variables and convert to the Laplace domain, after which Eq. 5.38 becomes a modified spherical Bessel function of order 0. The equation is solved and the boundary conditions are applied, which after some rearrangement

results in the following expression for the adsorbed-phase transfer function.

$$G_n = \frac{1}{RT} \frac{3\lambda\eta_\delta \left(\delta/r_c\right) \left(\mathrm{E}_1/x_c\right) \left(l_3 + l_4\right) K_c}{s \left[\mathrm{E}_1 - \mathrm{E}_2\right] + 3\lambda\eta_\delta \left(\delta/r_c\right) \left[l_3\mathrm{E}_2 + l_4\mathrm{E}_1\right]} \tag{5.41}$$

$$l_3 = x_c\sqrt{s/\eta_s} \coth\left(x_c\sqrt{s/\eta_s}\right) - 1 \tag{5.42}$$

$$l_4 = \sqrt{s/\eta_s} + 1 \tag{5.43}$$

$$\mathrm{E}_1 = \frac{e^{-x_c\sqrt{s/\eta_s}}}{\sinh\left(x_c\sqrt{s/\eta_s}\right)} \tag{5.44}$$

$$\mathrm{E}_2 = \frac{e^{-\sqrt{s/\eta_s}}}{\sinh\left(\sqrt{s/\eta_s}\right)} \tag{5.45}$$

5.3 Discussion

The simpler of the CMS surface barrier models presented here (Eq. 5.36) has the same mathematical form as the thin sheet model of Srinivasan et al. (1995). However, by making allowance for a different adsorbent density and isotherm slope in the shell compared with the particle core, the transport parameters in this model have a different physical significance. For the sake of comparison, the adsorbed-phase transfer function for the model of Srinivasan et al. can be expressed as

$$G_n = \frac{kK_c}{RT\left(s + k\right)} \tag{5.46}$$

$$k = \frac{3}{r_c}\frac{D_s}{\delta} \tag{5.47}$$

By comparing Eq. 5.36 with Eq. 5.46, it can be seen that we have replaced k in the model of Srinivasan et al. with the term $3\lambda\eta_\delta$, where

$$3\lambda\eta_\delta = \frac{3\rho_s K_s D_s}{r_c\rho_c K_c\delta} \tag{5.48}$$

If the particle shell has the same density and isotherm characteristics as the core, the values of k and $3\lambda\eta_\delta$ will be identical. However, this more general case has one interesting and important implication, namely, that the more general surface barrier transport coefficient contains additional terms that depend upon the adsorbate loading in the shell. The loading dependence of k results solely from the loading dependence of the shell diffusivity, D_s, which assuming adherence to the Darken relation takes the form

$$D_s = D_{s0} \frac{\partial \ln P}{\partial \ln n} \tag{5.49}$$

or, for a Langmuir isotherm,

$$D_s = D_{s0} \left(1 + bP\right) \tag{5.50}$$

However, the parameter $3\lambda\eta_\delta$ contains two additional parameters, K_s and K_c, that depend upon the pressure at which the surface barrier transport coefficient is measured.

In our earlier work, we measured the pressure dependence of surface barrier transport coefficients on CMS, finding a stronger dependence than expected from Eq. 5.50. Thus, we suggested that the isotherm in the microparticle shell, which is the isotherm directly influencing the micropore diffusivity in the shell, could differ from the overall material isotherm; this possibility would allow for a $(1 + bP)$ term that could adequately capture the barrier coefficient pressure dependence without conflicting with measured isotherms on CMS. However, we have now shown that the existence of a different shell isotherm results in the rate parameter $3\lambda\eta_\delta$, which after substitution of Eq. 5.50 and expressions for the slope of a Langmuir isotherm into Eq. 5.48, has the actual pressure dependence

$$3\lambda\eta_\delta = 3\frac{\rho_s}{\rho_c} \frac{D_{s0}}{\delta r_c} \frac{n_{sat,s} b_s}{n_{sat,c} b_c} \frac{\left(1 + b_c P\right)^2}{\left(1 + b_s P\right)} \tag{5.51}$$

102

Thus, with Eq. 5.51 we refine our explanation of the pressure dependence of the surface barrier transport coefficient based on the isotherm characteristics of the thin shell, showing that the pressure dependence of the shell and core isotherm slopes should be considered in addition to the pressure dependence of the shell diffusivity.

Consideration of the shell and core model may be further refined using the concentric sphere diffusion model presented in this paper. This model is a more general form of the LDF-equivalent surface barrier model, accounting for the shell curvature and for an unsteady loading gradient in the shell. For a thin shell having the same isotherm and adsorbent density as the particle core, we find that the frequency response of the concentric sphere model is indistinguishable from the LDF-equivalent model. However, if the shell isotherm is allowed to differ, the amplitude ratio and phase angle curves of these two models begin to depart from one another. Figure 5.2 compares amplitude ratio and phase angle curves for the LDF-equivalent and concentric sphere models that include the contribution of the shell to the overall loading, with parameters given in the figure caption. As can be clearly seen, the existence of a different isotherm in the shell causes the frequency response of the concentric sphere model to exhibit a different high frequency asymptote, which is approached more slowly than that of the simple barrier model. This different isotherm also causes a noticeable difference in the phase angle behavior. Increasing the density of the adsorbent in the shell compared with the core has a similar effect.

The shell and core interpretation of the CMS surface barrier has been put forth to explain the observation of LDF rate behavior in CMS. The model shows that if different isotherm slopes in the shell and core are invoked to explain the loading dependence of the surface barrier transport coefficient, such an explanation should be subjected to close scrutiny, as different isotherm slopes in the shell and core can result in rate behavior that is no longer equivalent to the LDF model.
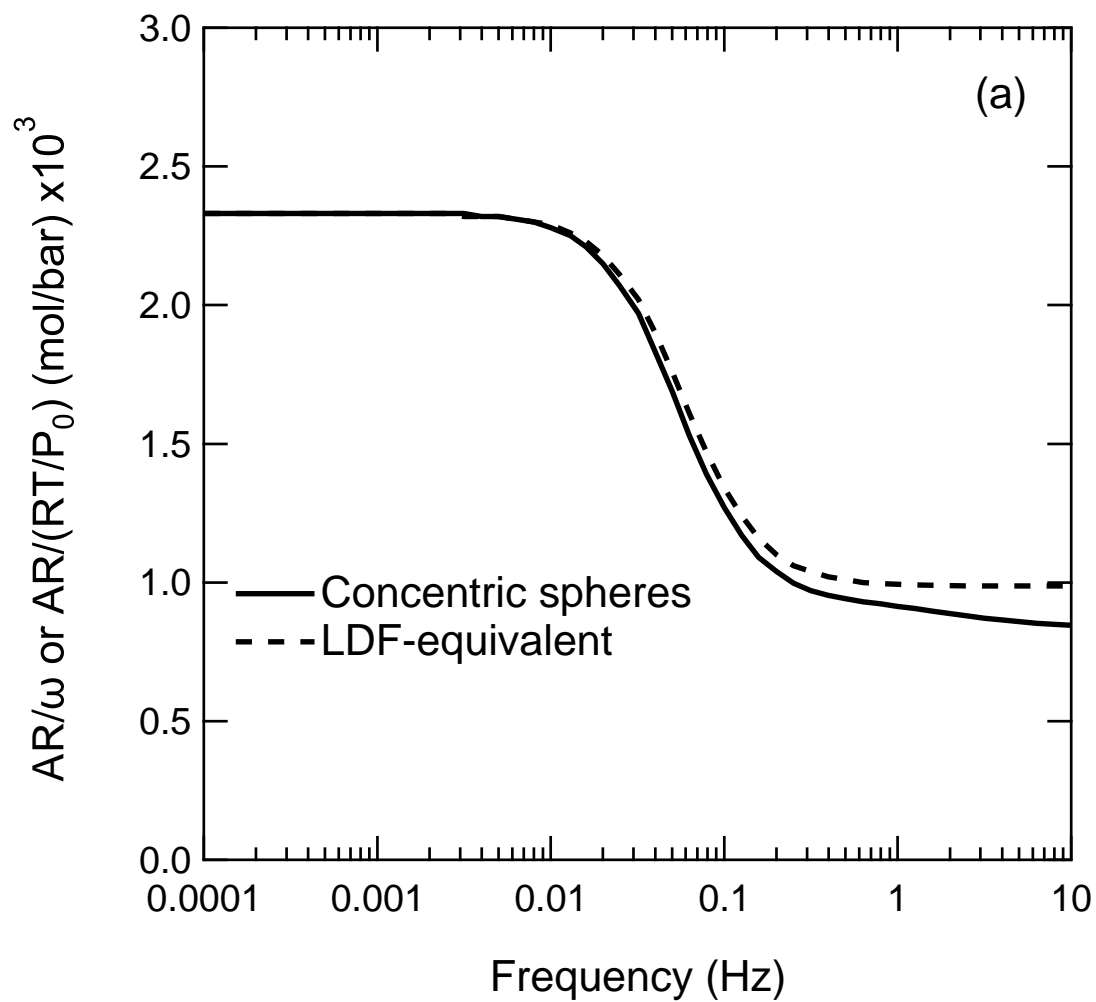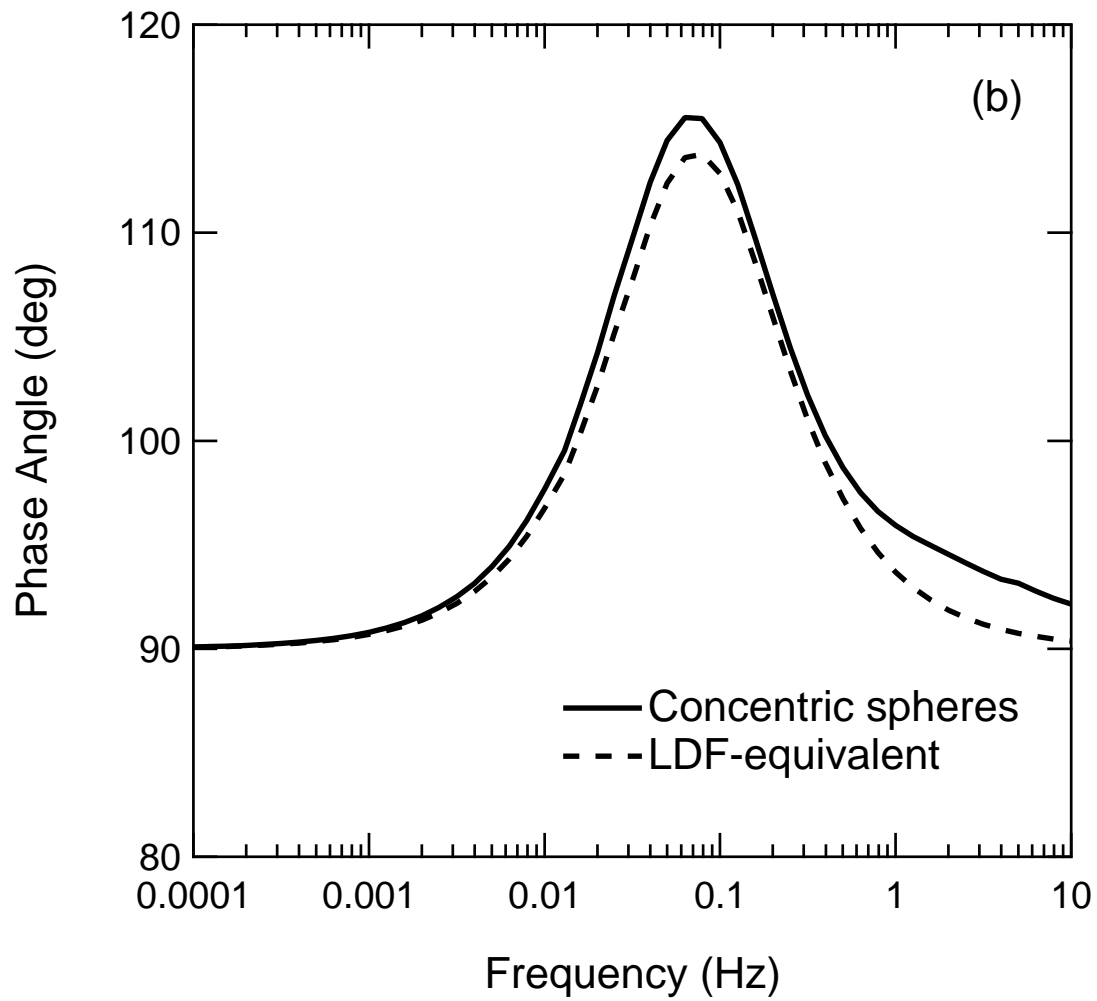
Figure 5.2 Comparison of the simple barrier and concentric sphere models with $K_s/K_c = 10$, $\eta_\delta = 1\,\mathrm{s}^{-1}$, and $\delta/r_s = 0.01$. a) amplitude ratio; b) phase angle.

5.4 Conclusions

Three adsorbed-phase transfer functions have been presented for use in analysis of adsorption rate data measured by frequency response. The first is a general model that combines the effects of micropore diffusion, macropore diffusion, a surface barrier, and temperature changes caused by the heat of adsorption. The remaining two models, which correspond to the shell and core interpretation of the CMS surface barrier, describe transport through a thin shell at the outermost region of a spherical microparticle with two different levels of complexity. The first of these two models ignores the curvature of the shell and assumes that transport through the shell reaches steady state instantaneously; the second makes neither of these simplifications. In both CMS surface barrier models, allowance is made for the existence of different isotherm characteristics in the shell and core. In the simpler model, this allowance results in a different loading dependence of the surface barrier transport coefficient than what has been previously supposed. Furthermore, if the difference in shell and core isotherms is large, the behavior of the two models begins to diverge, suggesting that there is a limit to the difference in shell and core isotherms that may be used to explain the loading dependence of the surface barrier transport coefficient in CMS systems exhibiting LDF-type rate behavior.

Notation

A	=	heat transfer area, m^2
b	=	Langmuir isotherm parameter, 1/bar
c	=	gas concentration, mol/m^3
c_p	=	macropore gas concentration, mol/m^3
C_p	=	heat capacity of an ideal gas, J/(mol K)
C_s	=	adsorbent heat capacity, J/(kg K)
D_p	=	macropore diffusivity, m^2/s
D_s	=	micropore diffusivity, m^2/s
D_{s0}	=	corrected micropore diffusivity, m^2/s
E	=	lumped parameter
F	=	gas flow rate in PSFR experiment, mol/s
G	=	transfer function for entire system
G_n	=	adsorbed-phase transfer function
G_T	=	energy balance transfer function
h	=	heat transfer coefficient, W/(m^2 K)
J	=	molar flux, mol/(m^2 s)
k_b	=	surface barrier transport coefficient, m/s
K	=	localized isotherm slope, m^3/kg
K_T	=	localized isobar slope, mol/(kg K)
l	=	lumped parameter
M_s	=	adsorbent mass, kg
n	=	adsorbate loading in a microparticle, mol/kg
$\tilde{n}$	=	adsorbate loading averaged over an entire macroparticle, mol/kg
$\hat{n}$	=	average loading in a macroparticle including gas in macropores, mol/kg
n^*	=	adsorbate loading in equilibrium with surrounding gas, mol/kg
n_{sat}	=	Langmuir isotherm saturation loading, mol/kg

P	=	gas pressure, bar
r	=	microparticle radial coordinate, m
r_c	=	microparticle core radius, m
r_s	=	microparticle radius, m
R	=	macroparticle radial coordinate, m
R_g	=	gas constant, $(\text{bar m}^3)/(\text{mol K})$
R_p	=	adsorbent particle radius, m
T	=	temperature, K
V	=	system volume, m^3
x	=	dimensionless microparticle radial coordinate
x_c	=	dimensionless core radius, r_c/r_s
x_p	=	dimensionless macroparticle radial coordinate, R/R_p

Greek Letters

α	=	lumped energy balance parameter
β	=	lumped parameter
β_{bm}	=	dimensionless transport parameter, $k_b r_s/D_s$
δ	=	shell thickness, m
ϵ_p	=	macropore porosity
η	=	diffusion parameter, D_s/r_s^2
η_δ	=	diffusion parameter, D_s/δ^2
η_m	=	lumped parameter
η_s	=	shell diffusion parameter, D_s/r_s^2
λ	=	heat of adsorption, kJ/mol
μ	=	chemical potential, kJ/mol
ρ	=	adsorbent density, kg/m^3
ϕ	=	phase angle, deg
ω	=	angular frequency, rad/s

Subscripts

0	=	equilibrium (mean) state
c	=	denotes a property in a microparticle core
i	=	value at shell/core interface
s	=	denotes a property in a microparticle shell

Superscripts

$^{-}$	=	Laplace domain

References

Boniface, H.A., Ruthven, D.M., 1985. Chromatographic adsorption with sinusoidal input. Chem. Eng. Sci. 40, 2053-2061.

Braymer, T.A., Coe, C.G., Farris, T.S., Gaffney, T.R., Schork, J.M., Armor, J.N., 1994. Granular carbon molecular sieves. Carbon 32, 445-452.

Deisler, P.F., Wilhelm, R.H., 1953. Diffusion in beds of porous solids: measurement by frequency response techniques. Ind. Eng. Chem. 45, 1219-1227.

Do, D.D., 1998. Adsorption Analysis: Equilibria and Kinetics. Imperial College Press, London.

Dominguez, J.A., Psaras, D., LaCava, A.I., 1988. Langmuir kinetics as an accurate simulation of the rate of adsorption of oxygen and nitrogen mixtures on non-Fickian carbon molecular sieves. AIChE Symp. Ser. 82, 73-82.

Evnochides, S.K., Henley, H.J., 1970. Simultaneous measurement of vapor diffusion and solubility coefficients in polymers by frequency response techniques. J. Polym. Sci. A2 8, 1987-1997.

Giesy, T.J., LeVan, M.D., 2013. Mass transfer rates of oxygen, nitrogen, and argon in carbon molecular sieves determined by pressure-swing frequency response. Chem. Eng. Sci. 90, 250-257.

Gunn, D.J., 1970. The transient and frequency response of particles and beds of particles. Chem. Eng. Sci 25, 53-66.

Huang, Q., Farooq, S., Karimi, I.A., 2003. Binary and ternary adsorption kinetics of gases in carbon molecular sieves. Langmuir 19, 5722-5734.

Huang, Q., Farooq, S., Karimi, I.A., 2004. Prediction of binary gas diffusion in carbon molecular sieves at high pressure. AIChE J. 50, 351-367.

Jordi, R.G., Do, D.D., 1993. Analysis of the frequency response method for sorption kinetics in bidispersed structured adsorbents. Chem. Eng. Sci. 48, 1103-1130.

Jordi, R.G., Do, D.D., 1994. Analysis of the frequency response method applied to non-isothermal sorption studies. Chem. Eng. Sci. 49, 957-979.

Koresh, J., Soffer, A., 1981. Molecular sieve carbons. Part 2. – Adsorption kinetics according to a surface-barrier model. J. Chem. Soc. Faraday Trans. 1 77, 3005-3018.

LaCava, A.I., Bülow, M., Fitch, F.R., 1994. Investigation of the mechanism for the separation of nitrogen-oxygen mixtures on carbon molecular sieves. Gas Sep. Purif. 8, 45-51.

LaCava, A.I., Koss, V.A., Wickens, D., 1989. Non-Fickian adsorption rate behavior of some carbon molecular sieves: I. Slit-potential rate model. Gas Sep. Purif. 3, 180-186.

Naphtali, L.M., Polinski, L.M., 1963. A novel technique for characterization of adsorption rates on heterogeneous surfaces. J. Phys. Chem. 67, 369-375.

Rouquerol, F., Rouquerol, J., Sing, K., 1999. Adsorption by Powders and Porous Solids: Principles, Methodology and Applications. Academic Press, San Diego.

Srinivasan, R., Auvil, S.R., Schork, J.M., 1995. Mass transfer in carbon molecular sieves – an interpretation of Langmuir kinetics. Chem. Eng. J. 57, 137-144.

Sun, L.M., Meunier, F., 1987. Non-isothermal adsorption in a bidisperse adsorbent pellet. Chem. Eng. Sci. 42, 2899-2907.

Sun, L.M., Meunier, F., Grenier, Ph., Ruthven, D.M., 1994. Frequency response for nonisothermal adsorption in biporous pellets. Chem. Eng. Sci. 49, 373-381.

Sun, L.M., Meunier, F., Kärger, J., 1993. On the heat effect in measurements of sorption kinetics by the frequency response method. Chem. Eng. Sci. 38, 715-722.

Sward, B.K., LeVan, M.D., 2003. Frequency response method for measuring mass transfer in adsorbents via pressure perturbation. Adsorption 9, 37-54.

Verma, S.K., Walker, P.L., 1992. Preparation of carbon molecular sieves by propylene pyrolysis over microporous carbons. Carbon 30, 829-836.

Wang, Y., LeVan, M.D., 2010. Master curves for mass transfer in bidisperse adsorbents for pressure-swing and volume-swing frequency response methods. AIChE J. 57, 2054-2069.

Wang, Y., Sward, B.K., LeVan, M.D., 2003. New frequency response method for measuring adsorption rates via pressure modulation: application to oxygen and nitrogen in a carbon molecular sieve. Ind. Eng. Chem. Res. 42, 4213-4222.

Yasuda, Y., 1982. Determination of vapor diffusion coefficients in zeolite by the frequency response method. J. Phys. Chem. 86, 1913-1917.

CHAPTER VI

CONCLUSIONS AND RECOMMENDATIONS

The work in this dissertation is centered on the characterization of mass transfer in gas/adsorbent systems relevant to the development of next generation PSA technologies designed to produce high-purity oxygen from air. The main contributions of this work are summarized below.

First, a new frequency response apparatus was developed capable of performing three different types of FR experiments: PSFR, VSFR, and CSFR. Combining these three techniques enables a broad range of experiments for the thorough and accurate characterization of mass transfer in a wide variety of adsorption systems. Between the PSFR and VSFR techniques, the apparatus can perform pure gas studies over the frequency range from 10^{-5} to 10 Hz. Using CSFR, the apparatus can study mass transfer of binary gas mixtures.

The new apparatus was first used to study mass transfer of CO_2 in 13X zeolite beads. Transport in this system was well described by a nonisothermal macropore diffusion model, where diffusion in the macropores took place via a Knudsen-type mechanism. The existence of a macropore diffusion resistance was confirmed by repeating experiments with smaller particles. Smaller particles were described only qualitatively by the nonisothermal macropore diffusion model, suggesting that unknown faster mechanisms govern transport in this system if the macropore diffusion resistance is decreased.

The apparatus was also used to study transport of pure N_2, O_2, and Ar in two carbon molecular sieve varieties. Transport of N_2 and Ar in both CMS varieties was found to be governed by a surface barrier resistance, while O_2 transport was best described by a combined-resistance model treating a surface barrier in series with a

micropore diffusion resistance. For both materials, transport of O_2 is much faster than transport of the other two gases, with Ar being the slowest. The pressure dependence of the surface barrier transport coefficient was stronger than predicted by previous interpretations of the CMS surface barrier. This stronger pressure dependence can be explained within the "shell and core" model of the CMS surface barrier by allowing the isotherm in the shell region to differ from the isotherm of the overall material.

Additionally, transport of binary mixtures of O_2 and Ar in one of the CMS varieties was studied using CSFR. Results for these binary studies show that transport of each gas in the mixture can be described well by the same transport models and parameters that describe transport of the pure gases. The data show that transport of O_2 is uninhibited by the presence of Ar. Because transport of Ar is much slower than transport of O_2, the effect of O_2 on Ar transport remains hidden. Nevertheless, linear isotherms for O_2 and Ar on this CMS suggest that the two gases can be treated as noninteracting, at least within the core of a CMS microparticle.

The work in this dissertation also includes important analytical models for interpretation of frequency response data in studies of mass transfer in adsorbents. The first model describes transport in a bidisperse adsorbent particle, accounting for transport resistances due to micropore and macropore diffusion, a surface barrier resistance, and nonisothermal effects caused by the heat of adsorption. Two other models offer a rigorous reconsideration of the "shell and core" interpretation of the CMS surface barrier, exploring the effects of different isotherms in the shell and core regions of a CMS microparticle. The models show that if the shell isotherm differs from that of the overall material, the pressure dependence of the barrier transport coefficient will be different than has been previously predicted. Furthermore, for a microparticle in which the shell isotherm is much stronger than the overall isotherm, the adsorption rate behavior will no longer resemble simple LDF rate behavior. These two models allow for a more thorough assessment of the shell and core interpretation

of the CMS surface barrier.

Finally, as shown in Appendix B, preliminary studies of mass transfer of N_2 and O_2 in LiLSX zeolite beads suggest that N_2 transport is limited by Poiseuille flow in the macropores, with nonisothermal effects present due to the high heat of adsorption for N_2. Due to the weak isotherm for O_2 on LiLSX, the frequency response of O_2 was too weak to be measured.

To continue this work, there are two directions recommended here. Most important among these is that a new experimental VSFR configuration be developed, such that the response of O_2 on LiLSX can be measured. The new configuration must be developed to ensure that the amount of O_2 adsorbing and desorbing during perturbation is significant compared to the overall amount of gas in the system. This criterion would suggest that the overall system volume should be smaller, with the amount of adsorbent used remaining on the order of what is used in the current apparatus. To keep the system linearized, the volume perturbation should also be reduced.

Lastly, the pressure dependence of the surface barrier transport coefficient that is predicted by the shell and core interpretation of the CMS surface barrier should be tested by measuring values of the barrier coefficient for different gases on CMS that are governed by a barrier resistance. Gases having strong isotherms on CMS should be chosen to minimize error in the fitting parameters. These values should be measured at closely spaced intervals over a wide range of experimental pressures, so that the pressure dependence can be confidently distinguished from experimental error in the measured parameter values.

APPENDIX A

DEVELOPMENT OF THE NONISOTHERMAL MACROPORE DIFFUSION MODEL

The macropore mass balance equation (Eq. 2.5) can be easily converted to the Laplace domain by defining the deviation variables

$$c'_p = c_p - c_{p0} \tag{A-1}$$

$$n' = n - n_0 \tag{A-2}$$

In the Laplace domain, the mass balance becomes

$$\frac{\epsilon_p D_p}{R^2} \frac{\partial}{\partial R} \left(R^2 \frac{\partial \bar{c}_p}{\partial R} \right) = \epsilon_p s \bar{c}_p + \rho_p s \bar{n} \tag{A-3}$$

The linearized equilibrium expression (Eq. 2.4) allows substitution for $\bar{n}$ with

$$\bar{n} = K \bar{c}_p + K_T G_T \bar{\bar{n}} \tag{A-4}$$

In Eq. A-4, the energy balance transfer function G_T is given as

$$G_T = \frac{\bar{T}}{\bar{\bar{n}}} = \frac{-M_s \lambda s}{M_s C_s s + \alpha} \tag{A-5}$$

and is found by converting the energy balance equation (Eq. 2.8) to the Laplace domain.

Introducing a dimensionless radial coordinate $x_p = R/R_p$ and rearranging, the

equation becomes

$$\frac{1}{x_p^2}\frac{\partial}{\partial x_p}\left(x_p^2\frac{\partial \bar{c}_p}{\partial x_p}\right) = \eta\bar{c}_p + \beta\bar{\tilde{n}} \tag{A-6}$$

The boundary conditions in the Laplace domain are

$$\bar{c}_p = \bar{c} \text{ at } x_p = 1 \tag{A-7}$$

$$\frac{\partial \bar{c}_p}{\partial x_p} = 0 \text{ at } x_p = 0 \tag{A-8}$$

Eq. A-6 is a nonhomogeneous form of a modified spherical Bessel equation, and can be solved analytically. The solution to the differential equation is

$$\bar{c}_p = \left(\bar{c} + \frac{\beta\bar{\tilde{n}}}{\eta}\right)\frac{1}{x_p}\frac{\sinh\left(\sqrt{\eta}x_p\right)}{\sinh\sqrt{\eta}} - \frac{\beta\bar{\tilde{n}}}{\eta} \tag{A-9}$$

To find $\bar{\tilde{n}}$, the following integration is performed using Eq. A-4.

$$\bar{\tilde{n}} = 3\int_0^1 \bar{n}x_p^2 dx_p = 3\int_0^1 \left(K\bar{c}_p + K_T G_T\bar{\tilde{n}}\right)x_p^2 dx_p \tag{A-10}$$

Noting that $\bar{\tilde{n}}$ does not depend on x_p, solution of the integral leads to the following expression for $\bar{\tilde{n}}$.

$$\bar{\tilde{n}} = \frac{3K\bar{c}l_1}{1 - K_T G_T + \dfrac{K\beta}{\eta}\left(1 - 3l_1\right)} \tag{A-11}$$

The expression for the adsorbed-phase transfer function G_n includes not $\bar{\tilde{n}}$, but $\bar{\hat{n}}$, which also accounts for gas in the intercrystalline voids of an adsorbent particle via

$$\bar{\hat{n}} = \bar{\tilde{n}} + 3\int_0^1 \frac{\epsilon_p}{\rho_p}\bar{c}_p x_p^2 dx_p \tag{A-12}$$

Upon solution of the integral, Eq. A-12 becomes

$$\bar{\hat{n}} = 3\bar{c}l_1 \left\{ \frac{K\left[1 - \dfrac{\epsilon_p \beta}{\rho_p \eta}(1 - 3l_1)\right]}{1 - K_T G_T + \dfrac{K\beta}{\eta}(1 - 3l_1)} + \frac{\epsilon_p}{\rho_p} \right\} \tag{A-13}$$

Noting that $\bar{c} \approx \bar{P}/RT_0$ and dividing both sides of Eq. A-13 by $\bar{P}$ yields the final expression for the adsorbed-phase transfer function.

$$G_n = \frac{\bar{\hat{n}}}{\bar{P}} = \frac{3}{RT_0}l_1 \left\{ \frac{K\left[1 - \dfrac{\epsilon_p \beta}{\rho_p \eta}(1 - 3l_1)\right]}{1 - K_T G_T + \dfrac{K\beta}{\eta}(1 - 3l_1)} + \frac{\epsilon_p}{\rho_p} \right\} \tag{A-14}$$

APPENDIX B

MASS TRANSFER OF N_2 AND O_2 IN LILSX ZEOLITE

Introduction

Because air is composed chiefly of N_2 and O_2, the ability of an adsorbent to separate these two gases is of particular importance to the development of next-generation rapid PSA technologies for separation of oxygen from air. Li-exchanged low-silica zeolite X (LiLSX) has been shown to be the most promising adsorbent for air separation due to its high nitrogen capacity and its high selectivity for N_2 over O_2.[1–11] Thus, the adsorption rates of N_2 and O_2 on LiLSX are of substantial interest and importance to the greater aim of this research project.

To date, there are apparently no investigations in the literature of N_2 and O_2 adsorption rates on LiLSX. In this Appendix, preliminary findings from our investigation of adsorption rates in the pure N_2/LiLSX and pure O_2/LiLSX systems are presented. This work provides valuable insights into the dynamic behavior of these systems and should offer significant aid to the development of PSA oxygen purification technologies.

Experiments

For this work, PSFR and VSFR experiments were performed using pure N_2 and O_2 on LiLSX zeolite (UOP OXYSIV™-MDX). The experiments were performed using the apparatus and technique described previously.[12] Between the two techniques, the overall investigated frequency range was 0.0001 to 10 Hz. Experimental pressures ranged from 0.125 bar to 1 bar. The zeolite sample was 6.66 g of 30-60 mesh spherical beads. Before experimentation, the zeolite sample was activated at 350 °C for 12 hours.

Results and Discussion

Transport of gases in zeolite X is expected to be fast, as the pore openings in faujasite cages are larger than those in other zeolites. An example of this principle is the rapid adsorption of CO_2 on 13X zeolite.[12,13] When transport in the zeolite micropores is fast, other transport resistances will govern the adsorption rate. For a zeolite particle composed of smaller crystals held together by a binder, the macropore diffusion resistance can be large enough to govern the rate of adsorption.

In the LiLSX (a zeolite of type X) system investigated here, relatively small particles are used. As the macropore diffusion resistance depends on the length of the diffusion path, i.e., the particle radius, even the macropore diffusion resistance in this system is expected to be quite low. Expecting fast transport, we first performed VSFR experiments with pure N_2 and O_2 on LiLSX, as the illucidation of faster transport mechanisms occurs at higher perturbation frequencies and the VSFR functionality of our apparatus covers higher frequencies (up to 10 Hz) than PSFR.

Figure B.1 shows sample VSFR data measured with N_2 at 0.25 bar fit to a transport model for diffusion in spheres, which is the model found to best describe the experimental data. The data are well described by this model at each of the experimental pressures.

Due to the close similarity between spherical transport models for micropore and macropore diffusion, it is difficult to ascertain simply by the model description whether micropore or macropore diffusion is limiting in this system. However, insight into which of these mechanisms is limiting may be gained by looking at the pressure dependence of the diffusion coefficient. For a pure gas, diffusion can take place via micropore diffusion or either Knudsen diffusion or Poiseuille flow in the macropores. Each of these mechanisms predicts a different pressure dependence of the diffusion coefficient. As shown in Figure B.2, the diffusion coefficients increase approximately linear with the experimental pressure, which is consistent with the expected trend
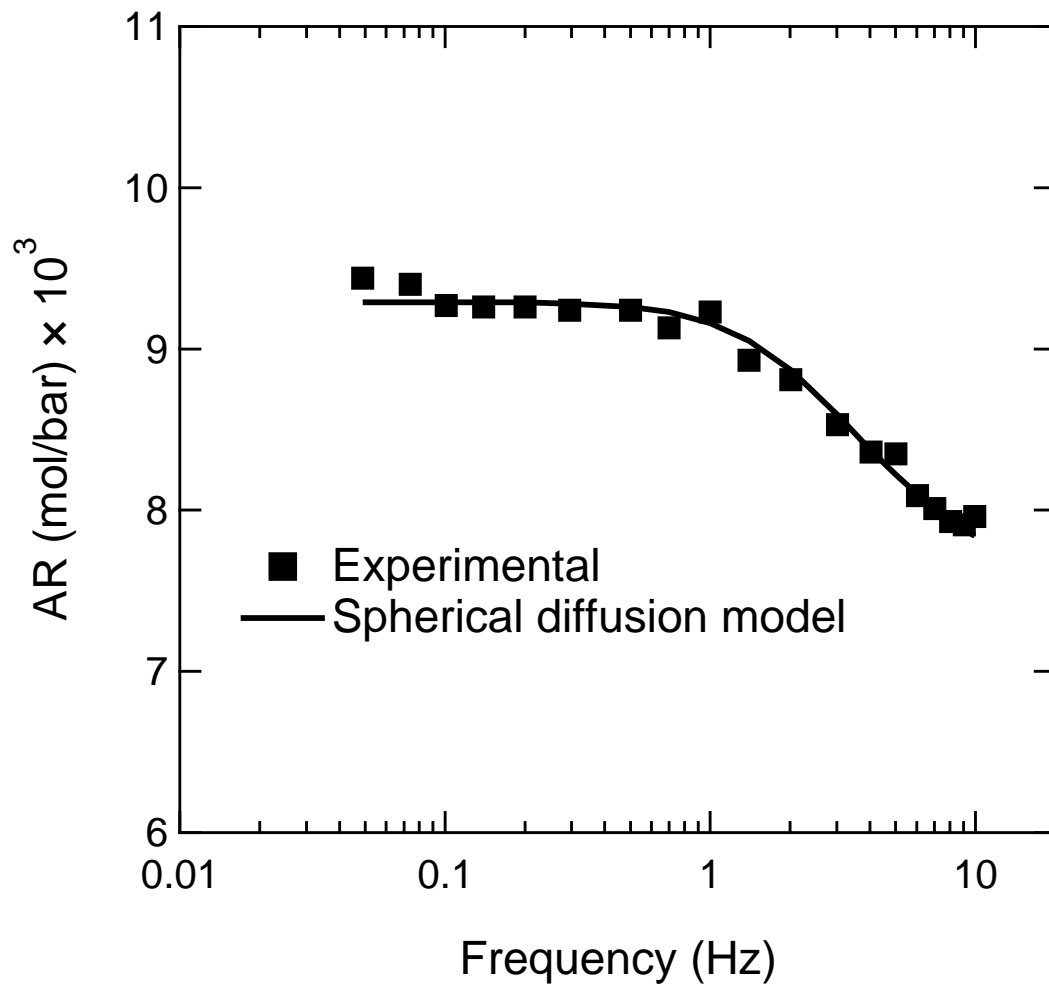
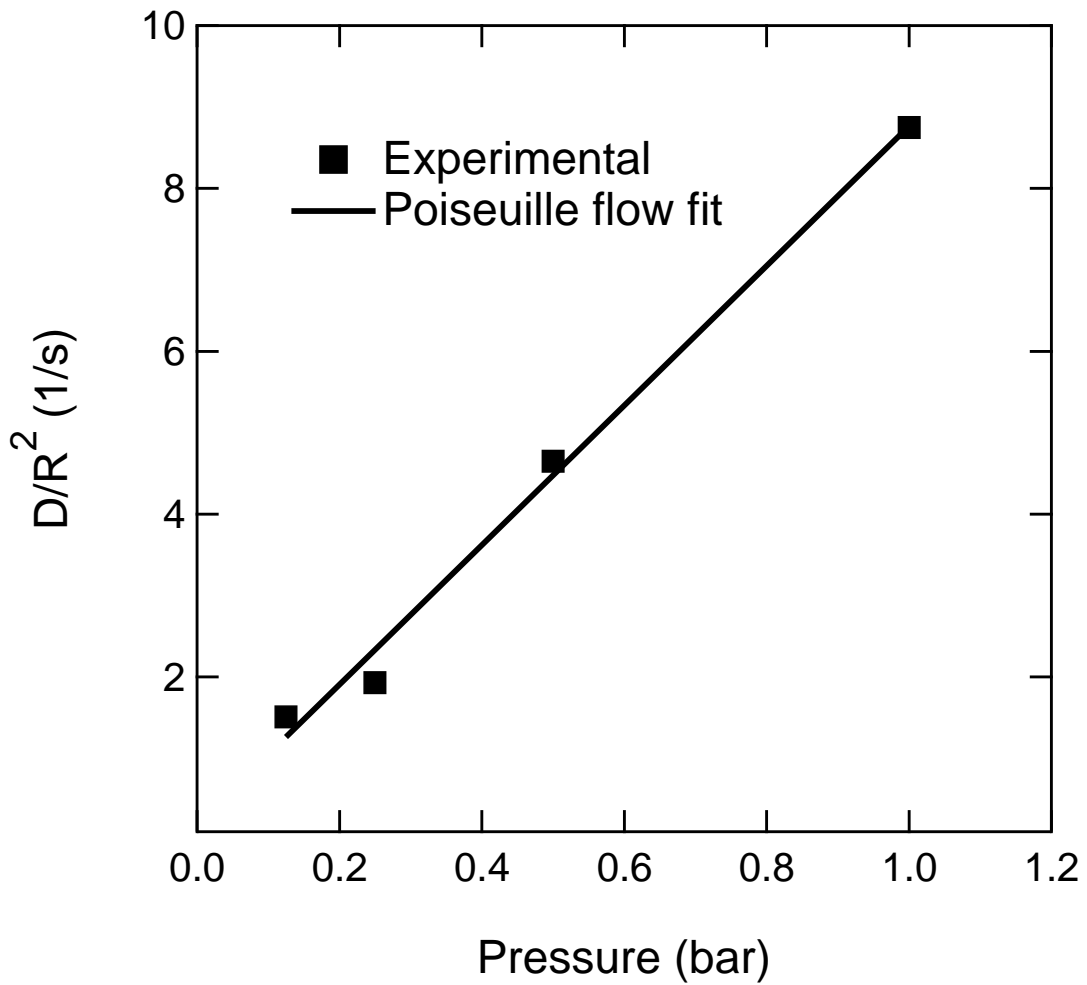Figure B.1 Sample VSFR amplitude ratio for N_2 on LiLSX compared with a spherical diffusion model fit.

Figure B-2 Values of D/R^2 for N_2 on LiLSX measured at pressures from 0.125 to 1 bar.

for Poiseuille flow.[14] These data suggest that Poiseuille flow in the macropores is the limiting transport resistance for N_2 in this system.

In analysis of FR data, the low-frequency asymptote in amplitude ratio occurs when the adsorbate loading is always at equilibrium with the surrounding gas. In this situation, decreasing the frequency further does not result in more gas adsorbed within the perturbation period. Thus, the value of the low-frequency asymptote depends on the local isotherm slope of the system at the experimental pressure. With the VSFR data for N_2, it was found that the isotherm slopes extracted from the low-frequency asymptotes are considerably smaller than those measured in parallel work using equilibrium techniques. It was thus desirable to investigate slower frequencies, to see if the real low-frequency asymptote had been reached in the VSFR experiments.

Figure B.3 shows sample PSFR amplitude ratio data measured using pure N_2 and LiLSX covering the frequency range from 0.0001 to 0.05 Hz. As shown in the figure, the amplitude ratio continues to increase in value toward the low-frequency asymptote as the frequency becomes slower, suggesting that the true asymptote has not been reached at the frequencies covered by the VSFR experiments. A possible explanation for this behavior is the existence of nonisothermal effects in the system caused by the heat of adsorption. Multiple studies have noted that N_2 has a particularly large heat of adsorption on LiLSX, making this system particularly susceptible to deviations from isothermality.[1,6] When energy is released upon adsorption faster than it can be transported away from the adsorbent, the temperature of the adsorbent increases, causing a change in the isotherm slope of the gas/adsorbent pair. The shape of the amplitude ratio curve is affected significantly by this isotherm slope, such that the low-frequency asymptote will not be reached until the perturbation frequency is slow enough that the adsorbent can maintain an isothermal condition via heat transfer.

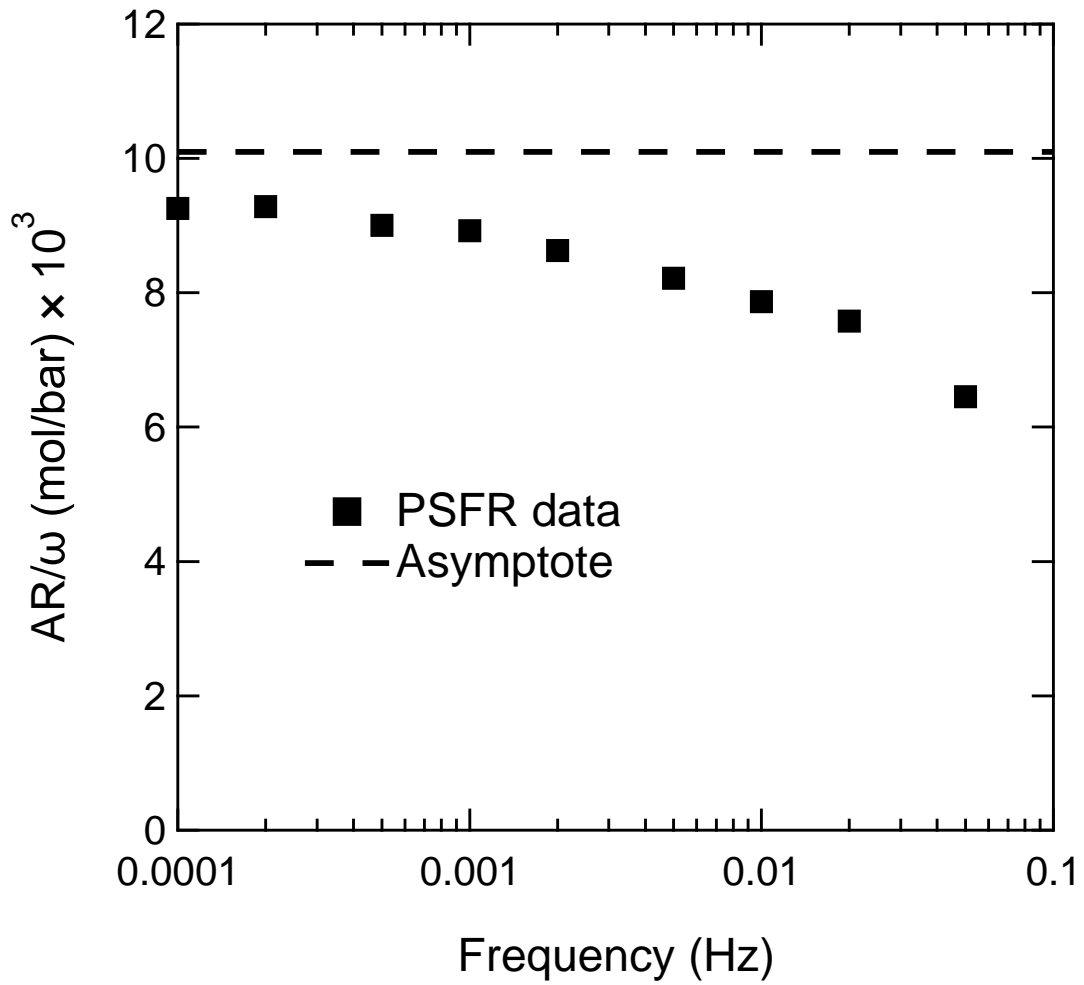In spite of the apparent nonisothermal effects in the system, the VSFR data

Figure B-3 Sample PSFR amplitude ratio data for N_2 on LiLSX measured at 0.25 bar compared with expected low-frequency asymptote.

still appear to exhibit some sort of low-frequency asymptote. This observation suggests that heat transfer in this system is much slower than mass transfer, such that the frequency ranges over which the effects of heat and mass transfer affect the amplitude ratio are separated by a relatively wide margin. Furthermore, while nonisothermal diffusion models generally differ in the shape of amplitude ratio curves compared with isothermal models, the isothermal model describes the VSFR data well; introducing additional parameters to account for the temperature affects would not enhance the ability of the transport model to describe the data. Thus, over the frequency range at which the affect of mass transfer is manifested, the temperature effects do not seem to affect the rate enough to necessitate the use of a more complicated transport model.

For O_2, PSFR and VSFR experiments were also performed. Figure B.4 shows sample VSFR amplitude ratio data for O_2 on LiLSX measured at 0.125 bar. The value of the amplitude ratio remains relatively constant across the whole frequency range, and similar behavior was observed at the other experimental pressures. This behavior can be attributed to the local O_2/LiLSX isotherm slopes, which are much smaller than the corresponding isotherm slopes for N_2. In PSFR and VSFR experiments, the magnitude of the isotherm slope dictates the size of the response to the perturbation: a small isotherm slope gives a small response. Thus, while the comparatively weak affinity of LiLSX for O_2 makes it an effective adsorbent for air separation, this weak affinity also makes FR investigations of O_2 adsorption rates difficult by resulting in a noise-level response to perturbation.

For the apparatus used in this work, PSFR data are much more sensitive than VSFR data to the response caused by gas/adsorbent pairs with small isotherm slopes; this is a result of the smaller system volume for PSFR. However, the PSFR technique has the disadvantage of a lower maximum investigable frequency, which is an important factor in the suitability of a FR technique to studying fast transport mechanisms. Figure B.5 shows sample PSFR amplitude ratio data for O_2 on LiLSX
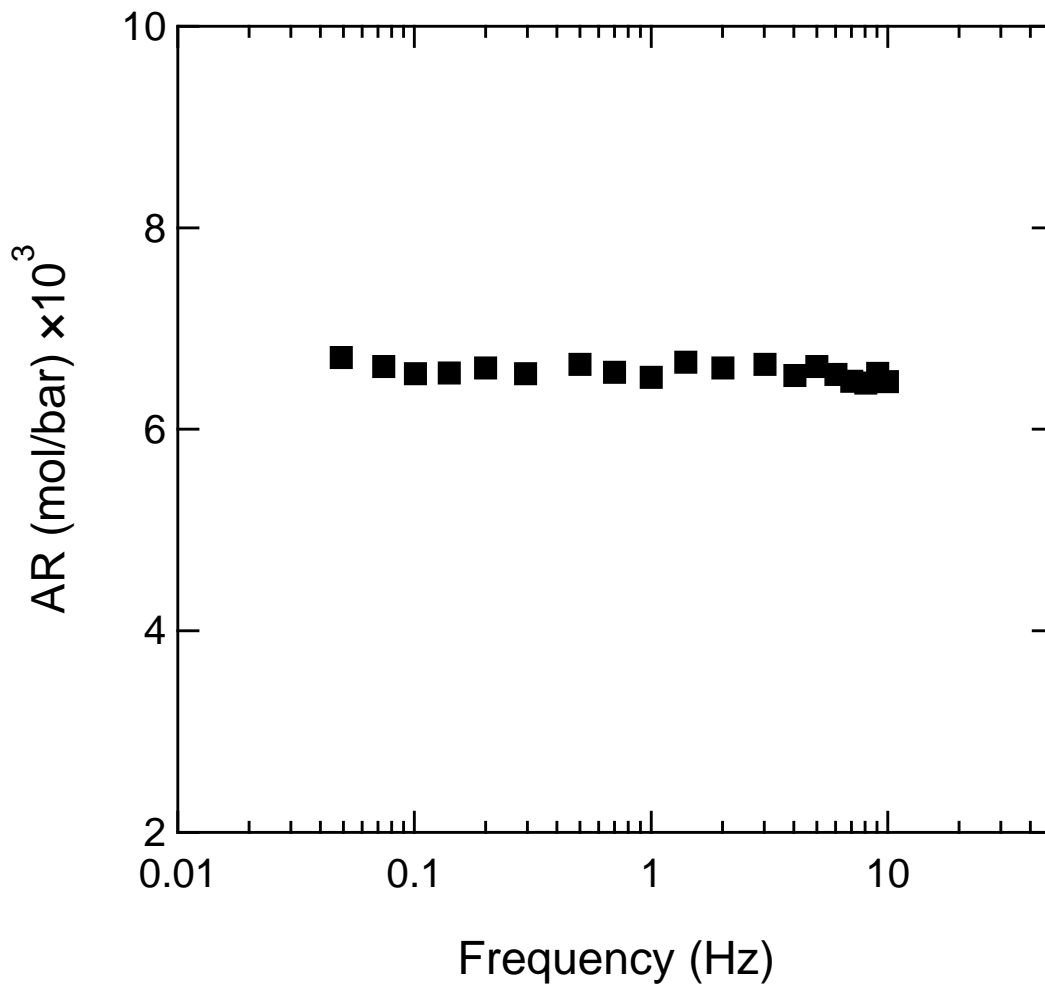
Figure B-4 Sample VSFR amplitude ratio data for O_2 on LiLSX measured at 0.125 bar.
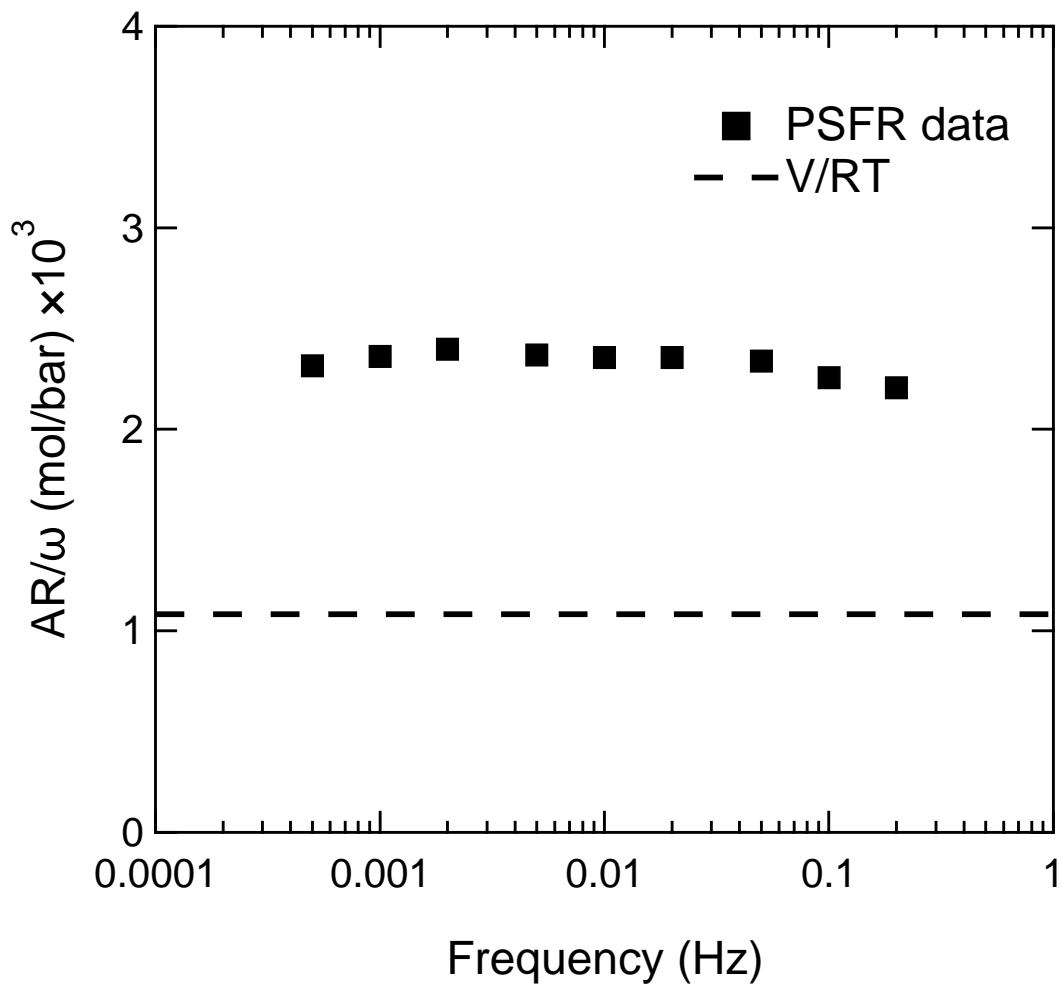
Figure B-5 Sample PSFR amplitude ratio data for O_2 on LiLSX measured at 0.5 bar compared with the expected amplitude ratio with no adsorption taking place.

measured at 0.5 bar. As with VSFR, the data here are largely flat across the whole frequency range. Given that the amplitude ratio values are discernibly higher than those expected for a system with no adsorption taking place (i.e., the value V/RT indicated by the dashed line), the flatness of the experimental data is not a result of the small isotherm slope, but is caused rather by the adsorbed O_2 being in equilibrium with the surrounding gas at all times. As with N_2, transport of O_2 in this system is fast, and the frequency range of PSFR experiments is not wide enough to make manifest the effect of O_2 transport on the amplitude ratio. As a result, the FR experiments of O_2 on LiLSX do not convincingly indicate anything regarding the governing transport mechanism(s) or the values of transport parameters for O_2 except that transport of O_2 is fast.

Conclusions

Frequency response experiments suggest that transport of pure N_2 in LiLSX is governed by Poiseuille flow in the macropores, with temperature effects being important. Experiments with pure O_2 were inconclusive, as PSFR experiments could not reach high enough frequencies to see the effect of O_2 transport on the amplitude ratio and the VSFR response was too small to resolve because of the weak O_2/LiLSX isotherm.

References

[1] Rege, S. U.; Yang, R. T. Limits for air separation by adsorption with LiX zeolite. *Ind. Eng. Chem. Res.* **1997**, *36*, 5358.

[2] Feuerstein, M.; Engelhardt, G.; McDaniel, P. L.; MacDougall, J. E.; Gaffney, T. R. Solid-state nuclear magnetic resonance investigation of cation siting in LiNaLSX zeolites. *Micropor. Mesopor. Mat.* **1998**, *26*, 27.

[3] Hutson, N. D.; Zajic, S. C.; Yang, R. T. Influence of residual water on the adsorption of atmospheric gases in Li-X zeolite: Experiment and simulation. *Ind. Eng. Chem. Res.* **2000**, *39*, 1775.

[4] Jale, S. R.; Bülow, M.; Fitch, F. R.; Perelman, N.; Shen, D. Monte Carlo simulation of sorption equilibria for nitrogen and oxygen on LiLSX zeolite. *J. Phys. Chem. B.* **2000**, *104*, 5272.

[5] Shen, D.; Bülow, M.; Jale, S. R.; Fitch, F. R.; Ojo, A. F. Thermodynamics of nitrogen and oxygen sorption on zeolites LiLSX and CaA. *Micropor. Mesopor. Mat.* **2001**, *48*, 211.

[6] Kazansky, V. B.; Bülow, M.; Tichomirova, E. Specific sorption sites for nitrogen in zeolites NaLSX and LiLSX. *Adsorption* **2001**, *7*, 291.

[7] Yoshida, S.; Hirano, S.; Harada, A.; Nakano, M. Nitrogen adsorption properties of cubic and orthorhombic Li-exchanged low silica X. *Micropor. Mesopor. Mat.* **2001**, *46*, 203.

[8] Zanota, M. L.; Heymans, N.; Gilles, F.; Su, B. L.; Frère, M.; De Weireld, G. Adsorption isotherms of pure gas and binary mixtures of air compounds on faujasite zeolite adsorbents: Effect of compensation cation. *J. Chem. Eng. Data* **2010**, *55*, 448.

[9] Chai, S. W.; Kothare, M. V.; Sircar, S. Numerical study of nitrogen desorption by rapid oxygen purge for a medical oxygen concentrator. *Adsorption* **2012**, *18*, 87.

[10] Chai, S. W.; Kothare, M. V.; Sircar, S. Efficiency of nitrogen desorption from LiX zeolite by rapid oxygen purge in a pancake adsorber. *AIChE J.* **2013**, *59*, 365.

[11] Rao, V. R.; Chai, S. W.; Kothare, M. V.; Sircar, S. Highlights of non-equilibrium, non-isobaric, non-isothermal desorption of nitrogen from a LiX zeolite column by rapid pressure reduction and rapid purge by oxygen. *Adsorption* **2014**, *20*, 477.

[12] Giesy, T. J.; Wang, Y.; LeVan, M. D. Measurement of mass transfer rates in adsorbents: New combined-technique frequency response apparatus and application to CO_2 in 13X zeolite. *Ind. Eng. Chem. Res.* **2012**, *51*, 11509.

[13] Ruthven, D. M.; Lee, L. K. Kinetics of nonisothermal sorption: Systems with bed diffusion control. *AIChE J.* **1981**, *27*, 654.

[14] Kärger, J.; Ruthven, D. M. *Diffusion in Zeolites and Other Microporous Solids*; Wiley-Interscience Publications: New York, 1992.